ABSTRACT

Development and application of a process-based,

basin-scale stream temperature model

By

Douglas McKinnon Allen

Doctor of Philosophy in Earth and Planetary Science

University of California, Berkeley

Professor Bill Dietrich, Chair

Over the past 150 years conversion of forested lands by industrial timber harvesting and other land use activities has resulted in elevated water temperatures throughout California and the Pacific Northwest and has significantly impacted native aquatic species. Recent regulatory and legislative efforts have focused on quantifying the basin-scale dimensions of stream temperature and its impacts on biological populations. Toward meeting these objectives, there is a need to develop stream temperature models which capture the essential physics of summertime stream heating, have limited input data requirements, and that have watershed scale application. Given anticipated increased drought intensity and frequency with global warming, such a model needs to account specifically for changes in summer baseflow.

To explore the necessary elements of such a model, I first present the basic physics controlling stream temperature and then perform a sensitivity analysis to see what matters most to temperature evolution along a river. Through this analysis I have elected

to focus on small streams in which both topographic and vegetation shading influence direct insolation reaching the channel. This simplifies the eventual structure of the model, and focuses it on uplands streams which are most often affected by forest management. The sensitivity analysis reveals that the heat flux and resulting stream temperature in this case are predicted to vary inversely with flow depth, leading to a nonlinear dependency on discharge. This analysis shows that there is an inverse relationship between flow depth and stream temperature, suggesting significant sensitivity to drought flow reductions.

The results of these analyses are used to guide the development of a simple, processed-based stream temperature model with application to entire river basins. The model assumes that direct solar radiation is the chief mechanism driving stream heating during summer months in mid-latitude regions. The key elements of the model are: 1) a simple heat balance model, 2) a model for riparian shading based on tree height adjacent to channels (and for shading due just to topography), 3) a groundwater inflow model that assumes inflow increases linearly with stream length, and 4) an optimization technique that uses a relatively small amount of field data to fit 3 free parameters.

The model was applied to Bull, Elder, and Rattlesnake Creeks, three sub-basins within the South Fork Eel basin in Northern California. Each sub-basin is characterized by different vegetation, relief, and lithologic characteristics. Model performance for the three sub-basins, measured by the root mean square error statistic, ranged from 0.25 ºC to 0.47ºC. Model predictions for all three sub-basins demonstrate the important interactions between relief, vegetation, and hydrology, and for one basin (Rattlesnake Creek), the important effects of lithology (expressed through topography, vegetation and groundwater inflow rates). The model also performed satisfactorily using pooled data for

the three basins, yielding an RMSE of 0.39°C. This test showed the model can be readily applied to larger watersheds and suggests that for calibration purposes data from about 7 thermographs per 100 km^2 are needed. As expected, model predictions are sensitive to increases or decreases in discharge. In particular, reductions in flow resulted in a highly non-linear temperature response, particularly for headwater streams.

A series of 12 numerical runs were conducted to explore the spatial sensitivity of stream temperature on changes in tree shading and baseflow. Three general vegetation states were assumed: current, no vegetation and forest in late seral, tall tree condition. Temperature predictions are generally significantly warmer for no-tree shade conditions, but local relief and aspect controls can offer sufficient shading to create intrinsically cool canyons and reaches on the mainstem that cool the flow. Also variation in groundwater inflow rates can reduce or amplify heating effects associated with either vegetation removal or growth to late seral stage. This analysis points to the local importance of topography and lithology in consideration of local stream temperature goals.

Finally, I explore the possible amplifying and moderating effects of varying both shade and baseflow. Eliminating riparian shade for the entire Bull Creek basin and reducing flow by 50% caused warming of stream temperatures relative to current conditions by about 5 to 6°C. Temperatures varied downstream but continued to warm down to the mouth. Converting the entire Bull Creek basin to full shade, and increasing the baseflow by 50% cooled the stream relative to current conditions by 3 to °C. Changes in just the tributary tree shading (full shade or no shade) produced smaller warming and cooling trends. By increasing the shade but reducing the flow or by decreasing the shade and increasing the flow, opposing effects were modeled that revealed the central role of

mainstem vegetation in moderating cumulative temperature effects. In essence, the warming due to loss of shading in the tributaries or of basin-wide reduced flows was partly compensated when flows entered the mainstem where current conditions (or assigned reference conditions) provide significant shading. This highlights the importance of mainstem shading by trees on stream temperature.

The stream temperature model proposed here can be easily applied to entire watersheds to explore management options. To do so requires some field data on stream temperatures at low flow (and some data on low flow downstream hydraulic geometry), which, in effect allows the model to retain its simplicity and yet make it applicable to specific locations throughout a watershed. One practical outcome of the model is the conclusion that stream temperatures of headwater channels may rise significantly during droughts, and that, in anticipation of the oncoming effects of global warming, broad efforts should be directed now towards the management of headwater and mainstem riparian forests into tall, shade providing trees.

Table of Contents

List of Tables

List of Figures

Chapter 1

Introduction

1.1 INTRODUCTION

The transformation of the Pacific Northwest and California landscape that followed the arrival of Europeans resulted in widespread conversion of forested land, either by clearcutting, selective logging, or conversion to a different land use altogether (Lichatowich, 1999, Sedell et al. 1991). This transformation was accompanied by, and more often at the expense of, significant changes in the quality and quantity of terrestrial and aquatic biological habitat. Water temperature plays a vital role in cold water aquatic ecosystems in California and Pacific Northwest and especially Pacific salmonid populations (Cafferata 1990). Water temperature directly governs almost every aspect of the survival and life history of Pacific salmon (Berman 1998). Numerous physiological processes are affected by temperature, including: (1) trophic effects (thermal effects on the energy base for fish), (2) tolerance effects – temperature effects on fish behavior, and (3) metabolic effects – temperature effects development and activity (Beschta et al. 1987, Groot et al, 1995, Spence et al, 1996). General temperature criteria for all salmonids for each life stage are outlined in Table 1.1. The criteria indicate that spawning life stages prefer temperatures less than 15.5ºC while rearing the life stages generally prefer temperatures below 18ºC. The rearing life stage is considered especially vulnerable to elevated water temperatures (Brown et al. 1994, U.S. EPA 1999, Stillwater Sciences 2002). For example the juvenile coho (*Oncorhynchus kisutch*) rearing life stage remain in freshwater streams for a full year while they mature (California Department of Fish and

Game 2002, U.S. EPA 1999). Table 1.2 details juvenile coho behavioral responses to different temperatures. Temperature effects on juvenile coho metabolism were studied by Averett (1968) who showed that juvenile coho require twice as much food to grow at 17°C than at 5°C. Juvenile salmonid life stages are especially vulnerable to elevated temperatures. For salmonid life stages, but particularly rearing juveniles, removal of shade-providing streamside vegetation has seriously reduced the quality and quantity of available freshwater habitat (Theurer et al, 1985).

Timber harvesting impacts on stream temperatures in California and the Pacific Northwest have been focus of attention since the 1960's (for example, Lichatowich 1999, Beschta et al. 1987, Brown 1983). Harvest impacts include eliminating riparian vegetation and exposing the channel to greater shortwave radiation loading leading to elevated water temperatures. Consequently the thermal regime is shifted to one which includes more extreme diurnal variability — increased warming during the day and cooling during the night. Eliminating riparian vegetation also reduces or eliminates bank stability resulting in erosion and aggradation, t and thereby tending to widen the channel and reduce its depth. Several studies have measured stream temperature response to timber harvesting. Tables 1.3 and 1.4 summarize results from studies in the Eastern United States and Japan (Table 1.3), and California and the Pacific Northwest (Table 1.4) and show significant increases in summer maximum stream temperatures. According to the Eastern US studies average summer maximum temperatures increase 3°C to 10°C (Table 1.3), while average summer maximum temperatures increase from 3°C to 8°C in California and the Pacific Northwest. Post-harvest, peak temperature changes of up to 19°C were recorded in one study in Oregon (Table 1.4, Amaranthus et al. (1989)).

The legislative response to the decline in salmon populations has been primarily focused through the Federal Endangered Species Act (ESA), and the Federal Clean Water Act (CWA). The Clean Water Act has established the legislative basis for water quality standards programs and defines water quality goals to meet those standards. Fresh water bodies throughout Coastal California and the Pacific Northwest now contain streams listed as water quality limited due to elevated temperatures. A broad range of analytical and empirical tools have been applied to assess and quantify elevated stream temperature conditions to guide management decisions (Deas and Lowney 2000). In addition, there is a demand for tools that address salmonid habitat concerns at the population level, and therefore a demand for models with landscape-scale focus (Dunham et al. 2001).

In many practical watershed-scale applications there is a need for a rapid assessment of the magnitude and controls on stream temperatures in order to guide restoration measures. Typically data availability is limited. In California and the Pacific Northwest the primary concern with regard to management controls on stream temperature has been the removal of riparian vegetation (e.g. Beschta et al. 1987). This concern is dictated by the fact that for unregulated streams, riparian manipulation is the only management response available to tackle elevated stream temperatures (LeBlanc and Brown 2000). For regulated systems, increasing reservoir releases is typically the only management strategy available to tackle elevated stream temperatures. Regulated rivers are generally deeper and wider and respond less to solar heat input and more to point-source flow adjustments, and the temperatures of those flow adjustments (Gu et al. 1998).

There is a need for watershed scale stream temperature models to guide management decisions. Simple empirical models (e.g. Mitchell 1999) and rudimentary

3

reach-based mechanistic models (Brown 1969) are inadequate or inappropriate for large basin applications. Reach- based mechanistic models (Bartholow 2000, Boyd and Kaspar 2003) are not applicable at basin-scales, while spatially-distributed physical models (e.g. Theurer et al. 1984, Bicknell et al. 1997) require substantial field-measured input data to run. These data are usually unavailable and are prohibitively expensive to collect.

Here I develop a spatially-explicit, process-based model for predicting stream temperatures during the hottest part of the year which applies to fine scale reaches (approximately 25-meters) throughout the entire stream network. The model assumes that direct shortwave radiation dominates the heat flux arriving at the stream surface. Furthermore the model assumes that riparian vegetation and terrain shading are the primary controls over the amount shortwave radiation reaching the stream surface, and hence provide important controls over stream temperature. The model assumes that lateral inflow of cool water enters the stream at a rate which is a linear function of distance. Heat is advected downstream by the steady-state low flow model, accounting for the advection of cool or warm water to downstream reaches. The model requires digital elevation data, vegetation information, discharge data, and limited observations of observed temperature data for the basin of interest. A key component of the model is a three parameter optimization technique that uses field measured temperature data to improve model predictions. The optimization technique permits the model to retain simplicity and limits its input data requirements.

The model demonstrates: (1) important shading effects due just to ridge and valley topography, revealing significant spatial differences in stream heating within watersheds; (2) significant shading effects associated with riparian vegetation; and (3) the

4

strong sensitivity of stream temperatures for small streams to heat loading and reductions in discharge.

1.2 ORGANIZATION

This dissertation is organized into four chapters. The second chapter reviews the general stream heating physics and presents the general equations for the different heat flux mechanisms. I then present the results from a general sensitivity analysis of stream heating physics which show that stream temperature is highly sensitive to the combination of high solar heat loading and stream depth. From the perspective of this review, I proceed to survey the relevant theoretical and empirical research on stream temperature. Based on this review and the results of the general sensitivity analysis I conclude that there is a need for a basin-scale, process-based stream temperature model which captures the dominant summertime stream heating mechanisms within a simple model structure.

In the third chapter I present the model and describe all the main features which comprise the model. I then apply it to three basins in Northern California. Together these basins reveal the influence of topography, vegetation, lithology, and hydrology on stream temperatures. The results for each basin indicate the model performs well despite simplifying assumptions embedded in the model. Finally I examine the sensitivity of model predictions to these assumptions. Temperature predictions are shown to be very sensitive to adjustments in flow. Changes in predicted temperature are shown to be highly non-linear when flow is reduced by 25% and 50%.

In the final chapter, I explore the effects of adjusting riparian tree heights on predicted temperatures. Here the motivation is to explore the role of different shade scenarios on predicted stream temperatures locally, and their effects (if any) cumulatively downstream. The need for riparian shade management has been a central conclusion to many watershed investigations. There remains some controversy, however, amongst different researchers over what are the dominant stream heating mechanisms. Most of the research indicates that riparian shade is essential to moderate summertime stream heating. I show results that support this research. I also show, however, that the effects of flow reductions (and thus simulating potential drought conditions) combined with reduced shade can lead to greatly increased stream temperatures. When I first embarked on this research, I considered the role of riparian shade to be the dominant control over stream heating and the component which demanded the most attention when considering model development. It has become apparent from the modeling reported here that considering shade effects alone without consideration of changes in discharge (particularly reductions in flow), only captures part of the stream temperature story. Climate change impacts on stream temperature in California and the Pacific Northwest are likely twofold: (1) increase ambient air temperatures (Webb 1996), and (2) reduced flows (Gleick 2000). As shown in the general sensitivity analysis in chapter 2, and the model results presented in chapters 3 and 4, reductions in flow are likely to have a much greater impact on stream temperature.

Table 1.1   Temperature criteria for salmonids[1]

Criteria	Temperature Range (°C)
Properly functioning	10 – 14 °C
At risk	14 – 15.5 °C (*spawning*)
	14 – 17.8 °C (*migration and rearing*)
Not properly functioning	> 15.5 °C (*spawning*)
	> 17.8 °C (*rearing*)

[1]Source: NMFS (1996), NMFS and USFWS (1997)

Table 1.2   Temperature tolerance ranges for juvenile coho[1]

Behavioral response	Temperature Range (°C)
Optimum rearing habitat in summer:	10 – 15 °C
Habitat unsuitable if temperature exceeds:	20 °C
Growth ceases at temperatures of:	≈20.5 °C
Upper incipient lethal temperatures:	22.9 – 25 °C

[1]Adapted from McMahon (1983)

Table 1.3   Summer stream temperature response to harvesting. East Coast and Japan examples

Location	Treatment	Temperature metric	Change (°C)	Source
Georgia	Clearcut with partial buffer	Avg. Jun-Jul Max	+ 6.7°C	Hewlett and Fortson (1982)
Maryland	Riparian harvest	Avg. summer Max.	+ 4.4 to 7.6°C	Corbett and Spencer (1975)
New Jersey	Riparian herbicide	Avg. Summer Max.	+ 3.3°C	Corbett and Heilman (1975)
North Carolina	Deadened cove vegetation	Avg. Summer Max.	+ 2.2 to 2.8°C	Swift and Messer (1971)
	Complete clearcut	Avg. Summer Max.	+ 2.8 to 3.3°C	
	Understory cut	Avg. Summer Max.	0 to 0.3°C	
Pennsylvania	Riparian harvest	Avg. Summer Max	+ 3.9°C	Lynch et al. (1975)
Pennsylvania	Clearcut with herbicide	Avg. Jun-Jul Max.	+ 10 to 10.5°C	Rishel et al. (1982)
	Commercial clearcut with buffer strip	Avg. Jun-July Max.	+ 0.6 to 1.6°C	
West Virginia	Clearcut	Avg. Summer Max.	+ 4.4°C	Kochenderfer and Aubertin (1975)
Virginia	Riparian vegetation removal.	Avg. Jul Max.	+ 1 to 3.0°C	Pluhowski (1972)
Japan	Clearcut	Daily Max.	+ 4.0°C	Nakamura and Dokai (1989)
Japan	Cleacut	Summer Maximum	+ 6.0°C	Sugimoto et al. (1997)
New Hampshire	Clearcut	Daily Avg. for hottest month	+ 4.0°C	Likens et al (1970)
West Virginia	95% clearcut with thin buffer	Avg. weekly for growing season	+ 1.7°C	Aubertin and Patric (1974)

Table 1.4   Stream temperature response to harvesting. California and Pacific Northwest examples

Location	Treatment	Temperature metric	Change (°C)	Source
Alaska	Clearcut, natural openings	Δ temperature per 100m	+ 0.1 to 1.1°C per 100m	Meehan (1970)
Alsea Watershed, Oregon	Clearcut	Mean of monthly maximum	+ 5.5°C	Harris (1977)
Alsea Watershed, Oregon	Clearcut	Maximum summer Temperature	+ 2°C	Harris (1977)
British Columbia	Clearcut	Maximum difference between observed and predicted daily maximum	+ 5°C	Moore et al. (2005)
British Columbia	Logged	Average Jun-Aug diurnal range	+ 0.5 to 1.8°C	Holtby and Newcombe (1982)
British Columbia	Logged and burned	Average Jun-Aug diurnal range	+ 0.7 to 3.2°C	Holtby and Newcombe (1982)
Oregon Cascades	Clearcut	Avg. Jun-Aug Max.	+ 4.4 to 6.7°C	Levno and Rothacher (1967)
Oregon Cascades	Clearcut and burned	Avg. Jun-Aug Max.	+ 6.7 to 7.8°C	Levno and Rothacher (1967)
Oregon Coast Range	Clearcut	Avg. Jul-Sep Max.	+ 2.8 to 7.8°C	Brown and Krygier (1967)
Oregon Coast Range	Clearcut and burned	Avg. Jul-Aug Max.	+ 9 to 10°C	Brown and Krygier (1970)
Oregon Cascades	Mixed clearcut	Δ Temperature per 100m	+ 0 to 0.7°C per 100m	Brown et al. (1971)
Oregon Cascades	Tractor stripped	Δ Temperature per 100m	+ 11.8°C per 100m	Brown et al. (1971)
Oregon Cascades	25% clearcut, thin buffer	Avg. Daily for hottest 3-weeks	+ 2.5 to 3.0°C	Harr and Fredricksen (1988)
British Columbia	66% clearcut, no buffer	Avg. Daily for July	+ 1.0°C	Feller (1981)
British Columbia (interior)	89% clearcut	Maximum change of the weekly mean temperature	+ 3.8°C	Macdonald et al. (2003)
Alaska	Clearcut	Annual Maximum	+ 10.0°C	Moring (1975)
Alaska	Clearcut	Maximum diurnal Flux	+ 11.2°C	Moring (1975)
Oregon Cascades	Paired study, Clearcut vs undisturbed	Mean Weekly Max.	+ 1.4 to 6.4°C	Johnson and Jones (2000)
Oregon Cascades	Patch cut	Maximum summer temperature	~ 7°C	Johnson and Jones (2000)
Oregon Cascades	Clearcut and burned	Avg. daily Max. for hottest 10-days	+ 6°C	Beschta and Taylor (1988)
Oregon	Burned	Maximum change	+ 3.3 to 19°C	Amaranthus et al (1989)
Northern California	Logged and 'roaded'	Maximum change	+ 3.3 to 9.4°C	Kopperdahl (1971)

Chapter 2

Theory, models, and measurement

2.1 INTRODUCTION

In this chapter I review the basic physics of stream heating and then report the results from a simple sensitivity analysis which quantifies stream temperature dependency on meteorological and stream geometry parameters. Next, I review previous stream temperature models and then summarize the findings of those field studies which have focused on measuring the dominant stream heating mechanisms during the summer time. Based on the sensitivity analysis and reviews of previous work, I show that there is an important need for a process-based model with watershed-scale application which can be readily applied to basins of varying size and which has only limited input data requirements.

2.2 PHYSICS OF STREAM HEATING

The mechanisms responsible for stream heating are well understood, and comprehensive reviews can be found in TVA (1972), Theurer et al. (1984), Deas and Lowney (2000), and Boyd and Kaspar (2003). The temperature of a water body is a function of the total heat energy contained in a discrete volume of water,

$$T_w = \frac{H}{\rho C_p V} \qquad [2.1]$$

where H is heat energy (calories), V is the volume (m^3), C_p is the specific heat capacity of water (1000·cal/kg·K), ρ is water density (1000·kg/m^3), and T_w is water temperature (˚C).

2.2.1 The energy budget

Transfer of heat between the stream and its surrounding environment is comprised of the net heat exchange between the water and the atmosphere and the net heat exchange between the water and the streambed. The heat exchange between the air and the stream is governed by four main processes; heat input from solar radiation, heat loss or gain from longwave radiation, heat loss due to evaporation (latent heat) and convection of heat across the air-water interface (sensible heat). The heat exchange between the streambed and the stream is governed by heat loss or gain from conduction. The net heat flux (typically expressed as an energy flux density with units of W m^{-2} [Deas and Lowney 2000]), q_{net}, is given by,

$$q_{net} \; = \; q_{sw} + q_{atm} + q_b + q_l + q_h + q_g \qquad [2.2]$$

where q_{sw} is the shortwave (or solar) radiation, q_{atm} is downwelling longwave (or atmospheric) radiation, q_b is upwelling long-wave (back, or water surface) radiation, q_l is latent heat flux, q_h is sensible heat flux, and q_g is conduction between the water and the stream bed. When energy gained exceeds energy lost from the system, q_{net} is positive, with a resulting rise in water temperature. The reverse is true when energy leaving the system exceeds energy received.

Shortwave radiation (q_{sw})

Shortwave radiation drives the physical and biological processes at the earth's surface during the day and is the flux in the energy balance most affected by changes in streamside vegetation. Atmospheric constituents (including water vapor, CO_2, ozone, aerosols, dust particles, and so forth) interact with the direct beam radiation scattering or

11

attenuating some fraction, the amount depending on the concentration of gases and particulate matter in the atmosphere and also the distance direct beam radiation travels through the atmosphere (referred to as the path length). The attenuated portion results in heating of the atmosphere or is re-radiated as longwave radiation back out to space or toward the earth's surface. Derivations and full descriptions of the all the empirical formulae necessary to compute the amount of shortwave radiation reaching the stream surface can be found in TVA (1972), Iqbal (1983), or Deas and Lowney (2000).

Longwave radiation (q_{atm} and q_b)

  Longwave radiation is the net black body radiation emitted by the atmosphere incident on the surface and black body radiation emitted by the earth's surface. On average the surface of the earth is warmer than the atmosphere resulting in a net loss of energy from the surface. Over the course of a day the net longwave radiation remains relatively constant compared to the shortwave radiation which peaks at solar noon. The downward flux of longwave radiation from the atmosphere is higher under cloudy conditions and the upward flux from the surface tends to be higher in the summer. Longwave radiation (W m^{-2}) is computed using the general form of the Stefan-Boltzman equation (Deas and Lowney 2000),

$$q_{lw} = \varepsilon \sigma T^4 \qquad [2.3]$$

where ε is emissivity, σ is the Stefan-Boltzmann constant (5.67 x 10^{-8} W m^{-2} K^{-4}), and T is temperature (K). Downwelling long radiation is computed using an empirical relationship described in TVA (1972),

$$q_{atm} = 0.97 \sigma \alpha_0 \left(1 + 0.17 C_L\right) T_a^6 \qquad [2.4]$$

12

where T_a is air temperature (K), C_L is the faction of sky covered by clouds, and α_0 is a proportionality constant. Upwelling longwave radiation is given by (TVA 1972),

$$q_b = -0.97\sigma(T_w + 273.16)^4 \qquad [2.5]$$

where T_w is the water temperature (K).

Latent heat flux (q_l)

Latent heat is the energy associated with phase changes and is not released until the phase change occurs. The rate of heat loss by evaporation is a function of the vapor pressure gradient between the air and water, and is strongly dependent on wind conditions, humidity, and the net radiation flux. The general form of the latent heat flux equation is given by,

$$q_l = \rho_w L_v E_r \qquad [2.6]$$

where ρ_w is water density (kg m^{-3}), L_v is the latent heat of vaporization (J kg^{-1}), and E_r is the evaporation rate (m s^{-1}) and is computed using the general bulk aerodynamic equation (TVA 1972),

$$E_r = \left(e_s(T_w) - e_a\right)f(U) \qquad [2.7]$$

where $f(U)$ is a wind function (mb^{-1} m s^{-1}), $e_s(T_w)$ is the saturated vapor pressure computed at water temperature (mb), and e_a is the measured vapor pressure (mb).

Sensible heat or convective flux (q_h)

Convection is the transfer of heat by moving air which results in a loss of sensible heat and is function of temperature gradient between the air and water, wind conditions

and an exchange coefficient. Sensible heat transfer is typically computed by rearranging

the Bowen's ratio (Deas and Lowney 2000),

$$B = \frac{q_h}{q_l} = C_B \frac{P}{P_{ref}} \left[\frac{T_w - T_a}{e_s(T_w) - e_a} \right]$$ [2.8]

where B is the Bowen's ratio (dimensionless), and q_h and q_l are the sensible and latent

heat fluxes (W/m^2), P is the atmospheric pressure (mb), and P_{ref} is a reference pressure at

mean sea level (mb), T_a and T_w are air and water temperatures respectively (K), and C_B is

a coefficient and equals 0.61 (mb). After rearranging equation [2.8], the sensible heat flux

is given by,

$$q_h = \rho_w L_v E_r f(U) C_B \frac{P}{P_{ref}} (T_a - T_w)$$ [2.9]

where the individual terms are defined above.

Stream bed conduction (q_b)

For some bedrock or coarse grain mantled streambeds, conduction of heat at the

water-substrate boundary can be considerable (Brown 1969, Chen et al. 1998, Sinokrot

and Stefan 1993). Conductance is the transfer of heat due to molecular interactions and

for the case of streambed-stream interactions is dependent on the thermal conductivity of

the streambed and the streambed temperature. The flux of heat between the stream and its

bed is given by (Deas and Lowney 2000),

$$q_g = -K_b \frac{\partial T_b}{\partial z}\bigg|_0$$ [2.10]

where q_g is streambed heat flux (W m^{-1} K^{-1}), K_b is the thermal diffusivity of the bed (m^2 s^{-1}), T_b is the temperature of the bed (K), and z is the vertical distance into the bed (m).

The remaining fluxes, including biochemical and frictional contribute only a small portion of the total heat budget for a stream during the summer months (TVA 1972).

2.2.2 Thermal longitudinal profiles

The implications of stream heating physics and the relative dominance of different fluxes downstream are revealed by the thermal longitudinal profile (stream temperature plotted against downstream distance) for a theoretical stream (Theurer et al. 1984). Here I show three conceptual illustrations of how stream temperature typically evolves downstream and the general controls on that evolution based on the physics reviewed above and published results (Gu et al. 1999, Deas and Lowney 2000).

Figure 2.1 illustrates the main features of a thermal longitudinal profile which, for groundwater-fed streams, demonstrates a characteristic asymptotic form (Theurer et al. 1984, Tague et al. 2007). Temperature at first increases rapidly then approaches an equilibrium stream temperature asymptotically. The downstream distance to where the temperature tends to level off I refer to as the 'transient phase' (shown on graph). The distance-temperature curve levels off when stream temperature converges to an equilibrium temperature (where the heat energy flux is zero) which is determined by meteorological conditions (Gu et al. 1999, Deas and Lowney 2000). The initial temperature reflects the temperature of groundwater feeding into a stream. Increasing downstream distance along a stream generally equates to increasing flow depth and hence

increasing thermal inertia. As water volume increases, more heat energy is required to warm a stream.

The difference in thermal long profiles between shaded and unshaded streams demonstrates the influence of available heat energy and, indirectly, the importance of discharge. Figure 2.2(a) and 2.2(b) shows how respectively the diurnal (maximum, mean, and minimum) thermal profiles for a hypothetical shaded stream and unshaded stream would differ. The two figures demonstrate three important differences. First, the daily maximum equilibrium temperature (the temperature of which is set by meteorology alone) is higher for unshaded profiles because unshaded streams received more incoming shortwave radiation. Second, the diurnal range is significantly larger for unshaded streams (particularly higher up in the profile) because unshaded streams receive more direct shortwave radiation during the day but experience more longwave radiation loss at night. By comparison, shaded streams limit nighttime longwave radiation emissions and also limit daytime shortwave radiation receipt at the stream surface. Third, the length of the transient phase (or the equilibrium temperature convergence distance) is much shorter for unshaded reaches.

Figure 2.2(b) also shows that increasing (or decreasing) discharge has two primary effects. Increasing discharge reduces the amplitude of the diurnal temperature range (Gu et al. (1998)) and while also extending the transient phase distance (Gu et al. 1999). Decreasing discharge operates in reverse for both effects.

2.3 GENERAL STREAM TEMPERATURE SENSITIVITY ANALYSIS

Stream temperature sensitivity analyses have generally focused on the sensitivity of specific models and model assumptions and the sensitivity of temperature predictions generated by those models (e.g., Adams and Sullivan 1989, Bartholow 1989, Gu et al. 2002, Sansone and Lettenmaier 2001, Mattax and Quigley 1989). Here I use the heat budget equations used in the SNTEMP model (Theurer et al. 1984) and applied by Railsback and Jackson (2004) to perform a general assessment of stream temperature sensitivity for a fully mixed, static water body, the volume of which is given by its channel depth and surface area.

The form of Equation [2.1] suggests a simple strategy for assessing stream temperature sensitivity, whereby a new water temperature, $newT_w$ (ºC), is found by computing the total heat content, q_{total}, of a volume of water, V (m^3). Thus, the new water temperature is given by,

$$new\,T_w\left(°C\right) = \frac{q_{total}}{\alpha V} \tag{2.11}$$

Where α, the specific heat capacity of water (J m^{-3} ºC^{-1}), is constant (4.186 x 10^6). The total heat content includes changes in heat energy flux, Δq (J). This energy change is calculated as the sum of five fluxes: incoming shortwave radiation (q_{sw}), upwelling longwave radiation ($q_{lw\uparrow}$), downwelling longwave radiation ($q_{lw\downarrow}$), latent heat flux (q_l), and convective heat flux (q_h),

$$\Delta q = q_{net} \cdot A \cdot t \tag{2.12}$$

where q_{net} (J m^{-2} sec^{-1}) is the sum of the five fluxes, A is the surface area of the water body (m^2), and t is time (seconds).

17

The water body's new total heat content, q_{total} (J sec^{-1}), is therefore,

$$q_{total} = (V \cdot T_w \cdot \alpha) + \Delta q \qquad [2.13]$$

where V is the volume of the water body (m^3), T_w (°C), is the initial water temperature.

The volume term, V, is the surface area of a river reach times its depth. Railsback and Jackson (2004) have implemented a stream temperature model based on Equation [2.11] **Error! Reference source not found.Error! Reference source not found.**which they included as part of the EcoSwarm software suite (Railsback and Jackson 2004). In their model, they compute the change in heat energy as the sum of five fluxes listed above (Appendix B). The steady-state heat flux equations are derived from the Stream Network Temperature Model (SNTEMP, Theurer et al. [1984]) and are very similar to flux equations used in several other environmental physics and stream temperature applications (Monteith and Unsworth 1990, Dingman 2002, Boyd and Kaspar 2003, LeBlanc et al. 1997, Sansone and Lettanmeier 2001).

As with Railsback and Jackson's (2004) implementation, hydrology is treated very simply – water is represented as a static volume of fluid (i.e. we will not look at the thermal evolution along a stream profile). To parameterize the model and make it relevant to the application in the next chapter, I use the width (Figure 2.3[a]) and depth (Figure 2.3[b]) relationships measured during low-flow in the South Fork Eel River basin in Northern California. The length (reach length) dimension (to get volume and surface area) is assigned a constant value of 25-meters. The simple depiction of hydrology used here requires only 5 parameters (reach length, width, depth, latitude, and initial water temperature) for specified air temperature, relative humidity, and wind speed.

The new water temperature is calculated by computing the change in heat energy for a given volume of water with a prescribed initial temperature (see above). The equations for the five heat fluxes are shown in full in Appendix B. Importantly, the calculated change in water temperature is a function of the change in total heat flux which is a function of area and the volume of water. Therefore, because surface area appears in both the calculation of total heat flux and flow volume, the most important stream geometric dimension is depth. Consequently I report predicted temperature sensitivity due to changes in water volume solely in terms of variations in depth. Also because the volume of water is static, 'lake-type' equations are used for both evaporation and convection heat fluxes (Railsback and Jackson 2004, Theurer et al. 1984) (Appendix B). As with Railsback and Jackson, I ignore the heat flux contribution from streambed conduction. Typically heat flux in and out of the bed contributes to less than 5% of the total heat flux (Theurer et al. 1984, Bartholow 1989, Bartholow 2000), although for small, bedrock channels, heat flux into the bed can be an important heat sink during the day (Johnson 2004, Brown 1969).

The change in predicted temperature is reported for incoming shortwave radiation for a timestep of one hour. Insolation values range from 0 to 400 ($J\ m^{-2}\ s^{-1}$), encompassing the full range of daily averaged shortwave radiation for mid-latitude regions (Boyd and Kaspar 2003, Deas and Lowney 2000). Temperature sensitivity after individually varying, (a) wind speed, (b) relative humidity, (c) air temperature, and (d) initial water temperature, is shown in Figures 2.4a to 2.4d respectively. The water depth used in all four cases corresponds to 2 cm (the low-flow depth associated with a drainage area of 1 km^2 for the South Fork Eel River, Figure 2.3b). Predicted temperatures are very

sensitive to the initial water temperature (Figure 2.4d, moderately sensitive to air

temperature (Figure 2.4c), and insensitive to wind speed and relative humidity (Figures

2.4a and 2.4b). In all four cases, predicted temperatures respond linearly to adjustments

in the individual parameters. Results for varying atmospheric pressure (which appears in

the convective heat flux term, Appendix B) are not shown. Predicted temperatures are

completely insensitive to adjustments in this parameter.

Temperature sensitivity to incoming solar radiation and low flow depth are shown

in Figures 2.5(a) 2.5(b) respectively. Water temperature varies linearly with incoming

solar radiation, but inversely with water depth. Figure 2.5a shows the expected linear

variations in temperature with shortwave radiation. This rate of temperature increase

varies significantly as a function of low flow depth. Figure 2.5b shows the inverse

relationship (i.e. nonlinear) relationship between stream temperature and low flow depth

against water temperature for the full range of incoming shortwave radiation values.

Simply put, very shallow water heats up much more in one hour than does deep water.

This simple observation has important implications throughout this study.

The results from this analysis corroborate results from other empirical and

modeling studies. Moore et al. (1999) assessed shade affects for shallow versus deep

artificial tubs and showed that temperatures in exposed, shallow tubs responded much

more rapidly and reached higher temperatures than shaded tubs. They concluded that

shade strongly affects the rate of heating or cooling and that depth strongly affects both.

They also showed that air temperature was of minor importance (Moore et al. 1999). Gu

et al. (2002) assessed the sensitivity of river temperature to discharge and showed that of

all the parameters tested, only discharge (presumably acting through the depth

dependency) showed a non-linear relationship with predicted river temperature. Adams and Sullivan (1989) and Sinokrot and Gulliver (2000) also showed the strong depth-dependency of predicted stream temperature in their models.

Two sensitivity analyses performed using the Stream Network Temperature Model (SNTEMP) and the Stream Segment Temperature Model (SSTEMP), both of which applied the steady-heat flux equations applied here (Bartholow 1989, Bartholow 2000) showed that predicted temperatures were most sensitive to air temperature, and rather less sensitive to solar radiation. Importantly, however, the flows used in both studies were large. For the SNTEMP sensitivity analysis (Bartholow 1989), the flows ranged from 0.28 m^3/s to 0.56 m^3/s. While for the SSTEMP sensitivity analysis, flows were varied from 0.425 m^3/s to 0.51 m^3/s. Comparison of these flows with flows recorded at USGS gages within the South Fork Eel River (Table 2.1) (my selected study watershed) show that they are associated with locations draining large areas. The Weott USGS gage in Bull Creek, for example, drains an area of 71 km^2, and the average 7-day for July 31st, recorded between 1961-2007, is just 0.14 m^3/s. On the Eel, Bartholow's modeled flows (Bartholow 1989, 2000) are crossed at rivers draining over 600 km^2 (Table 2.1). In such cases, it would seem likely that the river temperature would be far along its thermal profile evolution and close to equilibrium (e.g. Figure 2.1). Hence, at these downstream locations, air temperature most likely becomes the chief control over stream temperature. Large thermal inertia effects due to high flow depth also means that water temperature responds much more slowly to incoming shortwave radiation. Furthermore, these channels are sufficiently wide that either topographic or riparian

shading effects are minimal. The model I propose here that explicitly models shading effects is most relevant to headwater streams.

The results from this analysis indicate that stream temperature is sensitive to incoming shortwave radiation, inversely dependent on flow depth, and highly sensitive to the combination of both at shallow water depths (Figure 2.5b). At shallow depths, even moderate heat loading (e.g. 200 W m^{-2}) results in significant increases in water temperature.

2.4 PREVIOUS WORK ON STREAM TEMPERATURE

2.4.1 Stream temperature modeling

Early work on water temperature prediction focused primarily on modeling effluent discharge temperatures from reservoirs and other managed water systems (Raphael 1962, Brown 1969, Morse 1970). More recent temperature models focused on the (mostly deleterious) impacts of elevated water temperatures on aquatic ecosystems (e.g. Beschta et al. 1987, Deas and Lowney 2000, Bartholow 2000, Boyd and Kaspar 2003, Sansone and Lettenmaier 2001, Sridhar et al. 2004).

Stream temperature models can be broadly classified into empirical and mechanistically-based schemes (Figure 2.6). Empirical models are typically statistical relationships between one or more basin attributes and water temperature. The simplest and most commonly applied empirical approach is regression analysis. Typically air temperature is averaged over some time period and regressed against water temperature, averaged over the same period (e.g., Stefan and Preud'homme 1993, Smith 1981, Mitchell 1999). Empirical approaches take advantage of the strong correlative relationship between water temperature and various air temperature metrics, and the fact that air temperature is a commonly measured metric as opposed to stream temperature. Empirical models have several shortcomings that limit their utility and applicability. These include: (a) the relationship(s) are only applicable for the range of data used to compute the regression equation, (b) the relationship is non-transferable outside of the region where the data were collected, (c) no scenario-testing functionality, (d) the relationship(s) offer no insight(s) into causal mechanisms, and (e) the temporal resolution

of the temperature prediction is often long (for example, average monthly water temperatures).

Mechanistically-based water temperature models have two primary components: (1) a hydrodynamic and hydrological (flow) component, and (2) a heat flux and transport component (Deas and Lowney 2000). Most mechanistic models assume that the water column is fully mixed in both the transverse and vertical directions and therefore adopt a 1-D model structure (e.g. Theurer et al. 1984, Theurer et al. 1985, Gu et al. 1998, Boyd and Kaspar 2003). Accounting for both the hydrodynamic and the heat flux components is necessary for characterizing the thermal regime of rivers, and most of the effort in stream temperature modeling is typically devoted to quantifying the various fluxes contributing to heat transfer processes (Deas and Lowney 2000).

Simple reach-based mechanistic models

Simple deterministic schemes such as the Brown equation (Brown 1969, 1970, 1972, 1983) have been widely applied to assess stream temperature changes in response to timber harvesting (e.g. Cafferata 1990). The Brown equation predicts the temperature change, T_w, as the ratio of the energy received at the stream surface and the flow volume,

$$T_w = \left(\frac{\sum H \cdot A}{Q} \right) 0.000267 \qquad [2.14]$$

where T_w is the predicted temperature change (°F), H is the rate of heat absorbed by the stream in units of Btu/ft^2 min^{-1}, A is the surface area (ft^2), Q is the discharge (cfs), and the value 0.000267, is a constant converting discharge from cfs to lbs/minute. The advantages of a simple, reach-based mechanistic scheme such as the Brown equation is

24

that it is easily applied, requires little input data, and is transferable to other locations.

The disadvantages include, (a) the assumption that attributes are uniform for the entire length of the reach and hence the model is only applicable for comparatively short reaches (less than 500 meters), (b) the requirement of *reach-averaged* shade measurements neglecting the spatial heterogeneity of shade (consequently the model performs less well in fully-forested reaches), (c) the relationship has no facility to permit scenario testing of various shade levels along a reach, and (d) the model doesn't permit identification of causal mechanisms if the primary assumption (the amount of direct radiation striking the stream surface) doesn't hold.

Fully-mechanistic, reach-based models

Several models attempt to model the full physics of stream heating for single or a chain of connected reaches. The Stream Segment Model (*SSTEMP*) is the reach-based version of *SNTEMP,* the Stream Network Temperature Model (Theurer et al, 1984, Bartholow 2001). *SSTEMP* is a steady-state, 1-D heat balance model that predicts water temperature for a single time-step for an individual reach. *Temp-86* (Beschta and Weatherred 1984) is an energy budget model driven by solar radiation, the primary energy source. Significant effort was invested in accurately characterizing shading geometry for the modeled reach allowing evaluation of the effects of shade on stream temperature. The model predicts hourly temperatures for a given day. The *GIS-SRTEMP* model (Sansone and Lettenmaier 2001, Sridhar et al. 2004) couples a solar flux model and a 1-D energy balance model to predict 'worst-case' reach water temperatures (mean annual maximums) for low-flow conditions. *HeatSource* (Boyd 1996, Boyd and Kaspar

2003) is a reach-based analytical temperature scheme that models all the thermodynamic and hydrodynamic processes responsible for stream heating. It is also dynamic and can generate maximum and minimum temperature predictions. Both *HeatSource* and *GIS-STRTEMP* represent advances on previous reach-based models by taking advantage of the widespread availability of GIS, large georeferenced databases, and remotely sensed and aerial photographic information to improve the physical representation of channel reach-environment.

Physically-distributed, mechanistically-based models

Physically-based, basin-scale models apply governing equations for heat and mass transfer to predict water temperatures for entire channel networks and for different flow regimes and climate conditions. These models purport to capture the full physics of the thermal regime and hence are, theoretically, applicable to a broad range of channel systems and predict water temperatures for any time interval. Several groups (Raphael 1962, Morse 1970, Rutherford et al. 1993, Rutherford et al. 1997, St-Hilaire et al 2000) have developed stream temperature prediction models using well understood energy budget principles. The Stream Network temperature model (*SNTEMP*, Theurer et al. 1984) has been widely used to predict longitudinal stream temperature changes as a result of alterations in flow regimes, dam release, and impacts of canopy modification (Gaffield et al. 2005, Theurer et al. 1984, Mattax and Quigley 1989, Bartholow 1989). The model is a steady-state 1-D heat transport model that predicts daily mean and maximum temperatures. The Hydrological Simulation Program-Fortran (*HSPF*, Bicknell et al. 1997) simulates the hydrologic and associated water quality processes for land surfaces

26

and in streams. The model has been applied to assess the effects of land-use changes, reservoir operations, point or nonpoint source treatment alternatives, and so forth (e.g., Taylor 1998). Chen at al. (1998(a) and 1998(b)) developed shade and streambed conduction sub-models and incorporated them within *HSPF* to explore the interaction between riparian forest management and stream temperature. The updated model was tested in the Upper Grande Ronde basin in Oregon. The study highlighted the importance of collecting accurate riparian vegetation data. In the study, shade parameters were averaged over 1000-meter segments, and thus neglecting potentially important finer resolution heterogeneities in the riparian shading regime

Although these models are significant advances over earlier less mechanistic approaches, they also have considerable input data requirements. The model complexity and data demands make them less appropriate for broad practical application and less able to delineate benefits of specific land management practices (e.g. riparian forest recovery). To my knowledge, none of the spatially-explicit, physically-based temperature models have been used to quantify watershed-scale, cumulative downstream temperature effects as a result of upstream (or headwater) shade manipulation. Thermal infrared imaging techniques have been increasingly applied to watershed-scale stream temperature issues (Handcock et al. 2006, Beschta et al. 2003), but these data acquisition approaches offer limited insight into stream temperature response to alternative riparian shade strategies.

2.4.2 Stream temperature measurement

Several studies have sought to identify the dominant fluxes controlling summertime stream heating in mid-latitude regions. Brown (1969) measured the various heat fluxes over the course of a single day for two small headwater streams – one shaded and the other unshaded – in coastal Oregon. The peak shortwave flux was more than an order of magnitude larger for the open channel compared to the shaded stream, while the total shortwave radiation receipt at the open channel was approximately 30 times greater than that received for the shaded stream. Johnson (2004) measured the various heat fluxes for an unshaded and shaded stream in the H.J. Andrews Experimental Forest in Oregon. She showed that at mid-day, the total available heat energy was more than three times larger for the unshaded stream versus the shaded stream (Johnson 2004). Monteith and Unsworth (1990) estimated that direct shortwave radiation during summer months contributes up to 80% of the total solar radiation budget. Moore et al. (2005) summarized research from several studies which showed reductions in shortwave radiation receipt beneath riparian forest canopy. They reported direct shortwave radiation reductions of up to 90% below dense canopy (Brosofske et al. 1997, Chen et al. 1995) and reductions of 75% beneath more open stands (Spittlehouse et al. 2004). Brosofske et al. (1997) assessed changes in mean daily solar radiation within buffer strips and showed that following timber harvesting, shortwave radiation receipt at the stream surface increased approximately 200%, even when isolated trees were left in place. A heat budget analysis performed by Sinokrot and Stefan (1993) showed that sensible heat transfers comprise only a small portion of the heat fluxes influencing stream temperature. Several studies have shown that riparian vegetation is important in controlling the amount of shortwave

28

radiation reaching the stream surface. For example Oke (1987) estimated that riparian canopy transmits less than 20% of incident solar radiation but can be as low as 5%.

Two studies conducted by Webb and Zhang (1997, 2004) measured the spatial and seasonal variability of heat energy fluxes for several streams of different sizes and riparian conditions in Southwest England. During summer months, heat inputs were dominated by shortwave radiation, especially for small, exposed upland channels. For most sites heat loss was attributed to upwelling longwave radiation. The two studies highlight the importance of riparian vegetation and topographic shade, not just in reducing the amount of direct solar receipt at the stream surface, but also in suppressing longwave heat dissipation by evaporation and convection. After upwelling longwave radiation, evaporation was the next most important heat loss flux during summer months (Webb and Zhang 1997, 2004). Highest losses were recorded for small, exposed upland streams where higher wind velocities prevailed. Their 2004 study (Webb and Zhang 2004) showed that shortwave radiation accounted for more than 70% of the heat energy in exposed reaches, 63% in deciduous forest reaches, and 52% in coniferous forest reaches. Webb and Zhang's 2004 study demonstrates that forested reaches significantly limit longwave, evaporative, and sensible heat losses. The earlier study by Beschta et al. (1987) supports Webb and Zhang's conclusions regarding the role of riparian canopy in reducing evaporative and sensible heat fluxes. Beschta et al. indicate that heat dissipation from these two fluxes is small because both the temperature and vapor pressure gradients at the air-water interface below full riparian canopy, are low.

Brown (1969) showed that heat loss through the stream bed can be significant for shallow, bedrock channels. Johnson and Jones (2000), and Johnson (2004) showed that

streambed heat loss for small, gravel-bedded streams can be important. The two studies suggested that hyporheic exchange in gravel-bedded streams can be important in increasing residence time and hence conductive heat exchange. The longer hydraulic residence times resulted in increased heat losses through the bed (Johnson and Jones 2000, Johnson 2004). Both studies showed that bedrock reaches have significant summer diurnal temperature fluctuations compared to much narrower temperature fluctuations for gravel-bedded reaches.

The general conclusion drawn from these studies is that during the summer months, direct incoming solar radiation dominates the heat energy balance and that near-stream riparian vegetation, especially for smaller streams, blocks much or most of the direct incoming radiation from reaching the stream surface. At the scale of individual stream reaches, other mechanisms may exert stronger controls over local stream temperatures (e.g streambed conduction, hyporheic exchange, point-source contributions of cooler (springs) or warmer (geothermal sources) water). But at the scale of entire watersheds, most empirical research suggests that incoming shortwave radiation, especially the direct shortwave contribution, is the most important heat flux.

2.5 CONCLUSION

Based on the results of the general sensitivity analysis and from the previous work modeling and measuring stream temperature, it is apparent that for small streams direct solar radiation is the dominant mechanism determining summertime stream heating and that riparian shade is the most important control on the amount of direct shortwave radiation reaching the stream surface. Locally, other fluxes may dominate where favorable meteorological, channel, hydrologic, or vegetation conditions prevail. However, at the scale of entire watersheds, the majority of empirical research indicates that direct solar radiation is the dominant summertime stream heating mechanism. The strong sensitivity of stream temperature to the combination of incoming solar radiation and shallow water depths argues for a model which accurately represents the important components of the energy flux term (H) in Equation [2.1],and the hydrology term (V) in [2.1]. None of the existing watershed stream temperature models captured these basic requirements. For large-scale applications, the existing physically-based models have excessive input measured data requirements while still generating temperature predictions at overly-coarse spatial resolutions (reach lengths > 100-meters). Based on this information, it was determined that the essential components of summertime stream heating could be captured in a steady-state model where solar insolation dominates the heat budget fluxes and hydrology and stream geometry are captured in a model which assumes linearity in groundwater inflow rates. In the next chapter I describe the development and application of this model.

Table 2.1   Lowflow discharges recorded at several USGS gages within the South Fork Eel River basin, Northern.

Basin / Year	Drainage area at gage (km^2)	7-day mean daily discharge for the week-ending July 31st (m^3/sec)						
		Avg. 1968 to 1974	Avg. 1958 to 1974	Avg. 1961 to 2007[1]	1994	1997	Avg. 1994 to 1996	Avg. 2000 to 2001
Bull Creek (Weott gage), CA	71	—	—	0.136 m^3/sec	—	—	—	—
Elder Creek, CA	17	0.0452 m^3/sec	—	—	—	0.0481 m^3/sec	—	—
Tenmile Creek (Laytonville gage), CA	130	0.04 m^3/sec	0.05 m^3/sec	—	—	—	—	—
Mainstem South Fork Eel River (at Leggett), CA	642	—	—	—	0.64 m^3/sec	—	—	0.82 m^3/sec
Rock Creek, Oregon	249	—	—	—	—	—	1.3 m^3/sec	—

[1]Minimum 7-day mean daily discharge for this period was 0.031 m^3 s^{-1}, while maximum 7-day mean daily discharge for this period was 0.44 m^3 s^{-1}.

Figure 2.1   Characteristic asymptotic form of a thermal longitudinal profile
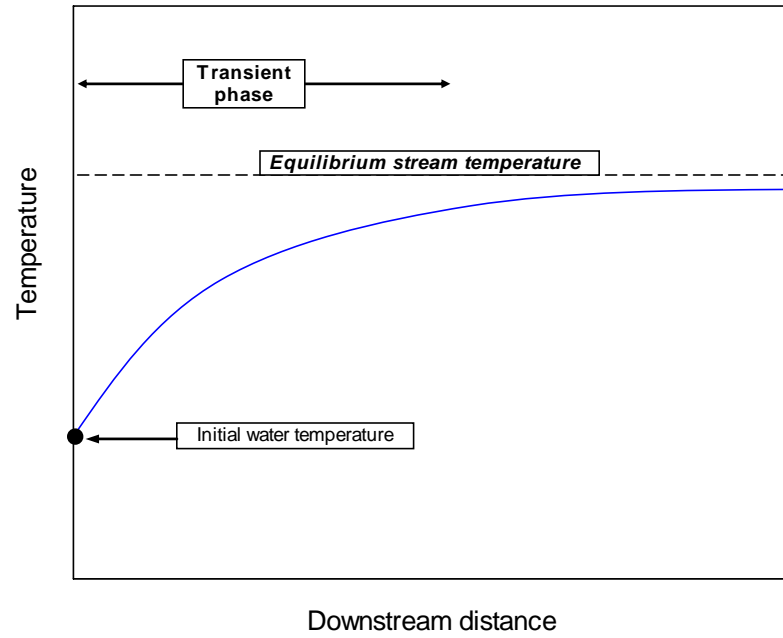
Figure 2.2   Characteristic thermal longitudinal profiles for, (a) shaded streams, and (b) unshaded streams

(a) Shaded longitudinal thermal profile
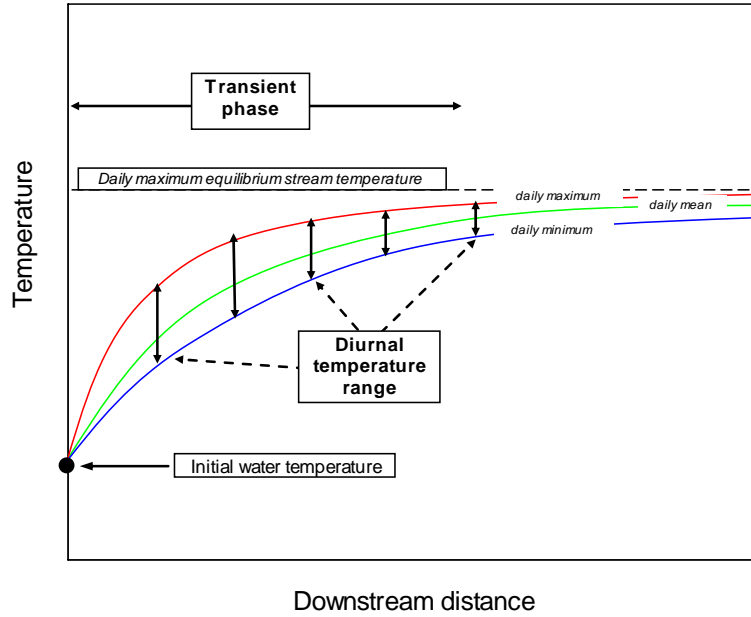
(b) Unshaded longitudinal thermal profile
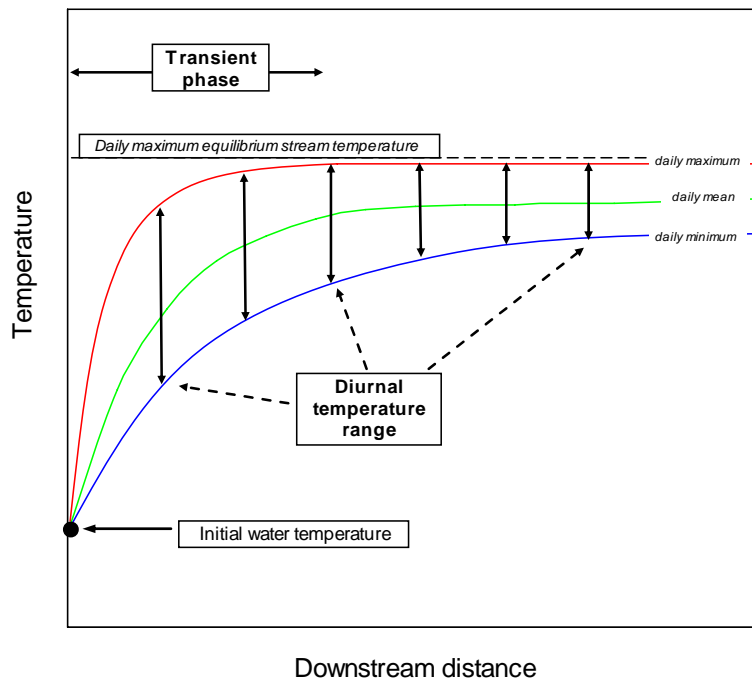
Figure 2.3   South Fork Eel hydraulic geometry[1]: (a) Drainage area versus lowflow width, and (b) drainage area versus lowflow depth.

(a) Drainage area versus lowflow width
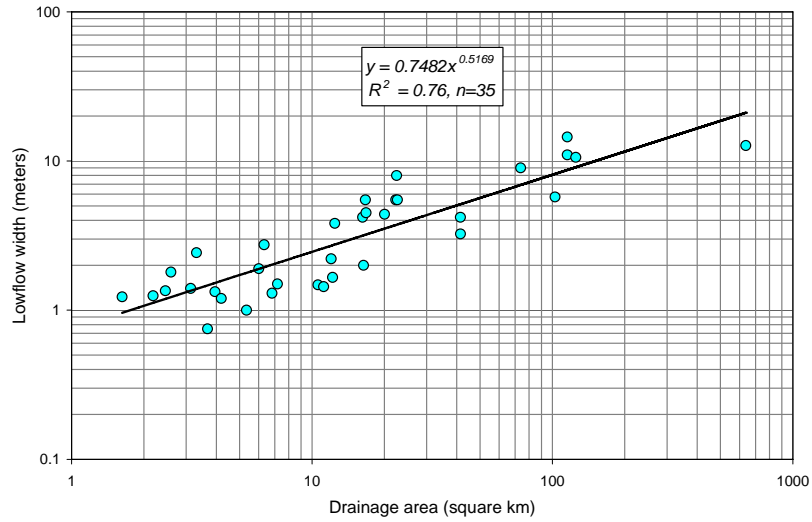
(b) Drainage area versus lowflow depth
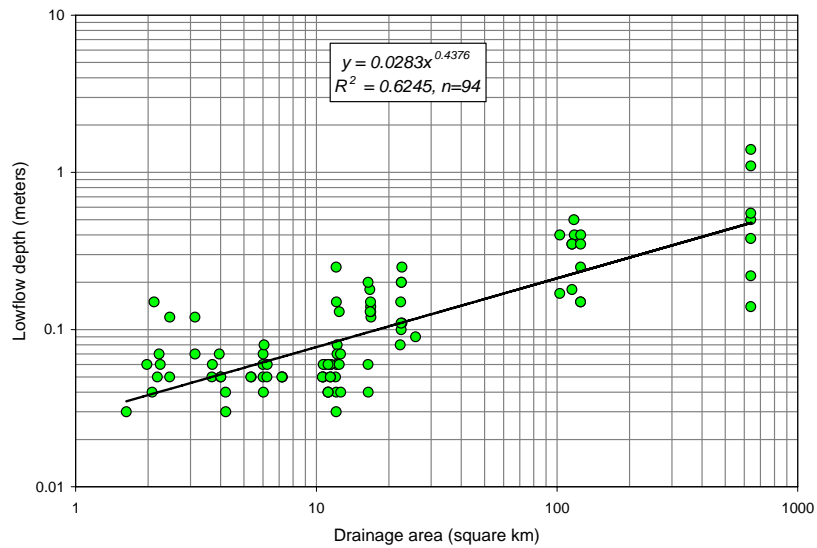
[1]Source: Stillwater Sciences unpublished data (1998)

Figure 2.4   Sensitivity of predicted water temperature to: (a) wind speed, (b) relative humidity, (c) air temperature, and (d) initial water temperature*.

(a) Sensitivity of predicted temperature to wind speed
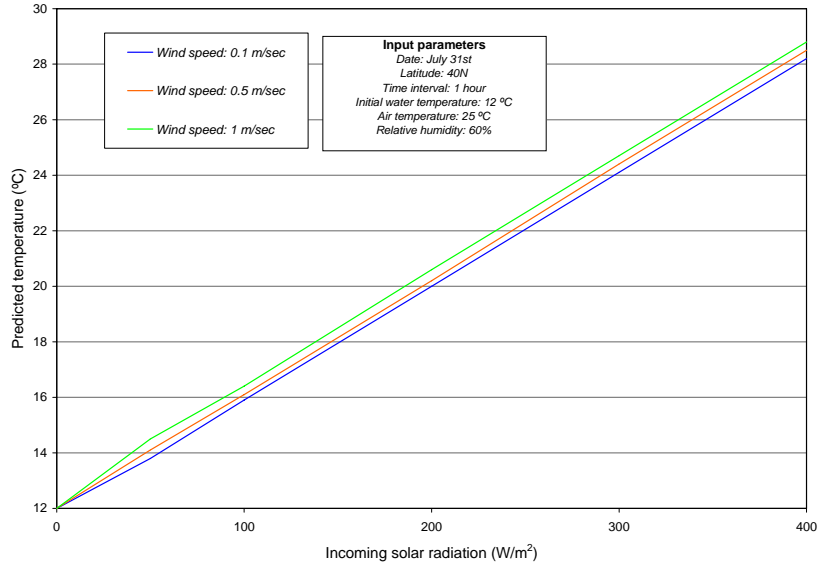
(b) Sensitivity of predicted temperature to relative humidity
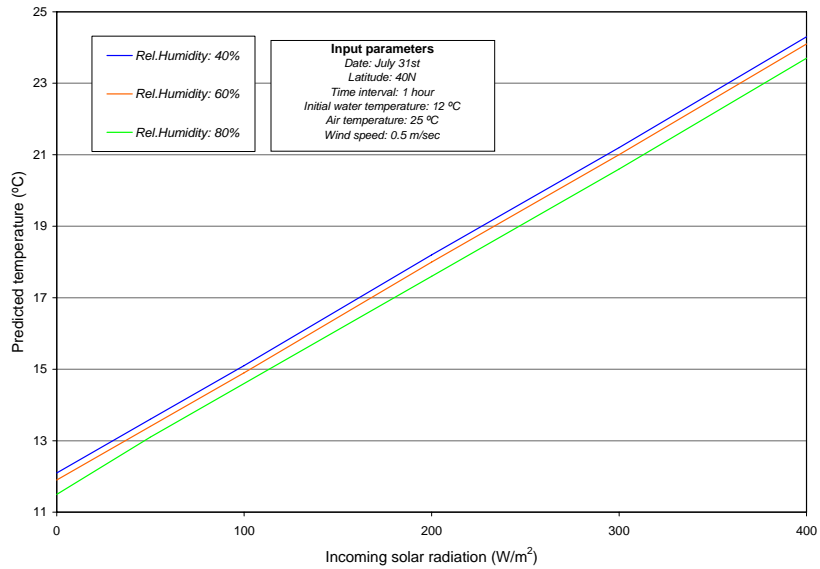
*Lowflow width and depth dimensions calculated using the relationships shown in Figure 2.5 for a drainage area of 1 km^2

(c) Sensitivity of predicted temperature to air temperature
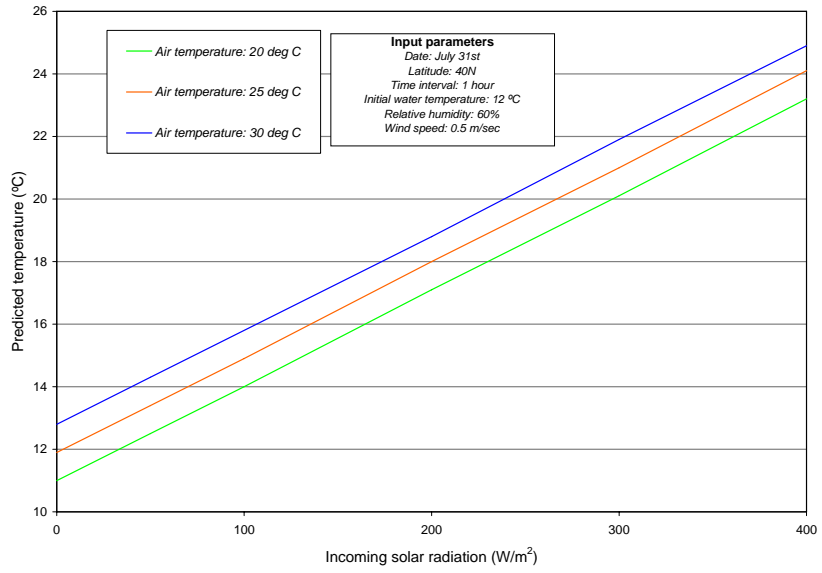
(d) Sensitivity of predicted temperature to initial water temperature
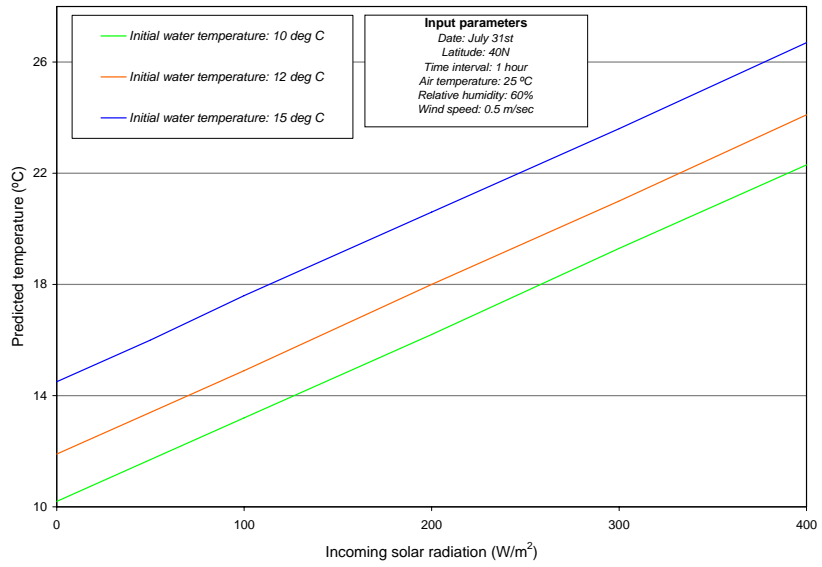
Figure 2.5   Sensitivity of water temperature to incoming shortwave radiation and depth.

(a) Sensitivity of water temperature to incoming shortwave radiation
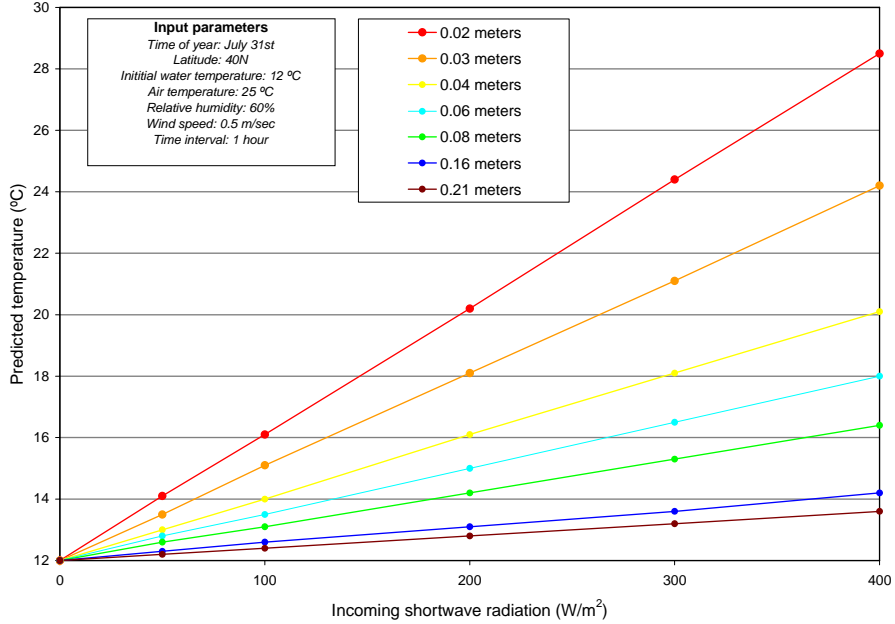
(b) Sensitivity of water temperature to depth
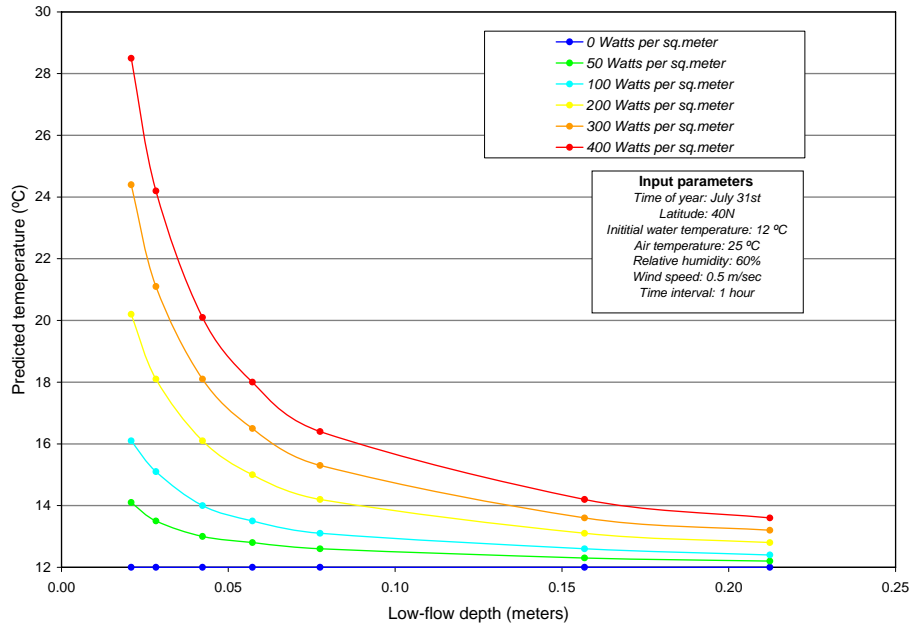
Figure 2.6   Stream temperature model classification
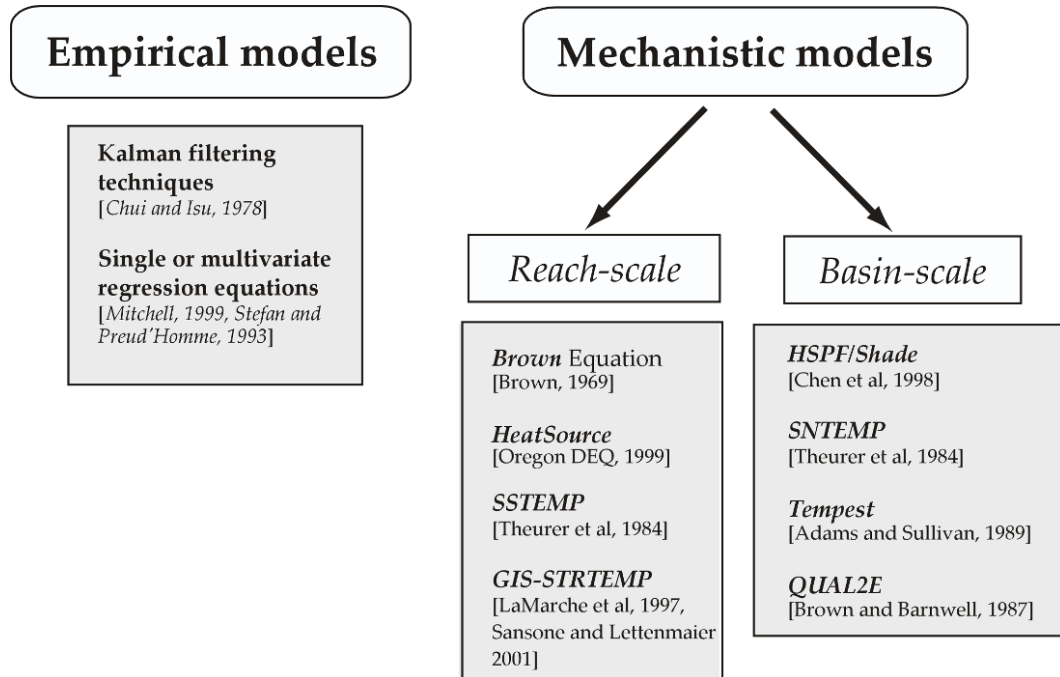
Chapter 3

Model development and application

3.1 INTRODUCTION

In this chapter I describe the development and application of a physically-based, large-area assessment stream temperature model, *BasinTemp*. The model is designed to predict stream temperatures for the hottest part of the year based on the essential physics responsible for summertime stream heating. I then apply the model to three watersheds located within the South Fork Eel basin in Northern California. For the simplifying assumptions embedded in the model and the limit input data necessary to run the model, *BasinTemp,* performs satisfactorily for each of the three watersheds. Finally I explore the sensitivity of model predictions, particularly to adjustments in flow which was shown in the previous chapter to be an important control over stream temperatures, particularly for smaller streams.

3.2 MODEL DEVELOPMENT

The stream temperature model, BasinTemp, is a one-dimensional basin-scale model that couples a GIS-based solar radiation model and a steady-state numerical heat balance model to predict water temperatures for the hottest time of the year. The model assumes that direct shortwave radiation receipt at the stream surface is the most important stream heating mechanism during the summer months in mid-latitude regions. Terrain shade and, most importantly, riparian vegetation shade, regulate the amount of shortwave

receipt at the stream surface and are therefore important controls moderating summertime stream heating. Figure 3.1 illustrates the main features of the model and the various processing steps. The model consists of: a GIS pre-processor which assembles vegetation, channel, and topographic data used in the solar radiation model; the solar radiation model which uses the tree height model assembled in the GIS to generate daily averaged, spatially explicit shortwave radiation predictions; a one-dimensional numerical heat balance model and hydrology model which inputs solar radiation predictions and then computes stream temperatures for every reach segment throughout the basin; and an optimization routine which uses locally measured temperature data to improve the temperature predictions.

3.2.1 GIS, solar radiation, and tree height model

The GIS pre-processor assembles the relevant topographic, channel, and vegetation information necessary to accurately characterize riparian geometry. The tree height model uses existing topographic data and vegetation information. A vector-based stream channel network is discretized into uniform segment lengths, where the length of each segment is scaled to match the resolution of the source elevation and vegetation data. Low-flow channel geometry is computed using a power relationship between GIS-extracted drainage area and field-measured low-flow widths for the basin of interest. Shortwave solar radiation predictions are generated using the Image Processing Workbench (Frew 1990, Dozier and Frew 1990, Marks et al. 1999). The Image Processing Workbench (IPW) includes several routines which compute spatially

distributed solar radiation for a specified time of year and a given latitude. The IPW routine, Topquad, is a sophisticated radiative transfer algorithm which computes the contributions from direct, diffuse, and reflected (direct and diffuse) radiation to the total short wave radiation flux. Topquad has been applied to a variety of physical environments for different meteorological conditions and for different times of the year (Frew 1990, Dozier and Frew 1990, Dubayah 1994, Dubayah 1991, Dubayah et al 1990, Marks et al. 1999).

IPW applies the two-stream approximation (Meador and Weaver 1980) to the computation of the shortwave radiation. The two-stream simplification provides a rapid approximation of radiative transfer processes by computing only the upward and downward fluxes and thus avoiding the formidable and time-consuming computation of the full angular distribution of scattered radiation. Scattering is strictly partitioned into a forward hemisphere and a backward hemisphere. All radiation propagating down toward the surface is aggregated into a single downward flux or 'stream' of energy. The stream combines the direct beam and any diffuse radiation scattered towards the Earth's surface (Dubayah 1991). All diffuse radiation propagating upward is combined with the upwelling flux. The general form of the approximation is given by two differential equations,

$$\frac{dF_\uparrow(\tau)}{d\tau} = \gamma_1 F_\uparrow(\tau) - \gamma_2 F_\downarrow(\tau) - \gamma_3 \omega_0 S_0 e^{-\tau/\mu_0} \qquad [3.1]$$

And,

$$\frac{dF_\downarrow(\tau)}{d\tau} = \gamma_2 F_\uparrow(\tau) - \gamma_1 F_\downarrow(\tau) - \gamma_4 \omega_0 S_0 e^{-\tau/\mu_0} \qquad [3.2]$$

where $F\uparrow$ and $F\downarrow$ are upward and downward fluxes, S_0 is the exoatmospheric flux incident

at angle $cos^{-1}\mu_0$; ω_0 is the single-scattering albedo, τ is the optical depth (see Appendix

A); γ is a function of g, the scattering asymmetry factor. The γ values parameterize the

scattering phase function (see Appendix A). Terrain effects on insolation can be

significant where relief, aspect, and hillslope gradient modify the amount of solar

insolation arriving at the earth's surface (Dubayah 1991, Dubayah et al 1990). Topquad

computes shortwave transmittance of radiation for a flat surface and then calculates the

direct irradiance as a function of slope, aspect, and solar altitude and azimuth. Shortwave

radiation reflected from terrain or vegetation can also contributes to the total shortwave

radiation budget and is third shortwave component computed by Topquad. The total

irradiance (F) on a slope is given by,

$$F = \left[V_d \bar{F}_\downarrow (\tau_0) + C_t \bar{F}_\uparrow (\tau_0) + \mu_s S_0 e^{-\tau_0/\mu_0} \right] \qquad [3.3]$$

where the three terms on the right hand side of Equation [3.3] are the diffuse flux,

reflected flux, and the direct flux respectively. V_d is the sky view factor, μ_0 is the cosine

of the solar illumination angle, μ_s is the cosine of the solar illumination angle on a slope,

S_0 is the exoatmospheric parallel beam flux, and C_t is a terrain irradiance term which

accounts for the anisotropic and geometric affects and is given by,

$$C_t = \frac{1 + \cos S}{2} - V_d \qquad [3.4]$$

where S is the terrain slope angle and the other terms are defined above.

Topquad computes daily averaged, spectrally integrated shortwave radiation for

basins of varying sizes for a specific day and latitude. The radiative transfer parameters,

optical depth (τ), the single scattering albedo (ω), and the scattering asymmetry factor (γ),

characterize transmission properties of the atmosphere. All three parameters were assigned values suggested by the developers of the Topquad algorithm (see Section 3.4). Table 3.1 list the full range of possible values for these parameters, and the values used in this study. These values may be obtained from atmospheric soundings measurements, published sources, or obtained from radiative transfer models (e.g., Berk et al. 1989, Ricchiazzi et al. 1998). Table 3.2 lists the source data requirements and parameters necessary to run Topquad, and Table 3.3 lists Topquad values applied in previous research applications. Previous applications of Topquad have shown that insolation predictions are considered very reasonable if predicted values are within 20 to 25 W/m^2 of the observed (Dr Danny Marks, personal communication 1998). For the temperature modeling applications presented here, the insolation model assumes atmospheric conditions appropriate for mid-latitude rural environments. Furthermore, because the temperature model focuses on the hottest part of the year, it is assumed that clear-sky conditions prevail. Consequently the optical depth parameter (τ) is assigned a globally fixed value (0.2) reflecting minimal atmospheric water vapor content.

The manner in which the tree height model and the solar radiation interact is illustrated in Figure 3.2, which shows the radiation receipt for a hypothetical North-South oriented stream. The figure demonstrates that the amount of direct shortwave radiation receipt (shown by unbroken red lines) is a function of tree height, terrain shade, and time of day. Thus, for late-seral tree heights, Figure 3.2 indicates that the stream only receives direct shortwave radiation around the noon time period. Earlier (or later) in the day, terrain and vegetation shade blocks direct shortwave radiation receipt (shown by dashed red lines). The contribution from shortwave radiation transmitted through the forest

canopy is ignored in the model. While important in locally-select cases, canopy-transmitted shortwave radiation is of secondary importance compared to the direct shortwave contribution (Reifsnyder et al. 1971, Reifsnyder and Lull 1965). Also relevant but only implied in Figure 3.2 are latitude and time of year.

Figure 3.3 shows the differences in incoming shortwave radiation for a hypothetical North-South versus and East-West oriented stream as a function of tree height. Predicted shortwave radiation receipt is similar for both cases for tree heights less than 20-meters. For taller trees, radiation receipt is less (but not significantly less) for North-South oriented streams. The two examples are shown for a flat, topographic surface. Incorporating terrain effects (not shown) can result in significantly different radiation predictions.

Insolation predictions are passed to the 1-D heat balance model which computes for every stream segment, the heat energy transferred out of the reach via stream flow.

3.2.3 One dimensional heat balance model

Water temperature and heat are related through discharge in the model by the relationship,

$$H = \alpha\, T_w\, Q \qquad\qquad [3.5]$$

where H is heat energy in Joules per second, T_w is water temperature (°C), Q is discharge ($m^3\ s^{-1}$), and α (equivalent to 4.186 x 10^6) is the number of joules per cubic meter of water per °C. Water is assumed to be fully mixed in the vertical and lateral directions. Within the model, the energy available to heat water is driven solely by insolation. Figure

3.4 illustrates the mechanisms accounted for in the 1-D heat balance model. The three main components of the model illustrated in Figure 3.4 are the insolation flux, the heat brought in by groundwater, and the remaining heat exchanges processes which are lumped in various fitting parameters (see below). The model assumes that the thermal system is in steady-state. The basic heat balance equation calculates the heat flux, *h* (joules), across a surface perpendicular to the reach at a distance *x* from the reach head:

$$\frac{dh}{dx} \;=\; \alpha T_{gw}\frac{dq}{dx} \;+\; \left(K_1 I + K_0 + K_2\left(T_a - \frac{h}{\alpha q}\right)\right)w \qquad [3.6]$$

The first term on the right hand side of Equation [3.6] (colored blue), $\alpha T_{gw}dq/dx$, is the heat brought in by groundwater. T_{gw}, is the temperature of net lateral inflow, and $q(x)$ is the water flux across a surface perpendicular to the reach. The second term on the right hand side of [3.6] (colored red) is the insolation term, where *I* is the predicted shortwave radiation flux at the stream surface (J m^{-2} sec^{-1})*,* and K_1 is a dimensionless insolation coefficient with a default value set equal unity. While the K_1 parameter may be allowed vary optimization, when allowed to vary, K_1 converged on 1.0. The total amount of predicted heat energy (in units of joules per second) available to heat each stream segment is the product of $K_1 I$ and the stream segment surface area (m^2). Stream segment surface area is product of, *x,* (reach segment length) and, *w,* (stream segment width). The various heat exchange fluxes which operate at the air-water interface (e.g., convection and evaporation) are lumped into the third term on the right hand side of [3.6] (colored green). T_a (°C) is a fitted parameter nominally related to air temperature. If available, measured air temperature data for the basin of interest can be used. In the absence of measured data, T_a is a fitted parameter generated during the optimization. K_0, and K_2, are

46

fitted parameters. K_2 multiplies the difference between the air (T_a) and water temperature ($h/\alpha q$).

Reach segment lengths are set to approximately match the resolution of the input vegetation data. By computing temperatures over such short reaches, the first term on the right hand side [3.6] can be added in its entirety to the upstream end. Adding all lateral flow to the upper end of each stream segment and setting $q\,/\,q(0) = 1$, Equation [3.6] becomes,

$$\frac{dh}{dx} = w\left(K_1 I + K_0 + K_2 T_a\right) - \left(\frac{K_2 w}{\alpha\, q}\right) h \qquad [3.7]$$

Which simplifies to,

$$\frac{dh}{dx} = a - c\,h \qquad [3.8]$$

where,
$$a = w\left(K_1 I + K_0 + K_2 T_a\right)$$
and,
$$c = \frac{K_2 w}{\alpha q}$$

Equation [3.8] has the general solution,

$$h(x) = \frac{a}{c} + \left(h(0) - \frac{a}{c}\right) e^{-cx} \qquad [3.9]$$

where $h(0)$ represents both the heat added from the upstream stream segment and all the lateral inflow for that stream segment. Table 3.4 lists the model parameters necessary to operate the 1-D heat balance model. All calculations in BasinTemp are performed in metric units. Heat is computed as rate of change in the heat energy content of a reach in units of watts (J sec^{-1}). Water temperatures downstream of tributary confluences are

47

computed using a general mixing equation (Bartholow 1989, Deas and Lowney 2000).

The predicted temperature downstream of a confluence, T_d (°C), is given by,

$$T_d = \frac{Q_m T_m + Q_t T_t}{Q_m + Q_t}$$ [3.10]

where Q_m and Q_t are mainstem and tributary discharges (m³/s) upstream of the

confluence, and T_m and T_t are mainstem and tributary water temperatures (°C) upstream

of the confluence.

3.2.4 Hydrology model

The model is developed for low-flow conditions – discharge leaving each reach is

computed as the sum of discharges from upstream reaches and local groundwater seepage

into the reach. The rate of groundwater seepage is assumed to be a fixed linear constant

of channel network length whose value is calculated so that predicted discharges at

references reaches match observed low-flow discharges at gages at those locations and

for the time period of interest. The model implicitly incorporates the affects of lithology

through the calculated groundwater seepage rates. Lithologic control over groundwater

seepage rates is explored further with a field example.

3.2.5 Optimization

The optimization routine finds values for the three parameters, K_0, K_2, and T_a,

which minimize the sum over all the calibration reaches. The objective function

minimized by the optimization is the root mean square error (RMSE) between predicted

and observed water temperatures at selected reaches,

$$RMSE(°C) = \frac{\sqrt{\sum\limits_{i=1}^{N}\left(T_{obs} - T_{pred}\right)^2}}{N} \qquad [3.11]$$

where T_{obs} is the observed temperature (°C), T_{pred} is the predicted temperature (°C), and N is the number of calibration sites. The optimization routine applies a model trust region method (Dennis and Schnabel 1996) which uses full second derivative information and is fully integrated within the 1-D heat balance model.

The model predicts steady-state water temperatures for time-steps of greater than a day.

3.2.6 Input data requirements

Table 3.5 lists the data used in this study to characterize the topography, vegetation, and runoff. The vegetation, channel, and digital elevation data are assembled within the GIS pre-processor. These data can all be obtained (at varying resolutions and accuracies) from freely-available, public domain sources. Digital elevation data are typically obtained from the USGS and at a resolution of 30-meters, although 10-meter resolution and occasionally higher resolution (for example, LiDAR) DEMs are increasingly becoming available. Measured low-flow discharge data required to parameterize the linear groundwater seepage rate parameter can be obtained from USGS stream gages data. The optimization procedure requires measured stream temperature data associated with the warmest part of the year from several locations within the study watershed.

The main features of the model are: (a) easy application to basins of varying size, (b) transferable to basins with very different physiographic, lithologic, and dominant

vegetation characteristics, (c) limited and flexible input data requirements, (d) prediction

of water temperatures for short, user-defined reaches, (e) advection of temperatures

downstream, permitting assessment of local and cumulative downstream temperature

effects, and (f) adjustable riparian tree heights for entire basins, or select areas within a

basin, permitting assessment of alternative riparian management scenarios on local and

basin-wide water temperatures.

In the next section I apply the model to three watersheds within the South Fork

Eel River basin in Northern California.

3.3 STUDY AREAS

The South Fork Eel river basin in Northern California drains an area of approximately 1,800 km^2 (Figure 3.5). The geology of the basin is dominated (83%) by sandstones, conglomerates, and shales of the Yager formation with 12% of the basin underlain by less competent, mechanically weaker Coastal Belt Franciscan formation (U.S. EPA 1999, James 1983). Floodplain deposits comprise the remaining 5% of the basin. Mixed hardwood-conifer woodland forest of varying age and maturity covers much of the basin. Old growth redwood forest is found in the Humboldt Redwoods State Park in the north of the South Fork Eel basin. Areas where shrub, forbs, and grassland vegetation dominate are associated with relatively recent land use activity, or exceptionally dry ridges. The climate is generally Mediterranean type and characterized by long, warm summers and cool, wet winters. Mean annual precipitation ranges from 1,500 mm to 1,800 mm most of which falls between October and April (James, 1983). Maximum summer temperatures can exceed 31°C (Mast and Clow 2000). Approximately 20% of the basin is owned by State Parks and the Bureau of Land Management and a small portion is owned by large timber companies, while the remainder is owned by small landholders, ranchers, and residential communities.

Temperature modeling focused on three sub-basins within the South Fork Eel River. The basins – Bull Creek, Elder Creek, and Rattlesnake Creek – capture a broad range of physiographic (Table 3.6), lithologic (Table 3.7), and vegetation (Table 3.8) characteristics, and landuse histories observed in the South Fork Eel basin. Elder Creek (drainage area 17 km^2) is a largely undisturbed basin containing one of the last remaining stands of old growth Douglas Fir in California. Rattlesnake Creek (drainage area 99 km^2)

is characterized by gently rolling terrain and broad areas of grassland and chaparral vegetation. Bull Creek (drainage area 112 km^2) is comprised of patches of old growth forest and recently logged areas

The model was initially tested on the Bull Creek sub-basin. Bull Creek offered several compelling features which made it valuable as a test basin. Relief in the basin is highly variable and includes steep, incised uplands and a broad, aggraded valley floor on the mainstem. A broad range of vegetation assemblages exist in the basin. Portions of Bull Creek are intensely managed, while in Humboldt Redwoods State Park, ancient stands old growth redwoods still exist.

Status of fisheries in the South Fork Eel basin

Historically coho salmon were abundant throughout the Eel basin and supported an important commercial salmon fishery (EPA 1999). Towards the end of the 19th century, commercial production of coho may have exceeded 500,000 fish (Lufkin 1996). In the early part of the 20th century coho numbers plummeted as a result of unrestricted harvesting. Commercial harvesting of coho was formally ended in the South Fork Eel in 1922. Population numbers recovered slightly between the 1930's and 1950's. The Department of Fish and Game estimated that the entire Eel system, including the South Fork Eel, produced around 160,000 salmon and steelhead in 1964 (Department of Fish and Game, 1997). More recently coho salmon have suffered a further decline in numbers. By the 1980's, estimates suggest that only 30,000 fish were extant in the entire Eel River basin (California Department of Fish and Game 1997). Despite the dramatic decline in numbers, the Department of Fish and Game considers the South Fork Eel to have a

significant remnant population of coho salmon (Steiner 1999 as reported in U.S. EPA 1999). University of California fisheries experts (Brown et al. 1994) found that the South Fork Eel population is important because it has little hatchery influence and thus is important for the genetic integrity of the stock.

3.4 SOURCE DATA

Table 3.5 lists the source data used in the model for the South Fork Eel temperature application.

3.4.1 Topography and channel network

Thirty meter digital elevation data (raster DEMs) and 1:24,000 digital line graph hydrography were obtained from the US Geological Survey. USGS 1:24,000 blueline hydrography adequately characterizes the larger channels and where channels were visible through forest canopy. Small, steep headwater channels are often omitted from these data. However, the focus is on mid-summer conditions when many of these ephemeral channels are dry. The channel network is discretized into equidistant (25-meters) segments approximately matching the resolution of the source vegetation data. For example, the Bull Creek channel network was discretized into approximately 5,700 individual segments. Each stream segment was attributed with a low-flow width generated from field-measured low widths and drainage area relationships developed for the South Fork Eel River (Figure 2.3a).

3.4.2 Vegetation data

Vegetation data (Figure 3.6) were obtained from 1994 Landsat Thematic Mapper (TM) imagery classified using a modified California Wildlife-Habitat Relations (CWHR) (Mayer and Laudenslayer 1988) scheme (Fox et al. 1997, Fox and Carlson 1996). The data are resolved at a horizontal resolution of 30-meters and were classified using both

supervised and unsupervised methods (Fox and Carlson 1996). Ground truthing was performed by several collaborating state and federal agencies (including the California Department of Fish and Game, U.S. Forest Service, and the Bureau of Land Management), by inspection and field validation of the Landsat vegetation classification (Fox et al. 1997).

Tree heights were computed using diameter-at-breast-height (DBH) conversions (Table 3.9) derived from theoretical DBH-to-height relationships (Hanus et al. 1999, Garman et al. 1995, Krumland and Wensel 1988) and published sources (Fowells 1975, Mayer and Laudenslayer 1988, Burns and Honkala 1990, Sawyer and Keeler-Woolf 1995, Whitney 1985). Generally the DBH-to-height relationship is asymptotic (Garman et al. 1995, Krumland and Wensel 1988) and is typically developed for individual tree species where the actual form of the DBH-to-height relationship depends strongly on site specific conditions (moisture content, exposure, soil type, and so forth).

3.4.3 Hydrology

Groundwater seepage rates were calculated using flow data obtained from USGS gages for each of the sub-basins. The rate is assumed to be a linear function of cumulative channel length with units of cubic meters per second per kilometer. The groundwater seepage rate was computed for each sub basin by iteratively adjusting the rate until the predicted mean low-flow discharge for the stream segment nearest to a local USGS gauging station matched the measured mean 7-day running mean low-flow discharge for the time period of interest. No currently active (or obsolete) USGS gage data exists for Rattlesnake Creek, so lithology-specific discharge data derived from

adjacent watersheds were used (see below). In the absence of measured groundwater temperature data (which was the case for the South Fork Eel River basin), the convention is to use local mean annual air temperature (Theurer et al. 1984, Bartholow 1989, Beschta et al. 1987, Deas and Lowney 2000, Sridhar et al. 2004). The groundwater temperature parameter (T_{gw}) was set to a value matching the mean annual air temperature (12°C).

3.4.4 Solar radiation model

The atmospheric transmission parameters (Equation [3.3]), optical depth (τ), the single scattering albedo (ω), and the scattering asymmetry factor (γ), were fixed using values suggested (Table 3.1) by the developers of IPW tools (Professor Jeff Dozier 1997, personal communication 1997, Dr Danny Marks, personal communication 1998, Professor Ralph Dubayah, personal communication 1998). All other attributes (slope, aspect, solar altitude and azimuth) are calculated directly from the DEM. Table 3.3 lists reported and literature values for the atmospheric transmission parameters, and reveals the range of values assigned to the parameters depending on local atmospheric conditions. The other input arguments to Topquad, include the spectral range (set from 0.3 μm to 3.0 μm), surface albedo (fixed at 15%), the date, and the latitude.

3.4.5 Temperature data

Temperature data for 1996 and 1997 collected and processed by the Humboldt County Resource Conservation District (Friedrichsen 1998, Lewis et al. 2000) were used for model calibration and optimization. The temperature metric used in the model was the 7-day running Mean Weekly Average Temperature (MWAT) for every stream segment. Empirical research has shown that coho salmon growth rates (Brungs and Jones 1977)

and the presence or absence of juvenile coho (Welsh et al. 2001) correlate well with the

MWAT metric. The metric is also widely applied by the National Marine Fisheries

Service and the U.S. Fish and Wildlife Service (NMFS and USFWS 1997).

3.5 RESULTS

3.5.1 Bull Creek

Predicted spatial distribution of solar radiation for topography-only, and existing vegetation conditions are shown in Figures 3.7 and 3.8 respectively. Predictions are daily average values for July 31st. The topography-only scenario (Figure 3.7) demonstrates strong aspect control over shortwave radiation receipt at the surface. For example, southern-facing slopes (particularly for the northern third of Bull Creek) receives considerable shortwave radiation receipt. By comparison, the current vegetation insolation scenario (Figure 3.8) displays a speckled appearance due to variable tree heights locally modifying insolation receipt. Comparison of the two scenarios reveals a significant reduction in shortwave receipt at the stream channel surface for the existing vegetation shade scenario. While this is partly a function of the way in which predicted radiation is attributed to grid cells in the GIS, it does reflect the effect late seral trees located in the near-stream environment have on direct solar radiation receipt at the stream surface.

Measured temperatures from seven thermographs recording MWAT for the week-ending July 31st, 1996 were used in the optimization exercise to generate fitting parameters. The groundwater temperature parameter, T_{gw}, is a global constant and set to a physically realistic temperature (12°C), approximately matching the mean annual air temperature. The coefficient of insolation parameter, K_I, is fixed at unity for all model runs. The 'air temperature', T_a, parameter was initially assigned a value of 20°C and then allowed to vary during the optimization. For the Bull Creek and Elder Creek (see below)

applications, the air temperature (T_a) parameter varied little from its initial value so it was fixed at 20°C for these two basins (Table 3.10). The remaining parameters, K_0 and K_2, were allowed to vary iteratively in order to generate optimized fitting parameters. The groundwater seepage was set using 7-day mean daily low flow discharge measured at the USGS Weott gage (Table 2.1).

Predicted MWATs for Bull Creek yielded a root mean square error of 0.25°C and an R^2 of 0.99 (Figure 3.9). No residual trend was found in the fit to the data. Hence we reproduced reliably both the local stream temperature and its spatial variation. The spatial distribution of predicted temperatures indicate general downstream warming and cooling which indicates general stream heating and tributary inflow effects. Along the mainstem Bull Creek, temperatures increase from 12°C to over 21°C downstream of Cuneo Creek. Mainstem Bull Creek cooling is also apparent downstream of the Squaw Creek tributary confluence where temperatures cool by almost 1°C (Figure 3.10). Tributary temperature patterns range from generally cool (Squaw, Harper, and Cow Creeks) to predominantly warm (Mill, Cuneo, Burns, Slide, and Panther Creeks). Predicted tributary temperature reflect dominant vegetation conditions (and hence level of shade provision) within each tributary sub-basin and also tributary orientation. Cooler tributaries (Squaw, Harper, and Cow Creeks) are associated with late seral vegetation (Figure 3.6) and are generally North-South oriented. As indicated by Figure 3.2, North-South oriented streams with late seral vegetation block most incoming direct solar radiation except during the mid-day period. Warmer tributaries, especially Cuneo Creek, are associated with shrub and grassland and secondary re-growth and are also generally West-East oriented channels.

3.5.2 Elder Creek

Elder Creek insolation predictions for July 31st are shown for topography-only

shade conditions (Figure 3.11a) and existing vegetation shade conditions (Figure 3.11b).

Aspect control over solar radiation receipt is very apparent in Figure 3.11(a) – steep,

north-facing slopes on average receive less than 50 W m^{-2}. By comparison south-facing

slopes receive as much as 400 W m^{-2} (Figure 3.11a). Reduction in predicted insolation in

the near streamside environment as a result of riparian shade provision is demonstrated in

Figure 3.11(b). Reduction of predicted insolation is apparent for the mainstem Elder

Creek and all its tributaries, but even more conspicuous for east-west oriented channels

(Figure 3.11b).

Measured thermograph data for Elder (and Rattlesnake) Creek for 1996 and 1997

were far more limited. Neither basin contained both synchronous and sufficiently reliable

observed MWAT data for 1996 or 1997. However both basins contained an adequate

number of thermograph stations recording the 7-day running mean of the daily average

(Weekly Average Temperature or WAT) for the week ending July 31st, 1997.

Groundwater seepage rate was set using measured low flows recorded at the USGS Elder

Creek gage (Table 2.1). As discussed above, the air temperature parameter, T_a, was fixed

at a physically realistic value of 20°C and K_1 was left at 1. The fitting process therefore

involved only two free parameters, K_0 and K_2. The final fitted and fixed parameter values

are shown in Table 3.10.

Predicted weekly average temperatures (WATS) for Elder Creek (Figure 3.12),

yielded a root mean square error of 0.40°C and an R^2 of 0.83. No residual data trend is

seen in the prediction comparison, hence, as with Bull Creek, the model matches the

observed spatial variation in stream temperature. Spatial temperature patterns indicate predicted temperatures are generally cool for the entire basin. Predicted temperatures for most of the mainstem Elder Creek are below 15°C, warming to 17.5°C for the downstream-most 1-kilometer of the mainstem. Tributary temperatures are all cool (< 15°C), especially deeply incised North-South oriented channels. Cooler predicted temperatures for North-South streams are the result of terrain shade and late seral riparian shade effects limiting the amount of incoming shortwave radiation (Figure 3.11b) reaching the stream surface.

3.5.3 Rattlesnake Creek

The model application to Rattlesnake Creek provided an opportunity to assess lithologic controls over riparian and topographic shade provision, and groundwater seepage rates. Figure 3.14 shows that Rattlesnake Creek is comprised of two dominant lithologic units (Franciscan mélange and Coastal Belt Franciscan) each of which is characterized by different physiography and vegetation. Franciscan mélange is characterized by gently rolling terrain and vegetation dominated by grasslands and sparse oak woodland (Figure 3.6). By contrast, areas of Franciscan Coastal Belt lithology are characterized by moderate to deeply incised relief where the dominant vegetation is mid-to-late seral conifer (Figure 3.6). Insolation predictions for topography-only shade (Figure 3.15) and existing vegetation shade conditions (Figure 3.16) reveal lithologic controls over the shortwave radiation receipt. Aspect controls are much more significant for Franciscan Coastal Belt areas notably the Western-most portion of the basin (Figure

3.15). Terrain shade effects are much less apparent with the gently rolling relief associated with Franciscan mélange (for example, the Foster Creek tributary in Figure 3.15). The insolation patterns as a function of lithology are also apparent for existing vegetation conditions (Figure 3.16). Areas characterized by grassland and forbs (Figure 3.6) within mélange lithology generally receive more insolation than Coastal Belt units. Notably, predicted insolation for the channels within Franciscan Coastal Belt units is considerably less than mélange unit channels (Figure 3.16).

The very different relief, and vegetation characteristics of mélange and Coastal Belt terrain suggests that hydrologic characteristic would also be very different for each unit. While no measured discharge data were available for Rattlesnake Creek, USGS discharge data were available from two adjacent basins (Elder Creek and Tenmile Creek). Lithology in Elder Creek is dominated by Coastal Belt Franciscan (Table 3.7), while Tenmile Creek is predominantly characterized by mélange lithology. Groundwater accretion rates were computed for both basins and then the rates were assigned to each unit for the Rattlesnake Creek application (Table 3.10). Significantly, the groundwater accretion rate for Coastal Belt Franciscan terrain is an order of magnitude larger than for mélange lithology (which is much greater than the precipitation difference within the somewhat drier inland Tenmile Creek watershed). It is also reasonable to assume that ambient air temperature patterns would vary across these two units. The model structure permits the air temperature parameter, T_a, to be varied spatially. This feature was implemented for the Rattlesnake Creek application by allowing T_a to vary according to each lithologic unit. As with the Bull and Elder Creek applications, the K_0 and K_2 parameters were also fitted during the optimization (Table 3.10).

62

Predicted weekly average temperatures (WATS) for the week ending July 31st, 1997 yielded an RMSE of 0.47°C and an R^2 of 0.77 Figure (3.17), with no residual trend to the data. Predicted temperature patterns are shown in Figure 3.18 and reveal very warm temperatures (> 21°C) for much of the basin. The headwater temperatures of the mainstem Rattlesnake Creek starts off warm (> 17°C) and increase downstream by more than 4°C. Tributary temperatures are generally warmer than the mainstem and several are very warm (> 21°C), including Foster Creek, Twin Rocks Creek, and Elk Creek. Figure 3.18 overlays lithology on to the predicted temperatures for Rattlesnake Creek and shows that the distribution of warmer temperatures (Franciscan mélange) and cooler temperatures (Coastal Belt Franciscan) is strongly associated with lithology.

3.6 DISCUSSION

The model predicts general stream temperature patterns, including downstream warming and cooling, spatially varying tributary temperatures, the cooling (or warming) effects of tributary inflow. A comparison of temperature predictions for the three South Fork Eel basins reveals both strong similarities and significant differences with stream temperature. For all three basins, temperatures increase downstream but at different rates. In the Bull Creek example, warm tributary inflow (Cuneo Creek), and cool tributary inflow (Squaw Creek) result in significant mainstem downstream warming and cooling respectively. Predicted Elder Creek temperatures are the coolest among all three basins, due to in part to its small size (17 km^2), and the shading effects imparted by steep terrain and tall trees. The groundwater inflow rate for Elder Creek is the highest among all three basins which also contributes to cooler temperatures.

For Bull Creek, predicted temperatures show strong spatial variability dictated primarily by riparian shade effects and to a lesser extent, terrain shade effects. Tributary temperature patterns follow the vegetation patterns shown in Figure 3.6, with cooler temperatures associated with late seral mid conifer vegetation in the Northeast portion of the basin. This area includes the Squaw Creek tributary which is contained within the Humboldt Redwoods State Park and contains large swaths of old growth Redwoods. Dominant vegetation changes significantly for tributaries in the Northwest portion of Bull Creek, particularly Cuneo Creek. Cuneo Creek has experienced considerable landuse manipulation in recent years as indicated by the large areas of grassland and shrubland particularly down toward its confluence with Bull Creek. Predicted temperatures for this tributary are significantly warmer due to the limited shade provision offered by grassland

64

and shrub vegetation. Tributary inflow warming and cooling effects are well illustrated by Cuneo and Squaw Creeks respectively.

Predicted temperatures for Rattlesnake Creek are generally warmer than Elder Creek and Bull Creek and reveal important interactions between lithology, relief, dominant vegetation, and hydrologic heterogeneity. Relief (Figure 3.5), vegetation (Figure 3.6), and predicted insolation (Figures 3.15 and 3.16) reveal significant differences between Franciscan Melange and Coastal Belt Lithology. Those contrasts manifest themselves most significantly with regard to groundwater inflow rates which were different by an order of magnitude between the two lithologies. Predicted temperatures for Melange terrain are significantly warmer demonstrating the temperature effects of both reduced water volume and generally higher heat loads due to less steep valleys and sparser vegetation (Figure 3.19).

The differences and similarities between all three basins are implicitly demonstrated by combining the data for all three basins and then running the model (Figure 3.20). This application tests the model robustness in three ways: (1) model predictions are generated for the equivalent basin area of 220 km^2 (Elder, Bull, and Rattlesnake Creek areas combined); (2) predictions are generated using two different stream temperature metrics (maximum weekly average temperatures [MWATS] and weekly average temperatures [WATS]); and (3) predictions are generated for two different discharge years (1996 and 1997). I use locally fitted air temperatures, T_a, and groundwater inflow rates that depend on lithology and basin location. The best-fit RMSE of 0.39ºC and an R^2 of 0.97 are comparable to model performance for each individual basin and also lack residual data trends. Model predictions for Elder Creek (blue dots)

and Rattlesnake Creek (red dots) bracket steady-state temperatures ranging from cold to very warm water temperatures. Predicted temperatures for Bull Creek (green dots) overlap both. This application suggests that spatially explicit model can be applied in large watersheds as long as local hydrologic conditions (as influenced by lithology) are incorporated.

Individual basin results (Figures 3.9, 3.12, and 3.17) and the results shown in Figure 3.20 offer some guidance into identifying the minimum number of thermographs necessary for model application. The root mean square error ranged from 0.25ºC (Bull Creek) to 0.47ºC (Rattlesnake Creek) for the individual basins, and was 0.39ºC for the combined result. These results suggest that a minimum of 6 to 7 thermographs per 100 km^2 is sufficient. An application of this model using 7 thermographs for a 259 km^2 basin in Southern Oregon (Stillwater Sciences unpublished data) generated much poorer results (RMSE = 1.1ºC, R^2 = 0.59). These latter results offer indirect support to the minimum required thermograph numbers indicated above.

The model reproduces, and demonstrates the importance of, discharge effects on stream temperature. Furthermore, important lithologic control over spatial hydrologic heterogeneity was demonstrated by the Rattlesnake Creek application. Tague et al. (2007) also demonstrated the importance of hydrogeologic controls on stream temperature. Their study showed that spring-fed streams emerging from High Cascade (recent volcanics) lithologic terrain remained cooler and flow volumes were higher compared to groundwater-fed streams flowing through Western Cascade terrain. The Rattlesnake Creek results support Tague et al.'s assertion (Tague et al. 2007) that numeric water quality standards (e.g, Poole et al. 2004, Ice et al. 2004) need to explicitly account for

hydrogeologic variability. Applying a single numeric stream temperature standard to basins such as Rattlesnake Creek would ignore the important controls on stream temperature exerted by different lithologic units.

Discharge effects are important when considered in the context of climate change. For a warmer climate in California, water is expected become increasingly scarce and its distribution (spatially and temporally) more restricted (Gleick 2000). The simple hydrologic model embedded in *BasinTemp* allows for the exploration of stream temperature response to reductions (and increases) in flow, and hence the impact of drought (or high flow) conditions on stream temperature. Figure 3.21 shows the change in predicted temperatures for a 50% reduction in flow for Bull Creek. The pattern of temperature change shows increases of up to 4ºC for the Western portion of the basin where dominant vegetation reflects disturbed conditions and hence shade provision is limited. Predicted temperatures also increase for the Northwest portion of the basin but only by 1 to 2ºC, suggesting that shade from tall trees limits the effects of reduced flow. Predicted temperatures are everywhere lower for a 50% increase in flow (Figure 3.22), but the magnitude of change is no more than 2ºC and is associated with the areas with higher predicted temperatures for the existing vegetation shade scenario. Thermal longitudinal profiles for four different flow scenarios – increasing and decreasing flow by 25% and 50% - are shown for the mainstem Bull Creek (Figure 3.23) and two of its tributaries (Figure 3.24 and Figure 3.25). For all three examples, the thermal longitudinal profiles show a strong non-linear response to increases or reductions in discharge. The non-linear relationship is much more significant for reductions in flow and for smaller, headwater channels. This effect is well illustrated for a 50% reduction in flow for the

67

Squaw Creek example (Figure 3.24). Predicted temperatures for reductions in flow are consistent with the results from the general sensitivity analysis presented in Chapter 2. Specifically the inverse dependency of stream temperature on flow depth will lead to the significant warming during drought flows and modest cooling during wet years. They also corroborate model predictions generated by the Stream Network Temperature Model (SNTEMP) for small streams in Wisconsin (Gaffield et al 2005). Results from this study also showed a non-linear relationship between predicted temperatures and increasing or decreasing flow by 50%, but the non-linearity was much more apparent for flow reductions (Gaffield et al. 2005).

One of central assumptions embedded in the model is the linearity of groundwater inflow rates. While discharge data for the three South Fork Eel river applications were insufficient to test this assumption, an on-going study for the South Fork Ten Mile River in coastal Northern California has provided useful support for the linearity assumption (Stillwater Sciences unpublished data, 2006-2009). Flow data from seven gages deployed throughout the South Fork Ten Mile River are shown in Figure 3.26. Lithology in the basin is dominated by Coastal Belt Franciscan. The graph plots observed versus predicted discharge for the end of July. The groundwater inflow rate was computed using flow data for the downstream most gage using the methods described above. This computed groundwater seepage rate was then used to generate predicted discharges for the remaining six gages higher up in the basin. Plotting observed versus predicted discharge for all seven gages (Figure 3.26) shows that the data fall on or near the 1-to-1 line. These results offer useful validation for the linearity groundwater seepage rate assumption, certainly for Coastal Belt Franciscan terrain. Nonetheless, the current form of this simple

hydrology model only works for networks where flow increases linearly throughout. Therefore the model is not appropriate for networks which contain losing reaches or which contain reaches characterized by strong hyporheic conditions.

The model has been shown to perform well for the simplifying assumptions described earlier. However, several of these simplifying assumptions render the model inappropriate or inapplicable for certain conditions or situations. For example, ignoring canopy transmitted radiation and treating vegetation as simple impenetrable walls precludes applying the model to assess how wide a forested buffer should be. Ignoring canopy transmitted radiation also precludes model application using higher resolution topography and vegetation information. Testing the model using a 5-meter and 10-meter DEM yielded RMSE's ranging from 7ºC to 8ºC. Under these conditions, higher resolution topography and tree height models block significantly more incoming shortwave radiation *throughout* the channel network with the result that stream temperature predictions are much cooler. This excessive cooling can not be corrected by adjusting the K_0, K_2, and T_a model parameters. Using a 30-meter DEM and tree height model for a constant 30-meter wide channel avoids these issues but at the expense of unrealistic simplification. Applying high resolution topography (e.g. LiDAR) which can both characterize near-stream relief *and* canopy geometry is desirable. However, the model will need to explicitly quantify canopy transmitted radiation in order to take advantage of these next-generation data sources.

The model in its current form is also inappropriate for conditions where incoming shortwave radiation is no longer the dominant heat energy flux. For example the model is inappropriate for applications to watersheds where coastal fog is important or for overcast

or cloudy conditions. Conditions where ambient air temperatures dominate the heat energy budget will also render model application inappropriate. These conditions were encountered during the July 2006 California heatwave (Koslowski and Edwards 2007). One of the significant features of the 2006 heatwave was the persistence of warm day time temperatures through the night. For small, exposed streams, daily maximum temperatures were generally higher, but daily minimum temperatures were significantly higher. Under these conditions, the heat energy flux component in the model which is dominated by insolation, does not account for important diurnal air temperature controls which are also function of riparian vegetation conditions.

3.7 CONCLUSION

A simple, physically-based model for spatially explicit stream temperature throughout a watershed during maximum weekly average temperatures is developed and applied to three basins. The key elements of the model are: 1) an approximate heat budget model, 2) a model for riparian shading based on tree height adjacent to channels, 3) a groundwater inflow model that assumes inflow increases linearly with stream length, and 4) an optimization technique that uses a relatively small amount of field data to set 3 parameters. The heat flux is dominated by direct insolation and stream temperature is predicted to vary inversely with flow depth, leading to a non-linear dependency on discharge, and consequently, on drought conditions. This model is most appropriate to relatively small channels that would experience strong shading from forested vegetation.

The model applied to three basins within the South Fork Eel River watershed is successively calibrated with no residual trend in the data. These basins present a diversity of topography, vegetation, and lithology, all of which explicitly and quantitatively influence stream temperature in the model. Deep north facing canyons with mature conifer forest are coolest and south facing, shallow valleys with brush and grass are warmest. These differences are driven in part by lithology: the coherent Coastal Belt of the Franciscan terrane supports deep canyons, whereas landscapes underlain by mélange support primarily gentle canyons covered with oak, brush or grass and yields much lower discharge.

In general, the stream temperature is predicted to increase downstream, but cool tributaries can reverse that trend and warm ones can amplify it. Forest removal causes significant warming, particularly in shallow flowing tributaries.

71

The model structure is such that it potentially has wide practical application, particularly in watershed management decisions. Field data, i.e. stream temperature at the hottest time of year must be collected at approximately 7 sites per 100 km^2 to achieve a good calibration. Once calibrated the model can be used to delineate sub-basins that are intrinsically warm or cool and permit "what if" testing regarding the effects of vegetation and water management. I explore this last point more extensively in Chapter 4.

Table 3.1   Numeric values assigned to atmospheric transmission parameters used by Topquad to compute insolation

Parameter	Value used	Potential Range
Optical depth (τ)	0.2	0 – 100+
Single scattering albedo (ω)	0.85	0 - 1.0
Scattering asymmetry factor (γ)	0.55	0 – 0.99

Table 3.2   Source data requirements for *Topquad*[1] parameters

Parameter	Source
Spectral range	Depends on application. A coarse spectral range (0.3 – 3.0 μm) was used in this study.
γ - scattering asymmetry factor (measures the strength of forward scattering)	Computed by radiative transfer models (e.g., MODTRAN, [Berk et al. 1997])
ω - single scattering albedo (the ratio of the scattering extinction to the total extinction)	Computed by radiative transfer code (e.g., MODTRAN), or from soundings measurements.
τ - optical depth	Computed by radiative transfer code (e.g., MODTRAN)
Land surface albedo	In the absence of direct measurements, assigning a global estimate is considered reasonable (Marks, pers. comm. 1998)
Mean Elevation	Extracted from DEM. Optical depth is a function of pressure which is in turn, elevation dependent.
Slope and aspect	Computed from DEM
Sky view factor	Computed from DEM
Terrain configuration factor	Computed from DEM

[1]*Topquad* is a set of routines included in the Image Processing Workbench (IPW) that calculate daily integrated radiation over a DEM using a two-stream atmospheric radiation model and 21-point Kronrod quadrature between sunrise and sunset (Marks et al. 1999)

Table 3.3   Literature and reported values for the atmospheric transmission parameters used in *Topquad*

Source	Optical depth (τ) (meters)	Single scattering albedo (ω)	Scattering asymmetry factor (γ)
Mammoth Mountain, CA, *clear* day (Dozier pers comm., 1998)	0.10	0.98	0.80
Mammoth mountain, CA, *cloudy* day (Dozier, pers comm. 1998)	3.0	0.995	0.80
Urban-industrial environments (Iqbal, 1983)	—	≈ 0.6	—
Rural-agricultural environments (Iqbal, 1983)	—	≈ 0.9	—
DHSVM model input (Arola, 1993, based on Dubayah, 1990))	0.20	—	—
Suggested values (Danny Marks, pers. Comm.., 1999)	0.20	0.85	0.55
Kansas, June 15 Clear Day (Dubayah, 1990). Spectral range 0.35-0.75µm	0.20	0.90	0.55
Kansas, June 15 Clear Day (Dubayah, 1990). Spectral range 0.75-2.8µm	0.20	0.75	0.65
Kansas, December 15, Clear Day (Dubayah, 1990). Spectral range: 0.35-0.75µm	0.20	0.90	0.55
Kansas, December 15, Clear Day (Dubayah, 1990). Spectral range: 0.75-2.8µm	0.2	0.75	0.65
Values used in this study	0.20	0.85	0.55

Table 3.4   *BasinTemp* heat balance model parameters

1-D heat balance model parameter	Units	Description
Groundwater temperature (T_{gw})	°C	Groundwater temperature. Global parameter. Set to a physically realistic value (approximately the mean annual air temperature for the basin of interest, e.g. Theurer et al. 1984)
Groundwater seepage rate	m^3/km	Calculated by matching the modeled mean daily discharge with the average of the 7-day running mean daily discharge at a gage (or gages) for the basin of interest
'Air temperature' parameter (T_a)	°C	The 'air temperature' parameter value is obtained either by allowing it to vary in the fitting exercise or by assigning measured air temperature data (if available) from the basin of interest.
K_0	—	Lumped fitting parameter (no direct physical interpretation)
Insolation parameter (K_1)	Dimensionless	Insolation parameter. Default value is set to unity.
K_2	—	Fitting parameter that multiplies the difference between air temperature parameter (T_a) and water temperature ($h/\alpha q$ in Equation 3.6).

Table 3.5   Data used in the South Fork Eel River *BasinTemp* modeling.

Data type	Source Data
Topography	30-meter USGS DEM
Tree height model	30-meter Landsat TM imagery classified according to the California Wildlife Habitat Relations (CWHR) system (Fox et al. 1997)
Stream network	1:24,000 USGS Digital Line Graph blueline hydrography
Channel geometry	Power-law relationship between drainage area and field measured low-flow width for reaches throughout the South Fork Eel (Figure 2.3a).
Low-flow Discharge	7-day mean daily discharge data recorded at USGS gages for Bull and Elder Creeks. No discharge data were available for Rattlesnake Creek so USGS discharge data from Elder Creek and Tenmile Creek were used (see text)
Observed stream temperature data	1996-1997 thermograph data compiled by Humboldt Country Resource Conservation District (Friedrichsen 1998, Lewis et al. 2000)

Table 3.6   Physiographic attributes of Bull, Elder, and Rattlesnake Creeks, South Fork Eel basin, Northern California

Basin	Lat/long of mouth	Area (km^2)	Relief (meters)	Mean elevation (meters)	Total Length of channel (km)	Drainage density[1] (km/sq.km)
Bull Creek	123.9W 40.4N	112	995	430	141	1.3
Elder Creek	123.6W 39.7N	17	874	850	25	1.4
Rattlesnake Creek	123.7W 39.8N	99	1081	710	141	1.4

[1]Based on USGS 1:24,000 blueline hydrography

Table 3.7   Dominant lithologies for Bull, Elder, and Rattlesnake Creeks, South Fork Eel basin.

Basin	Percent of basin contained in different lithologies[1]					
	Yager Formation	Franciscan Melange	Coastal Belt Franciscan	Modern Stream Deposits	Valley Floor and Terraces	Leggett Peridotite
Bull Creek	82.9	–	12.4	0.4	4.3	–
Elder Creek	–	–	99.5	–	0.5	–
Rattlesnake Creek	–	62.3	36.2	0.02	0.2	1.3

[1]Yager and coastal belt Franciscan geomorphic terrains are characterized by moderate to steep slopes and forested hillsides with straight profiles. Franciscan Melange lithology is characterized by open grasslands and oak woodland with gently rolling, hummocky relief (U.S. EPA 1999). Little timber production is associated with Mélange terrain (U.S. EPA 1999).

Table 3.8   Dominant California Wildlife Habitat Relations (CWHR) vegetation classes in Bull, Elder, and Rattlesnake Creeks, South Fork Eel basin.

CWHR vegetation class	Bull Creek	Elder Creek	Rattlesnake Creek
Late seral mixed conifer	16%	52%	38%
Late seral conifer-hardwood	42%	17%	—
Later seral mixed conifer	—	—	8%
Early to mid seral conifer-hardwood	26%	19%	11%
Early to mid seral mixed hardwood	8%	8%	—
Grassland and Shrubs	—	—	32%
Other	8%	4%	11%

Table 3.9   Diameter at breast height (DBH) to tree height conversions for existing California Wildlife Habitat Relations vegetation assemblages[1].

DBH range (inches)	Tree height (meters)						
	Mixed Hardwood	*Mixed Pine*	*Mixed Fir*	*Mixed Conifer and Hardwood*	*Mixed Oak Woodland*	*Mixed Hardwood and Conifer*	*Mixed Conifer*
1-6	10	7	7.5	7.5	5	10	10
6-11	15	10	15	15	10	15	15
11-24	20	17.5	20	22.5	15	20	25
> 24	25	25	30	30	20	27.5	35
> 36[2]	–	–	–	–	–	–	45

[1] Sources listed in main body of text

[2] Only applies to *Mixed Conifer* and *Mixed Conifer and Hardwood* classes.

Table 3.10   Final best-fit *BasinTemp* calibration parameters for each test basin.

Basin / Year	Temperature metric	Groundwater seepage rate (m^3/km)	Groundwater temperature (T_{gw} ºC)	K_0*	K_2*	'Air temperature' parameter (T_a ºC)	Best-fit RMSE (ºC)	Best-fit R^2
Bull Creek 1996	MWATS	0.001715	12	-295	9.2	20 ºC	0.25 ºC	0.99
Elder Creek 1997	WATS	0.002	12	-288	6.7	20 ºC	0.40 ºC	0.83
Rattlesnake Creek[2] 1997	WATS	0.000227 (*mélange)* and 0.002 (*coastal belt)*	12	-293	10.3	19.7 ºC and 20.8 ºC	0.47 ºC	0.77
Bull, Rattlesnake and Elder Creek combined 1996/1997	Bull Creek 1996 MWATS and Elder and Rattlesnake Creek 1997 WATS	*See note* (3) *below*	12	-293	8.3	*See note* (3) *below*	0.39 ºC	0.97

*   Units of K_0 and K_2 are dimensionless

Notes
1.   The dimensionless coefficient, K_1, was fixed at unity for every basin.
2.   Two lithology-specific (mélange and Franciscan Coastal Belt) groundwater seepage rates and two parameterized air temperatures (T_a) were applied to Rattlesnake Creek calibration.
3.   Basin and year-specific groundwater seepage rates were applied. Similarly year-specific, and in the case of Rattlesnake Creek, lithology-specific, parameterized air temperatures (T_a) were applied.

Figure 3.1   Temperature model processing steps
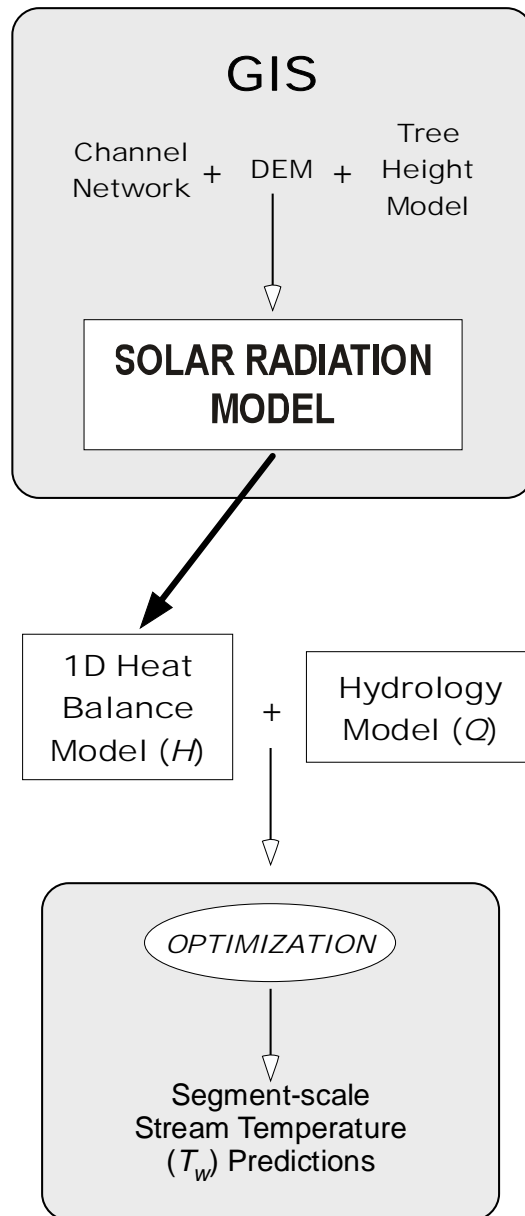
Figure 3.2   Features of tree height and solar radiation prediction model for a
hypothetical north-south oriented stream channel
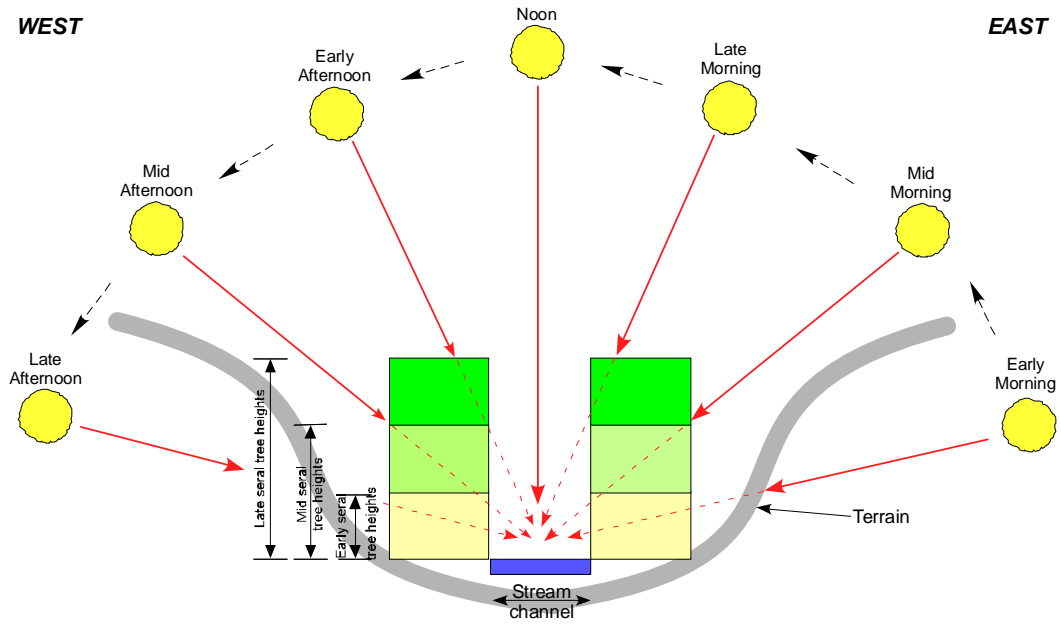
Figure 3.3   IPW shortwave radiation predictions as a function of assumed tree height and stream orientation[1]
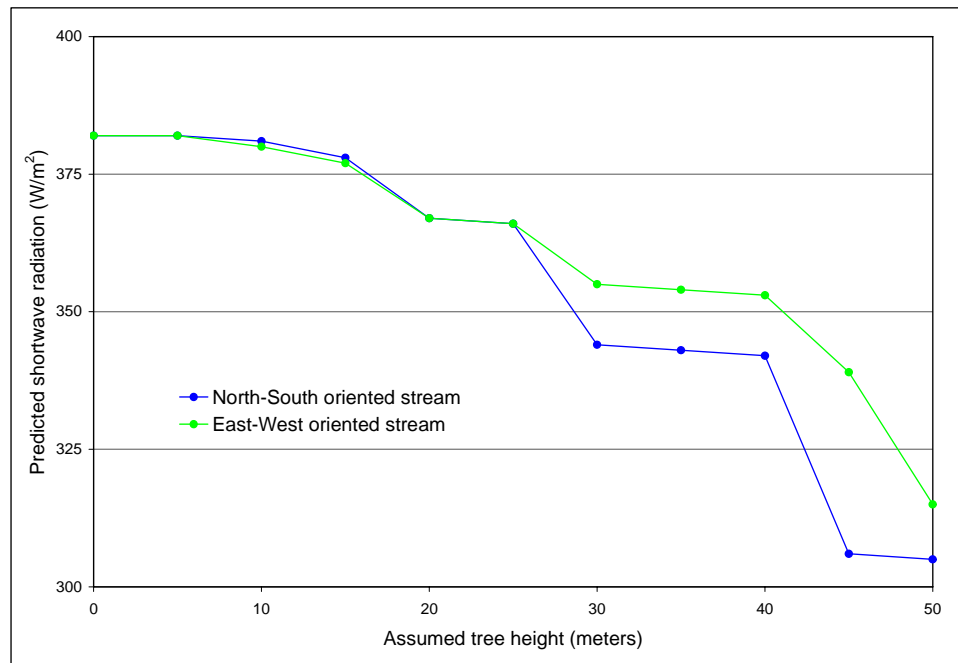
[1]Assumes a flat topographic surface at mean sea level

Figure 3.4   Heat exchange processes modeled in *BasinTemp*

Insolation
$w(K_1 I)dx$

Miscellaneous **heat exchange** processes:
$w(K_0 + K_2(T_a - h/a_* q))dx$

w

dx

Heat brought in by **groundwater**
$aT_{gw}dq/dx$

flow

Idealized slice of water column
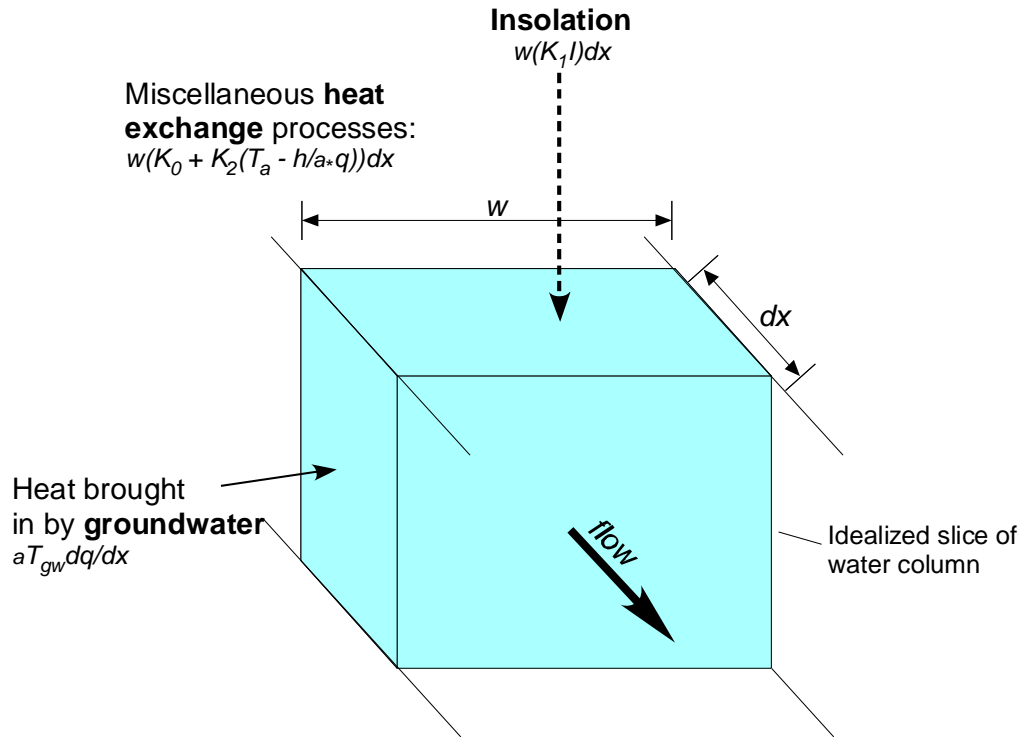
Note: a = Greek alpha

Figure 3.5   Bull, Rattlesnake, and Elder Creeks. South Fork Eel River basin, Northern California.
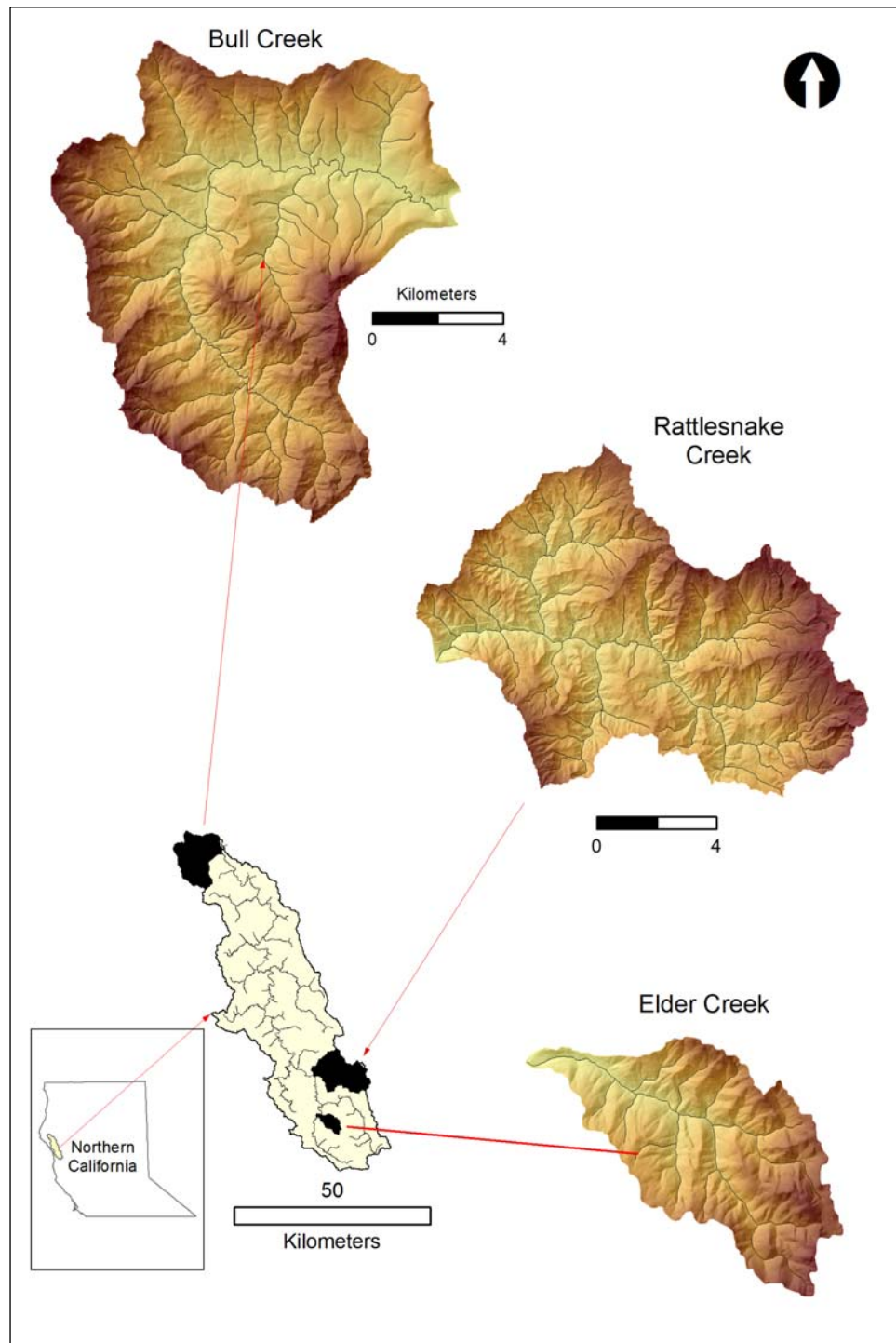
Figure 3.6   Modified California Wildlife Habitat Relations (CWHR) vegetation data[1]
used to generate tree height model
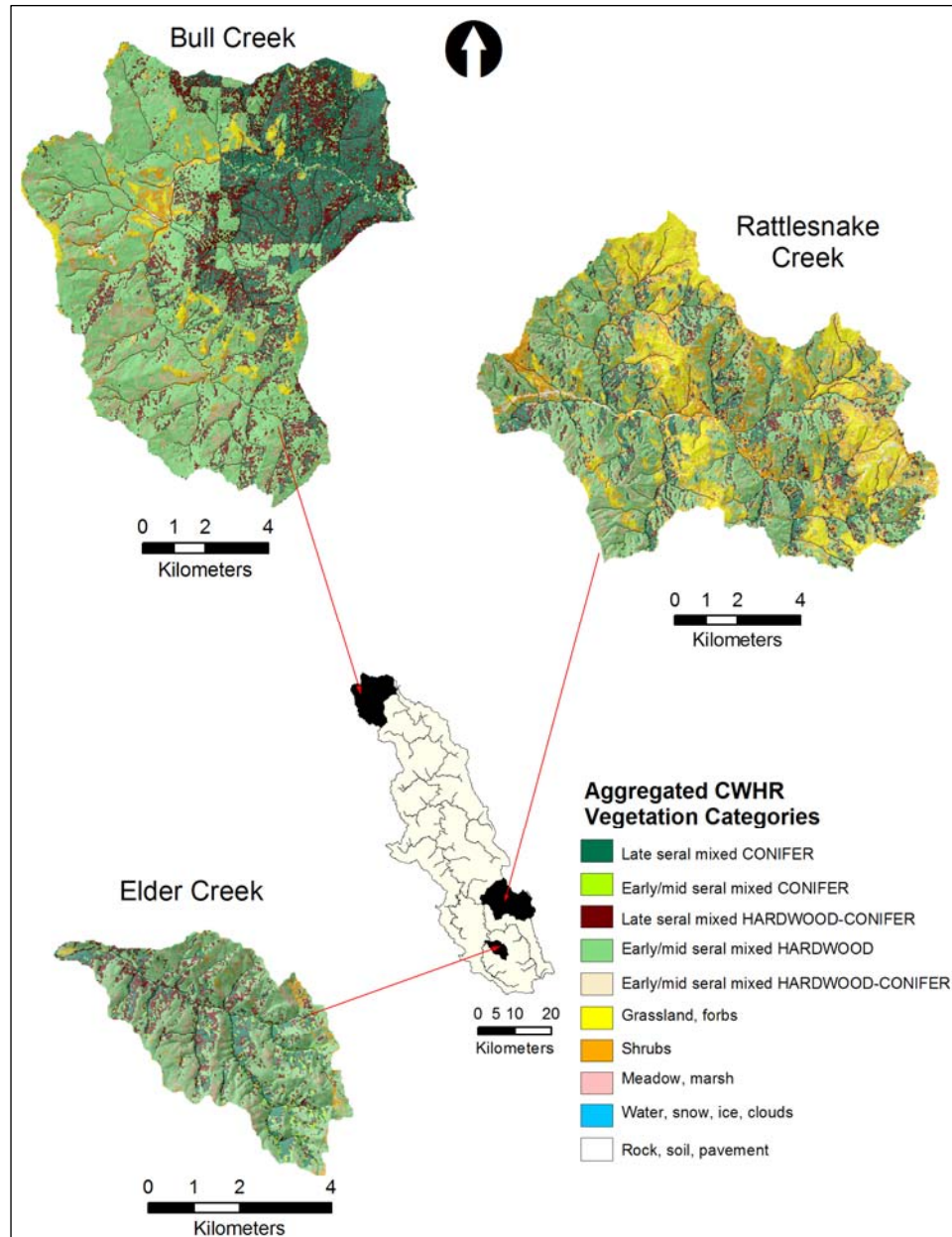
[1]Source: Fox et al. (1997), Fox and Carlson (1996)

Figure 3.7   Solar radiation predictions for topography-only shade conditions, Bull
             Creek

Figure 3.8   Solar radiation predictions for existing vegetation shade conditions, Bull Creek.

Insolation Predictions (W/m^2)

400

0

0   1   2   4

Kilometers

Figure 3.9   Observed versus predicted MWATS[1]. Bull Creek, South Fork Eel River

Best-fit MWAT Predictions		
Station	Observed (°C)	Predicted (°C)
1305	16.4	16.3
1532	16.4	16.4
1518	19.5	19.8
1511	20.0	20.0
1513	20.5	20.7
1590	21.3	20.8
1512	22.1	22.2
		RMSE = 0.25
		R-squared = 0.99

[1]MWAT predictions generated for the week-ending July 31st, 1996

Figure 3.10   MWAT predictions for existing vegetation shade conditions for week-ending July 31st, 1996. Bull Creek.
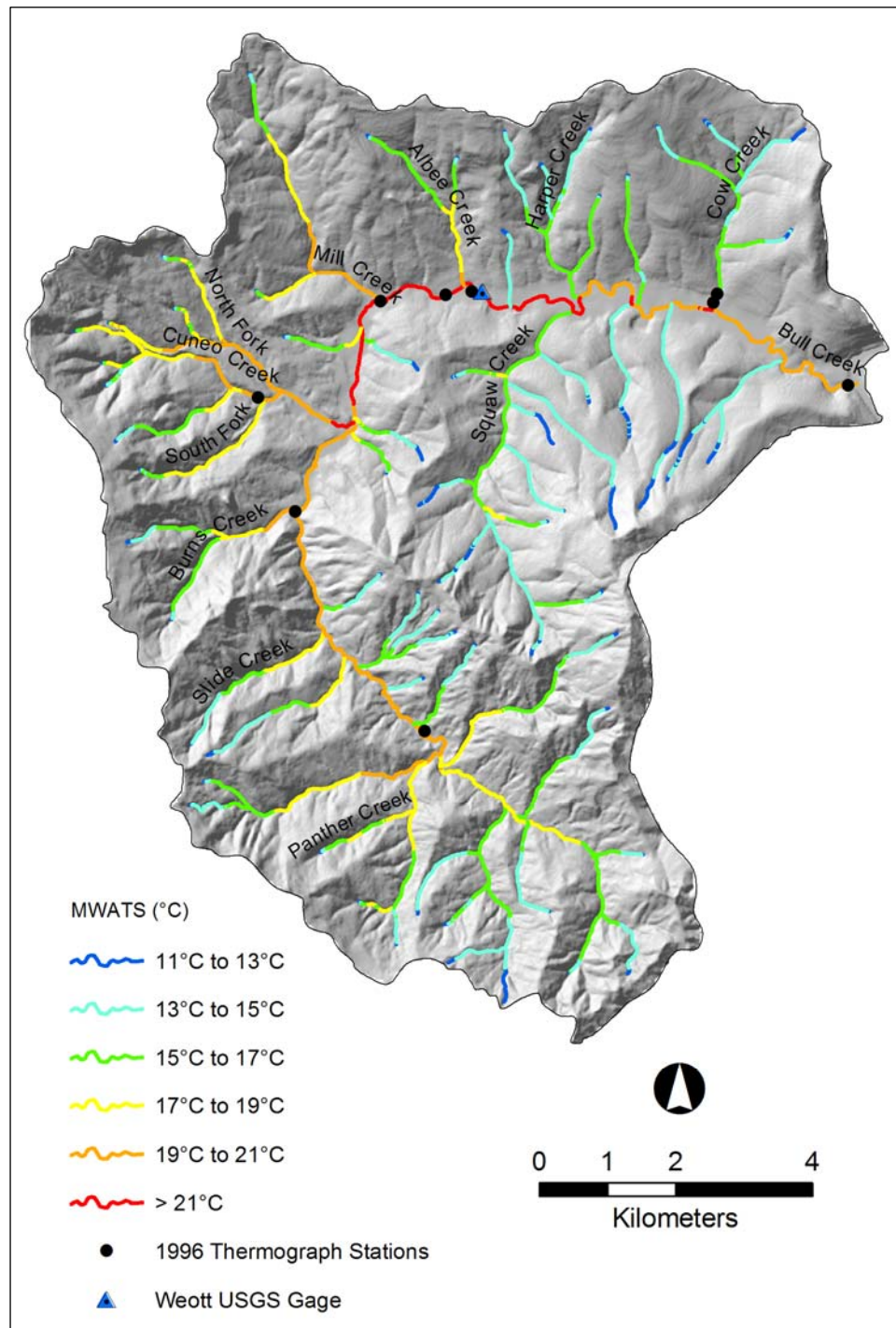
Figure 3.11   Solar radiation predictions. Elder Creek, South Fork Eel River basin.

(a) Insolation predictions for topography-only shade conditions

(b) Insolation predictions for existing vegetation shade conditions

Predicted Insolation (W/m²)

400

40

0   0.5   1   2
Kilometers
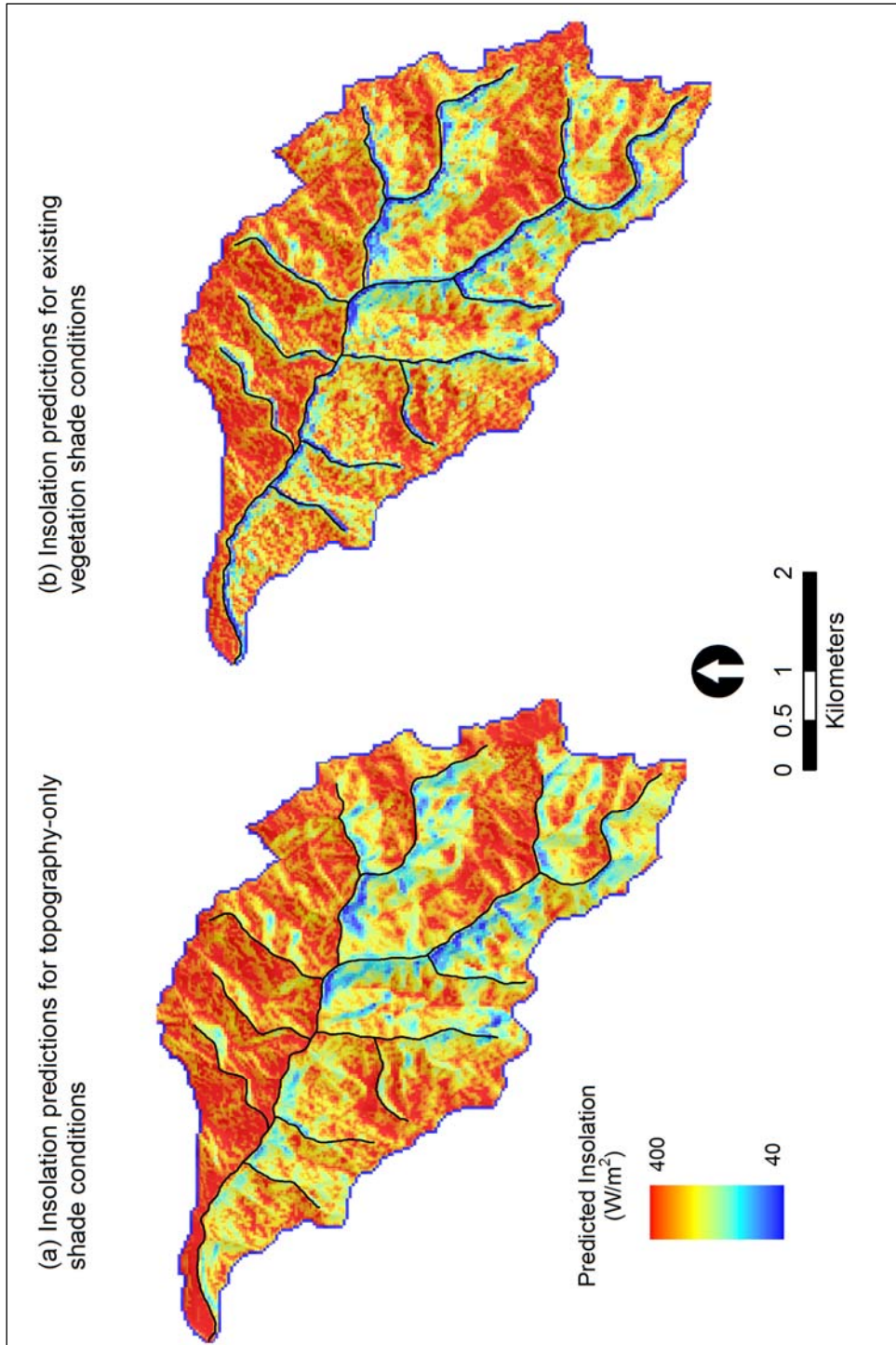
Figure 3.12　Observed versus predicted weekly average temperatures (WATS)[1]. Elder Creek, South Fork Eel River.

Best-fit WATS Predictions		
Station	Observed (°C)	Predicted (°C)
1540	17	17.0
1460	17.5	17.5
1461	17.8	17.5
1458	16.6	16.6
1457	16.4	15.8
1480	14.8	15.0
1456	15.8	16.6
	RMSE (°C)	0.40
	R^2	0.83
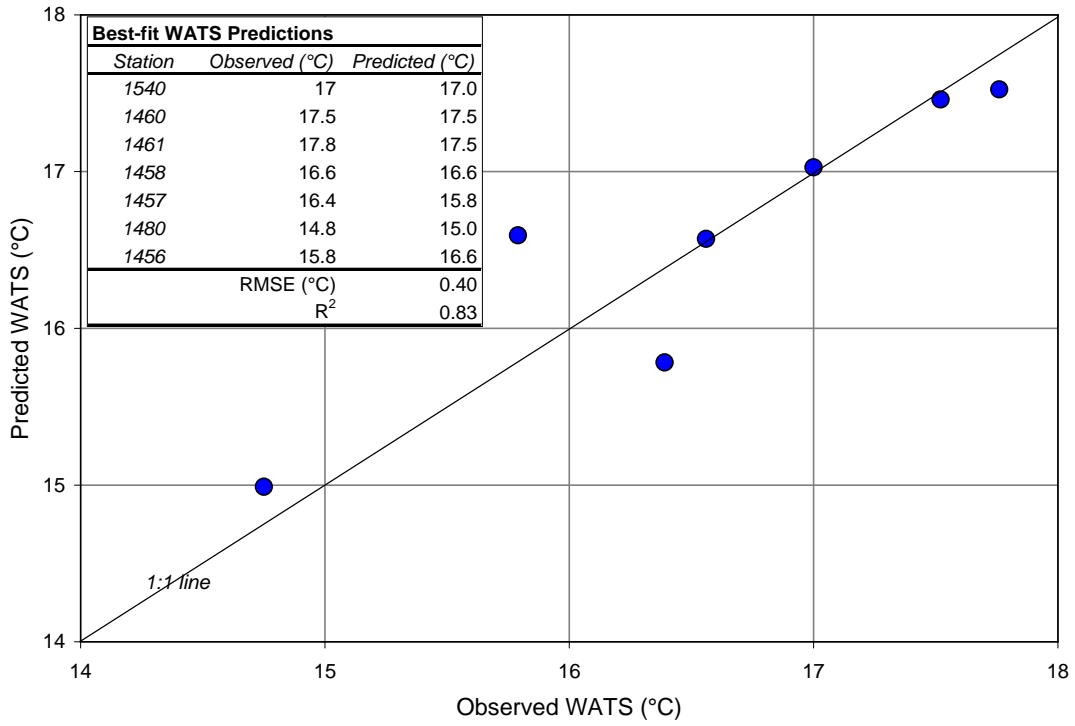
[1]WATS predictions generated for the week-ending July 31st, 1997

Figure 3.13   WATS (weekly average temperature) predictions for the week-ending July
31st 1997. Elder Creek, South Fork Eel River basin.
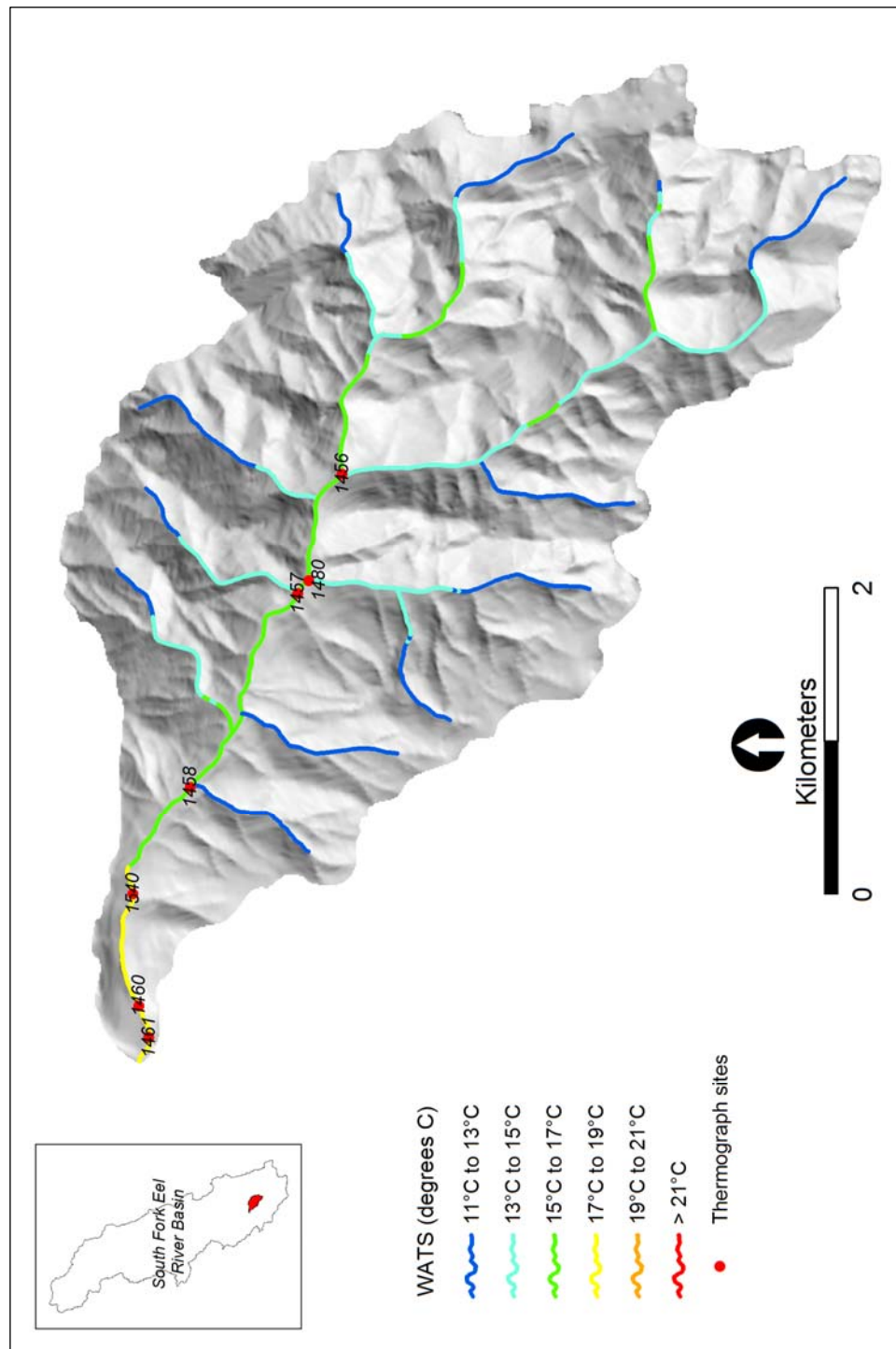
Figure 3.14   Rattlesnake Creek lithology[1]
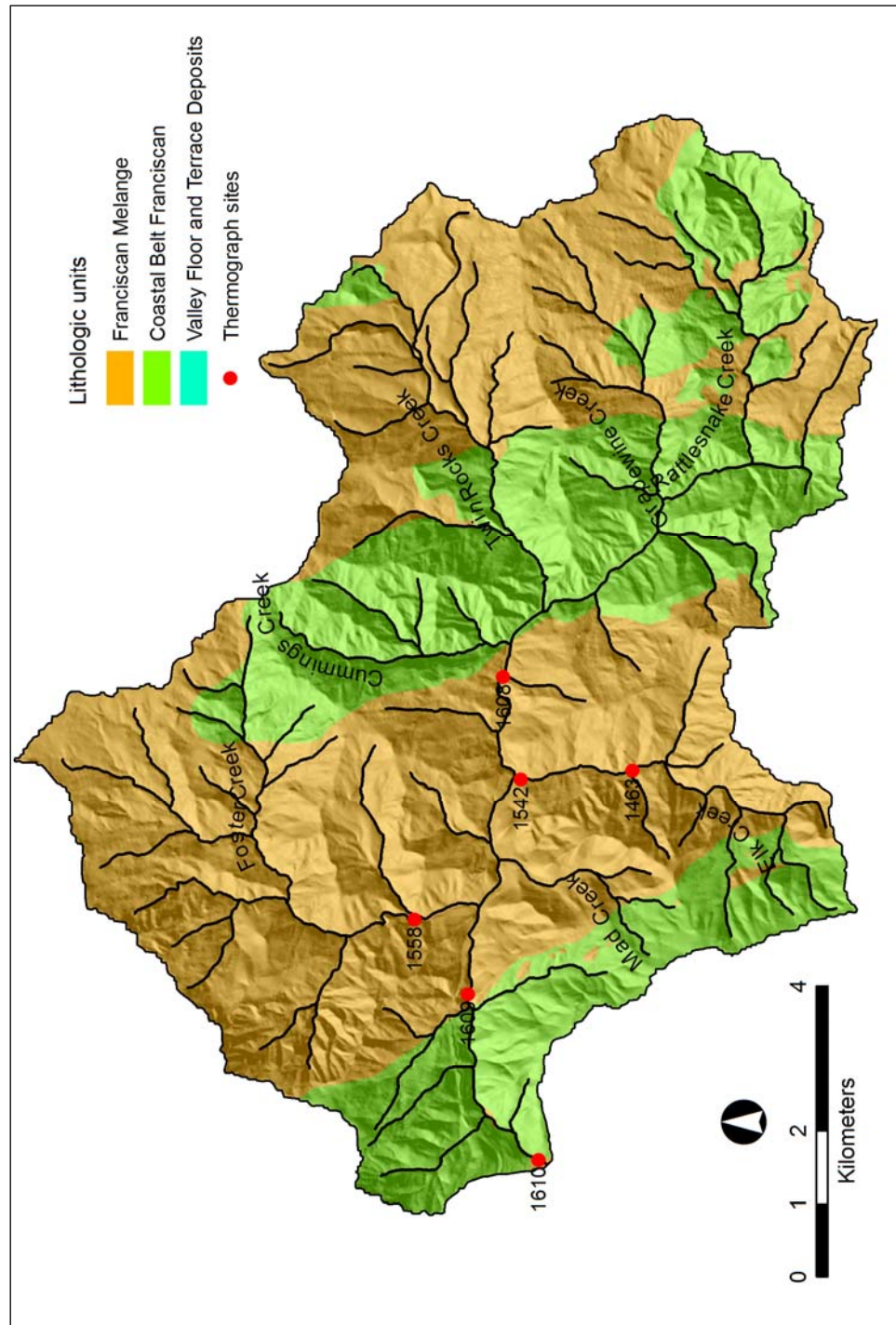
[1]Source: U.S. EPA (1999)

Figure 3.15   Solar radiation predictions for topography-only shade conditions,
Rattlesnake Creek
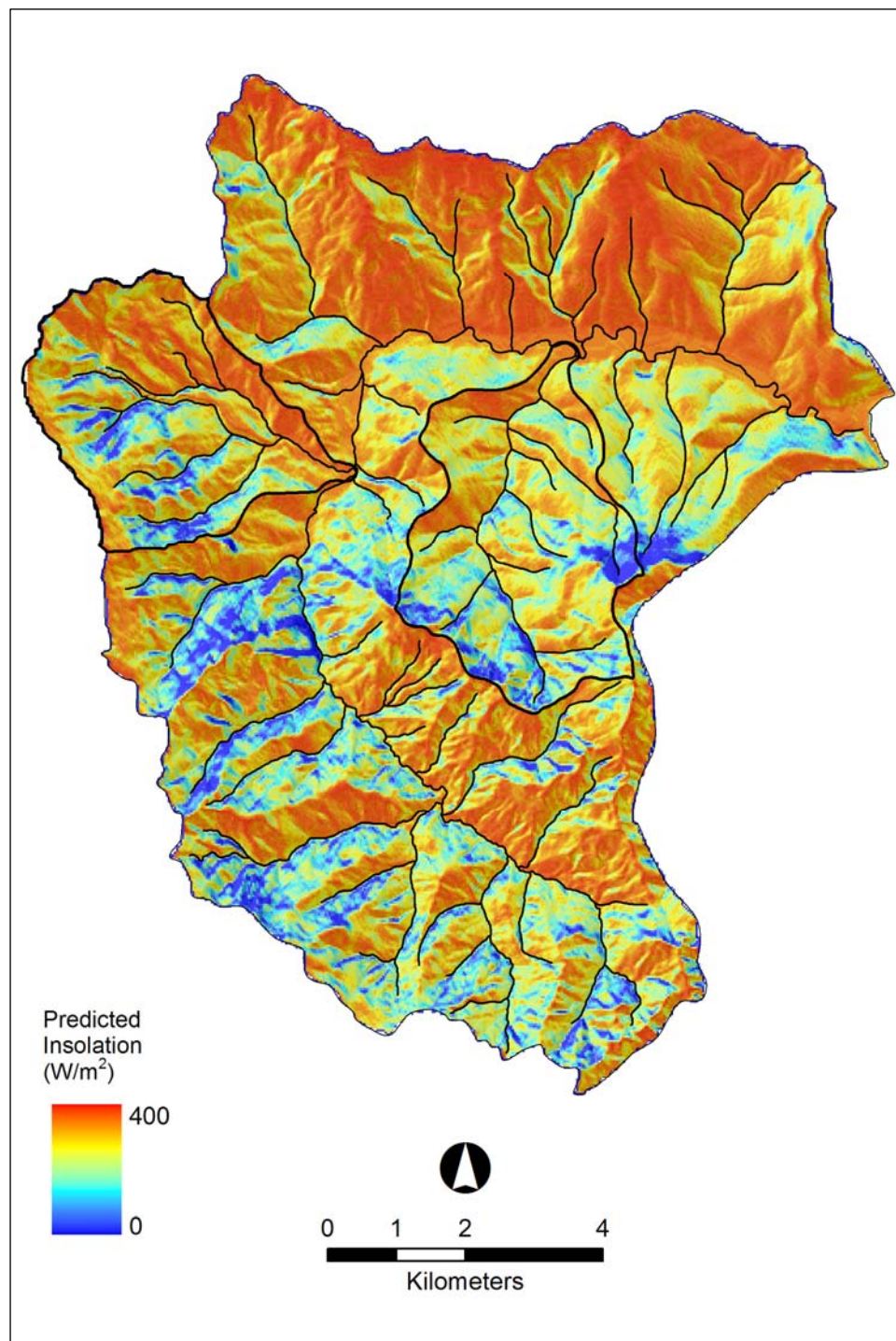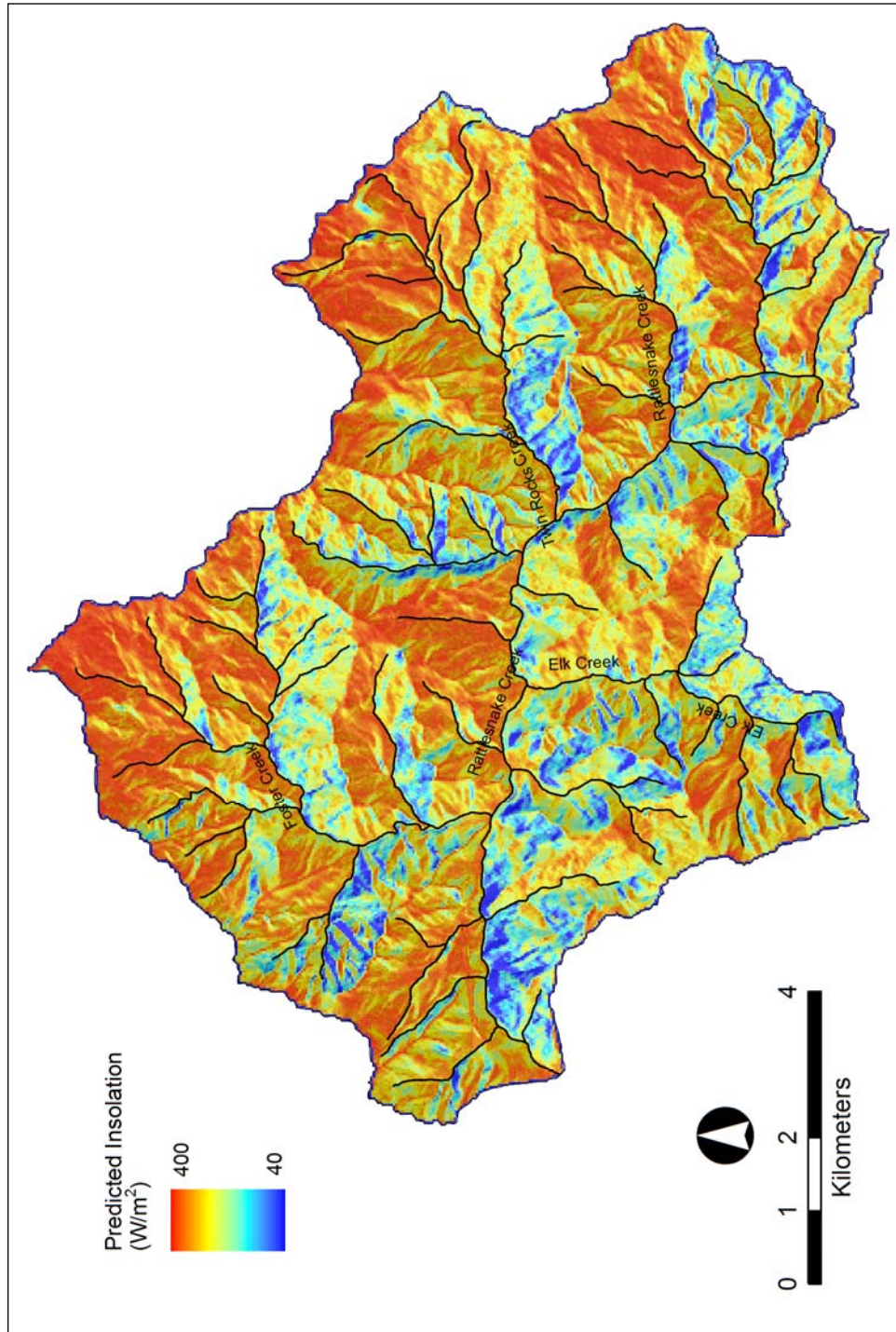
Figure 3.16   Solar radiation predictions for existing vegetation conditions, Rattlesnake
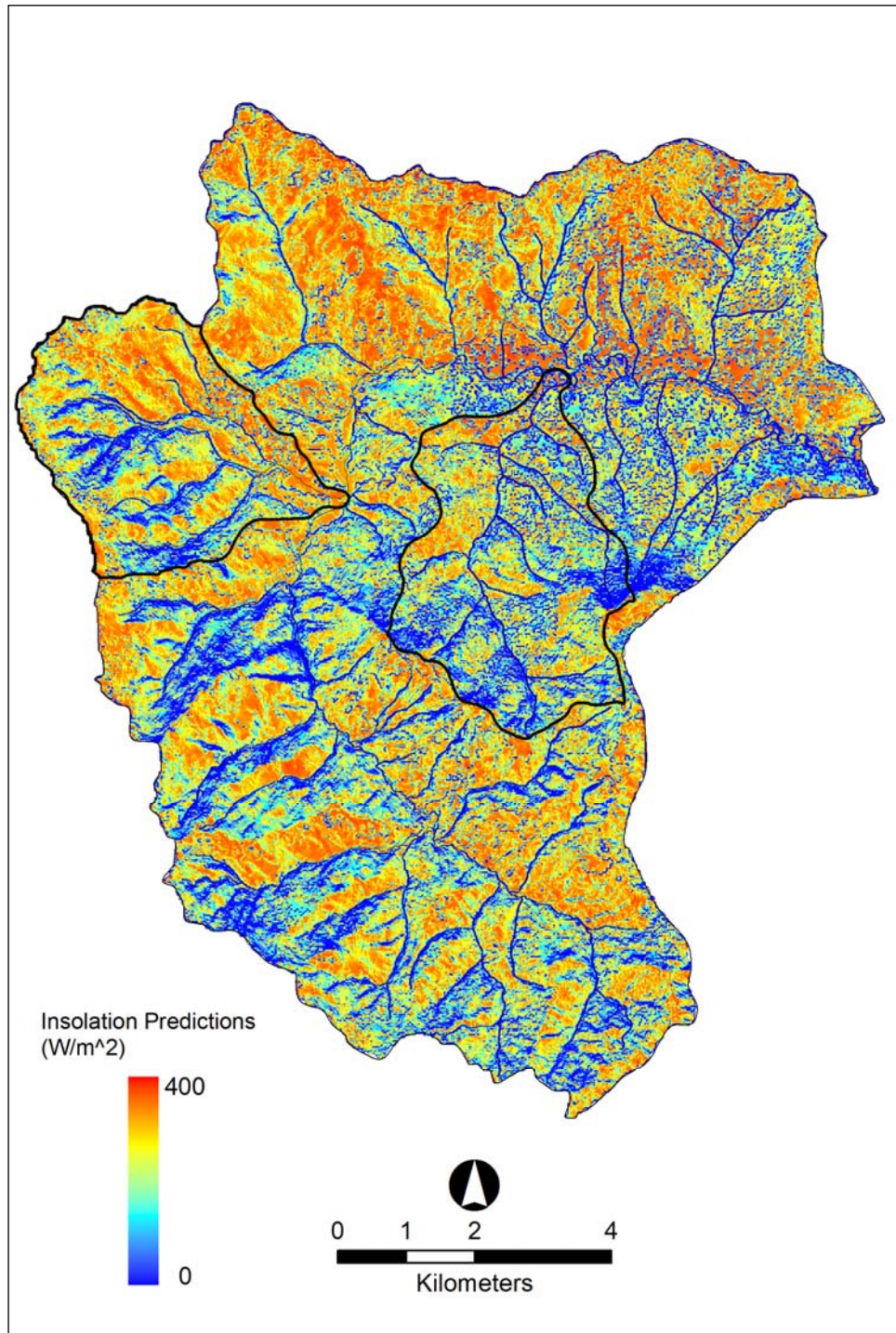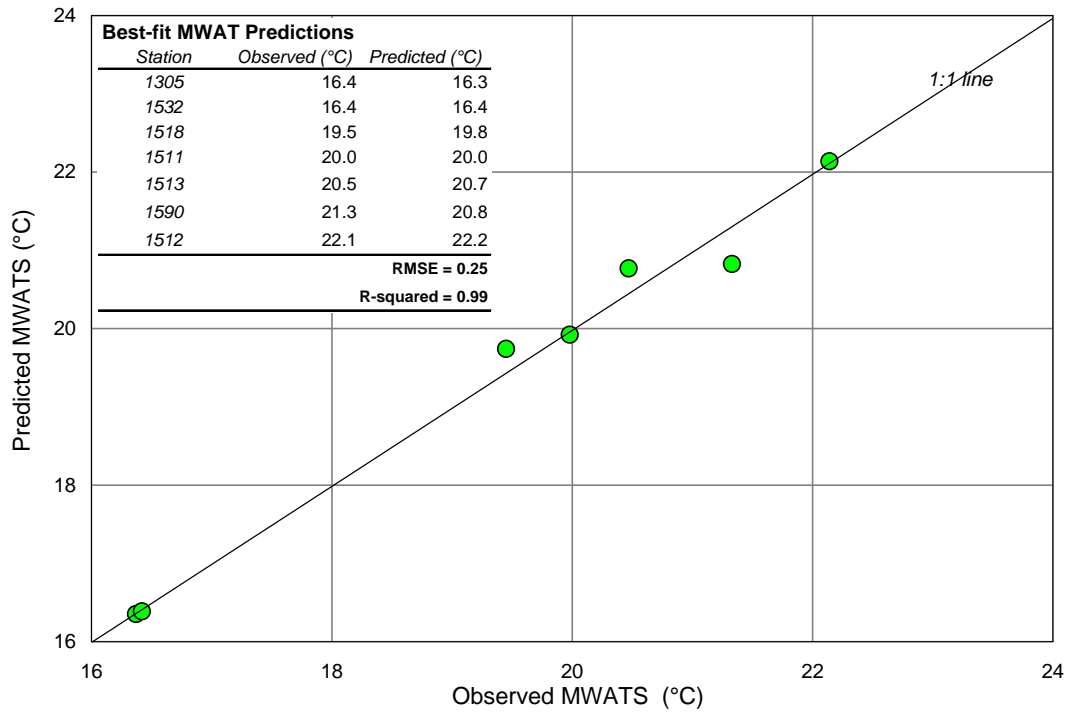Creek
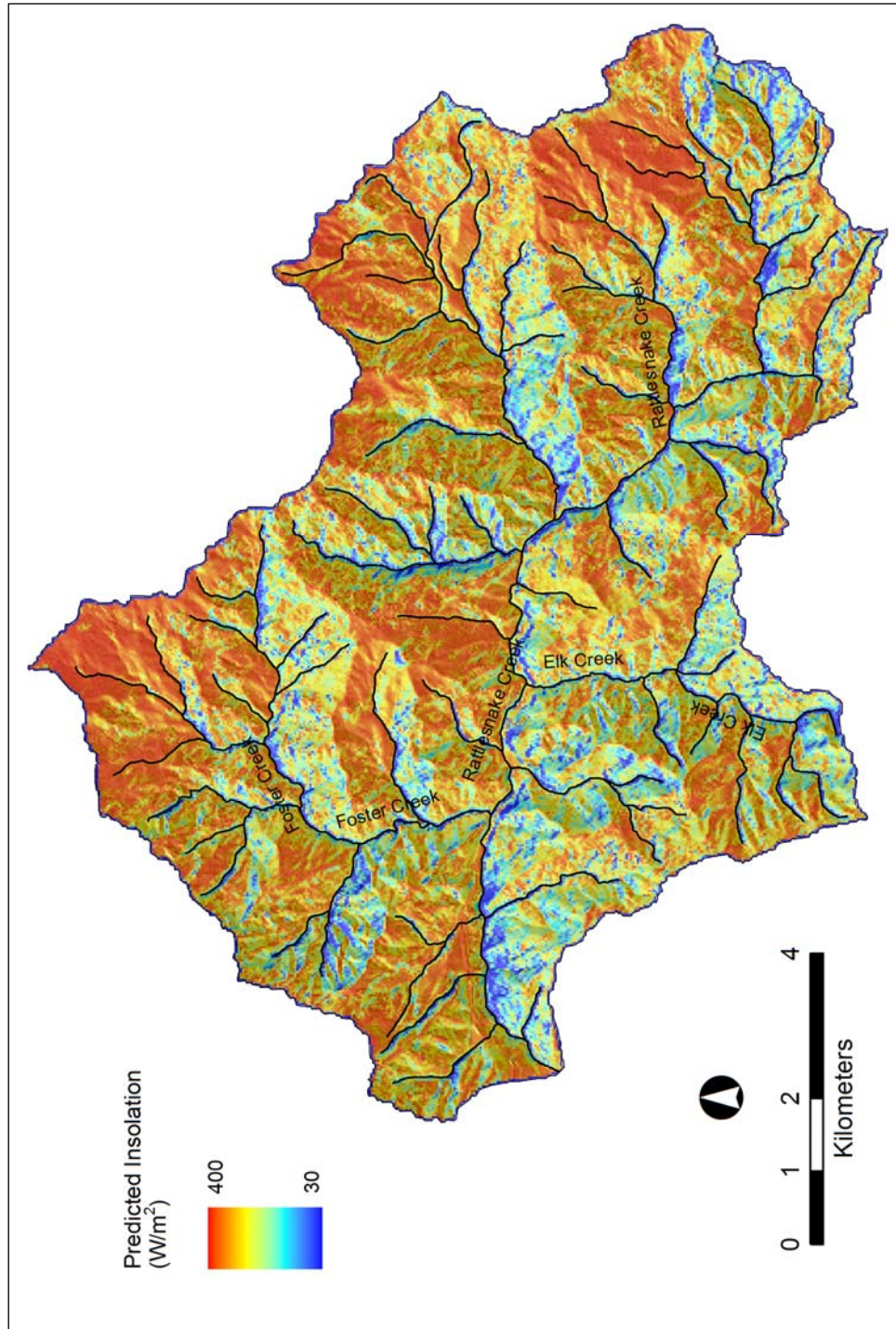
Figure 3.17   Observed versus predicted WATS (weekly average temperature)[1].
Rattlesnake Creek, South Fork Eel River basin

Station	Observed (°C)	Predicted (°C)
Best-fit WATS (weekly average temperature) predictions for the week-ending 7-31-97		
1558	19.8	19.9
1609	21.3	22.0
1542	20.4	20.0
1610	22.2	21.4
1463	19.5	19.4
1608	19.9	20.3
	RMSE (°C)	0.47
	R-squared	0.77
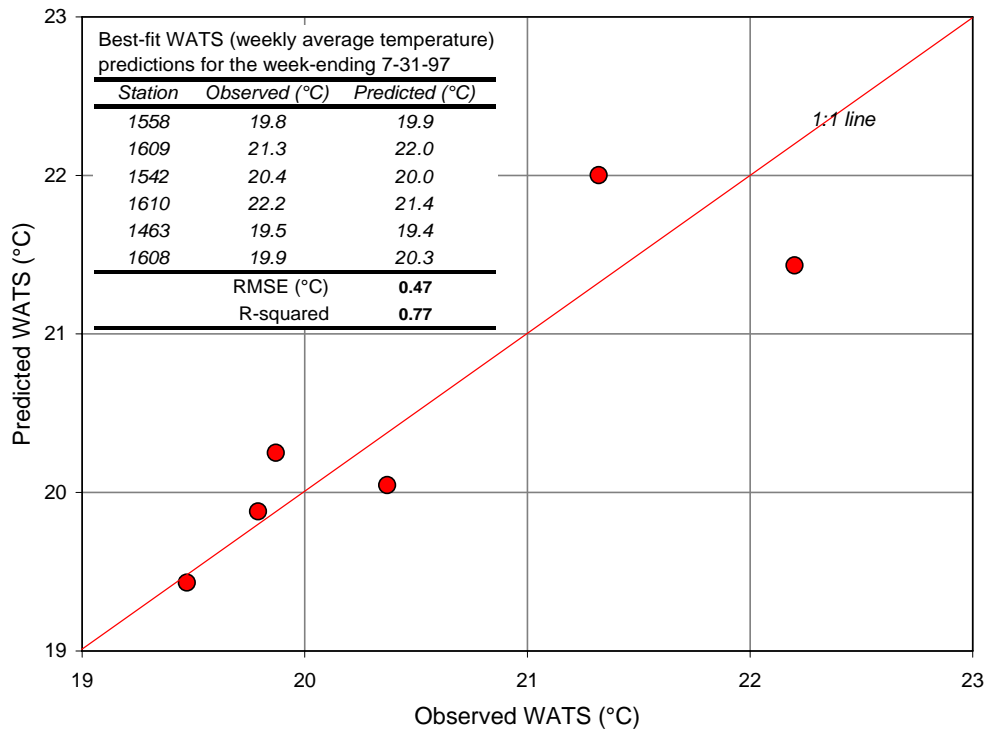
[1]WATS predictions generated for the week-ending July 31st, 1997

Figure 3.18   WATS (weekly average temperature) predictions for the week-ending July 31st 1997. Rattlesnake Creek, South Fork Eel River basin.

Figure 3.19   WATS (weekly average temperature) predictions overlain on mélange an
coastal belt Franciscan lithology for the week-ending July 31st 1997.
Rattlesnake Creek, South Fork Eel River basin. Overlying lithology.
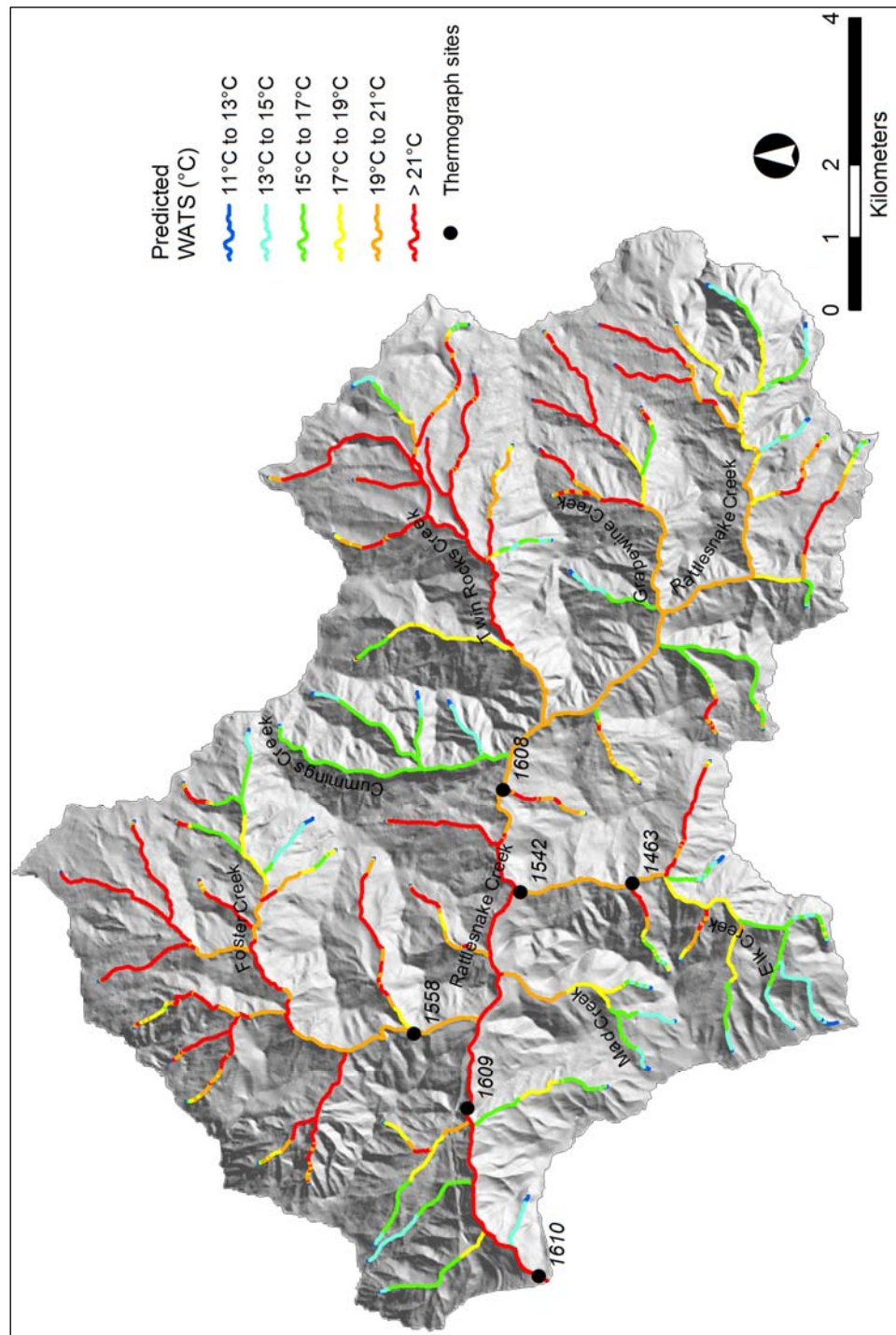
Figure 3.20   Combined observed versus predicted temperatures using observed
temperature data for all three South Fork Eel River sub-basins (Bull Creek
1996 MWATS, and 1997 WATS for Rattlesnake and Elder Creek)
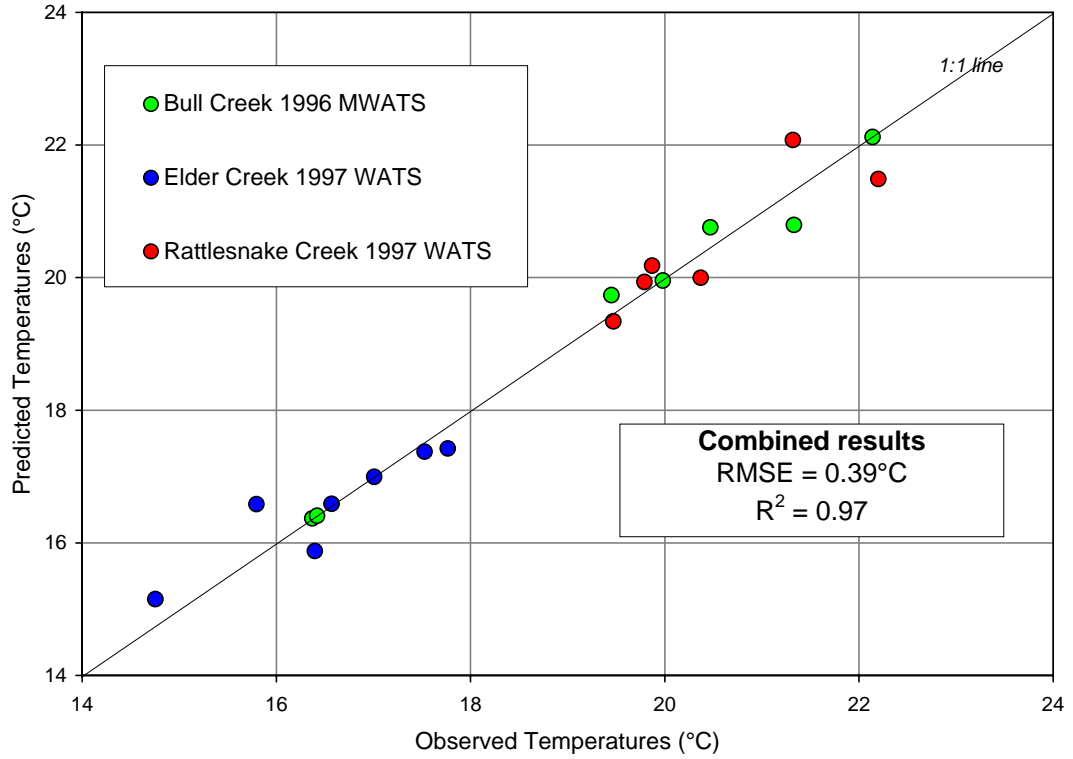
Figure 3.21   Change in predicted temperatures after *reducing* lowflow discharge by
50%. Bull Creek.
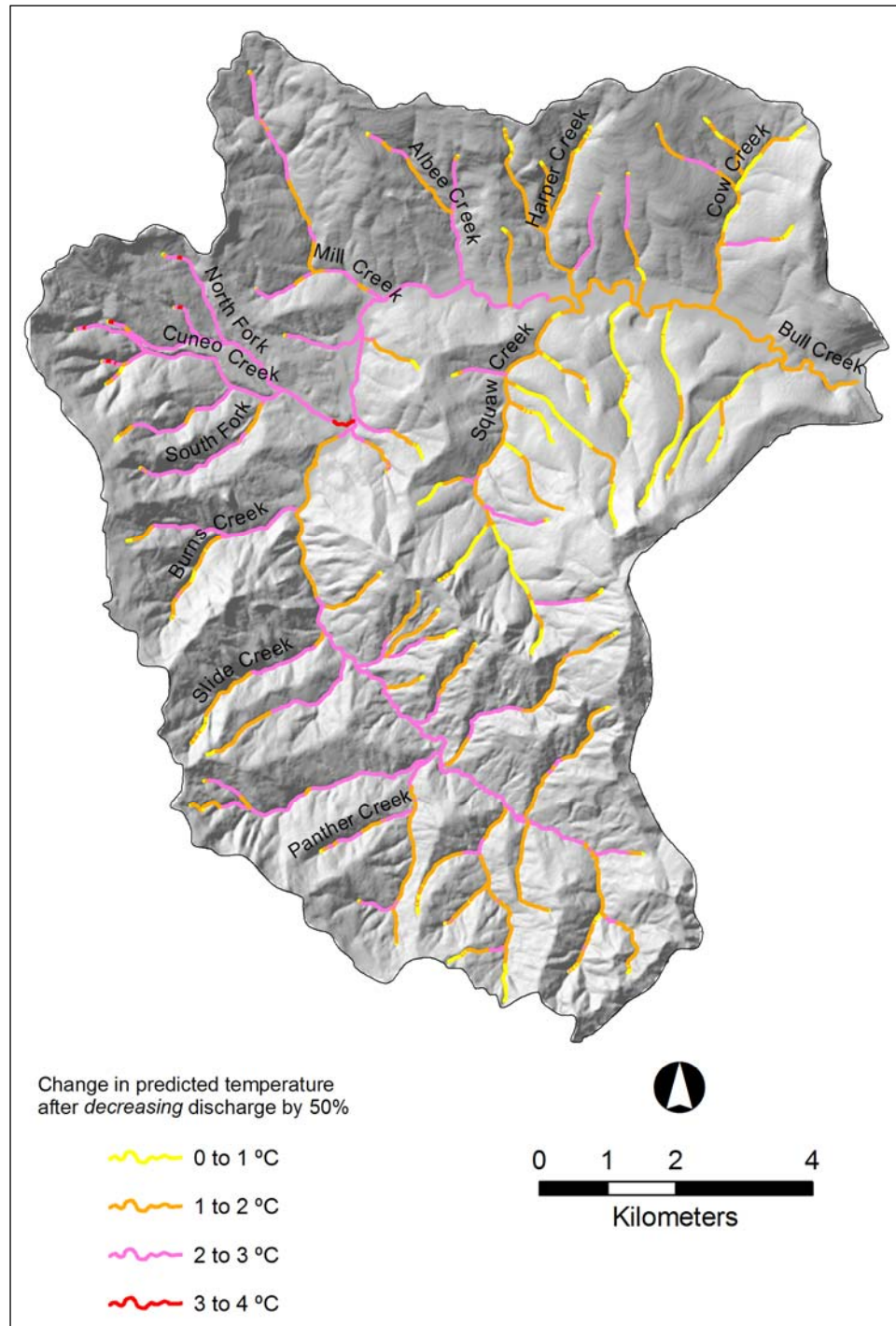
Figure 3.22   Change in predicted temperatures after *increasing* lowflow discharge by 50%. Bull Creek.
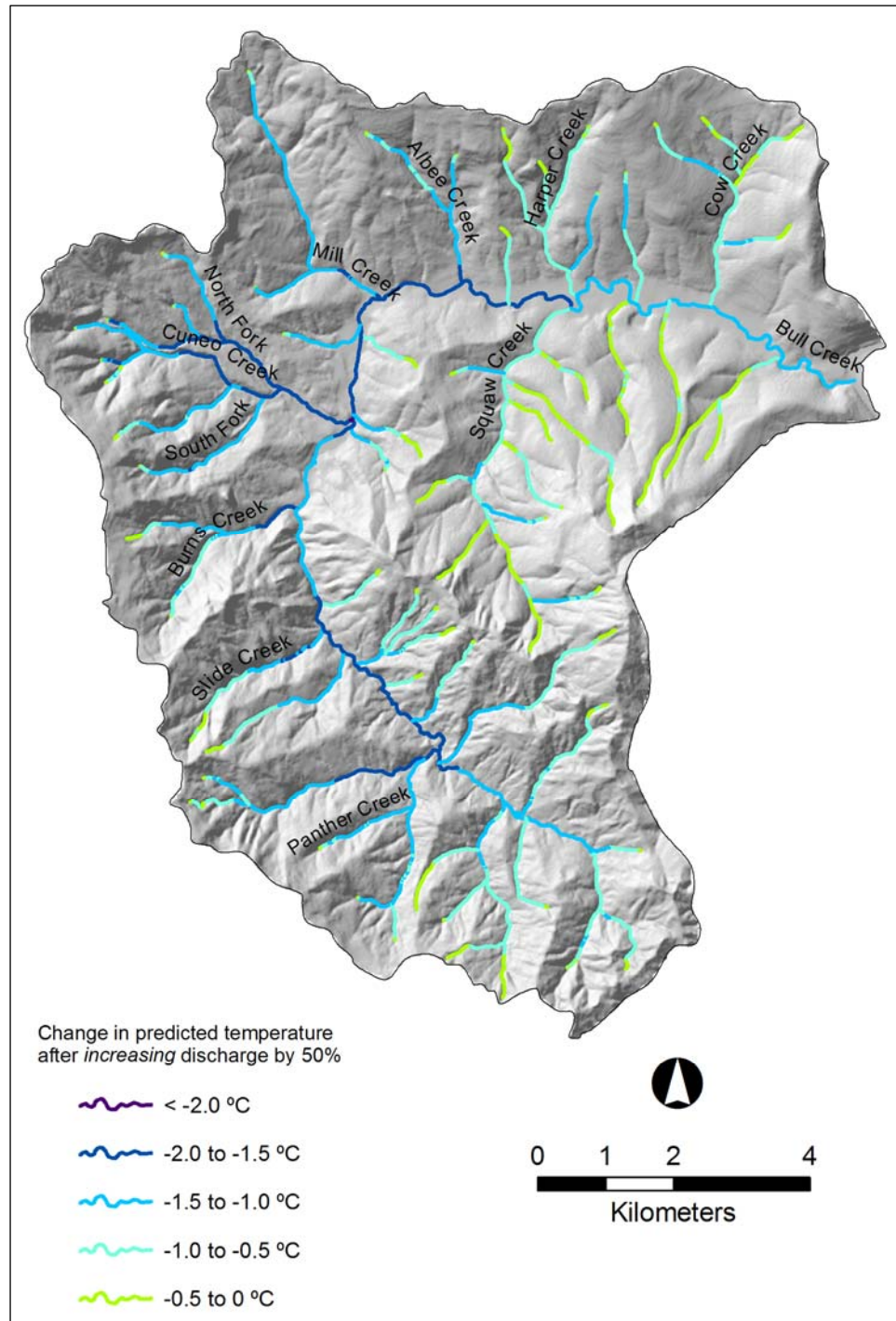
Figure 3.23   Bull Creek thermal long profiles: temperature effects of reducing (or increasing) flow by 25% and 50%
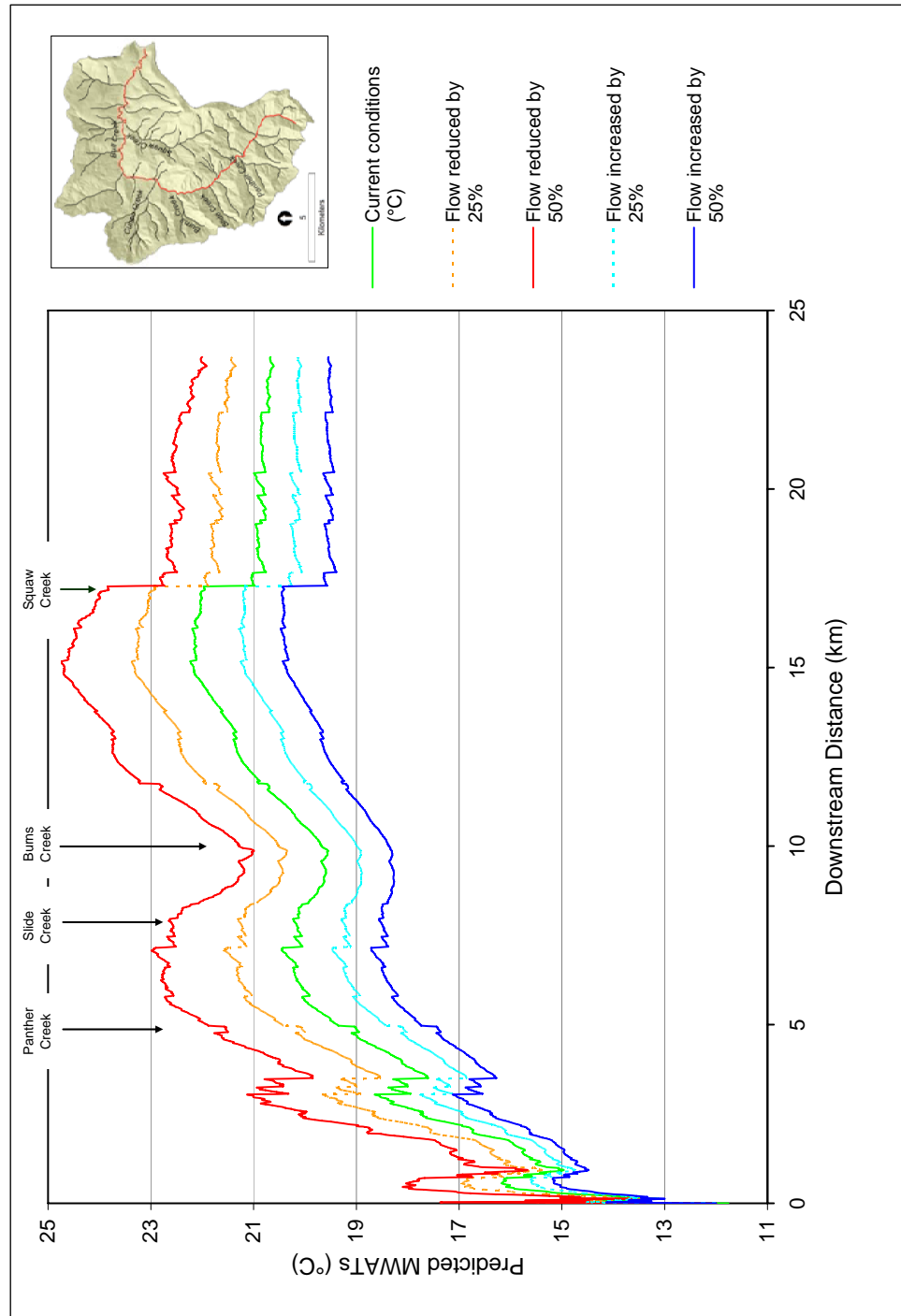
Figure 3.24   Squaw Creek thermal long profiles: temperature effects of reducing (or increasing) flow by 25% and 50%
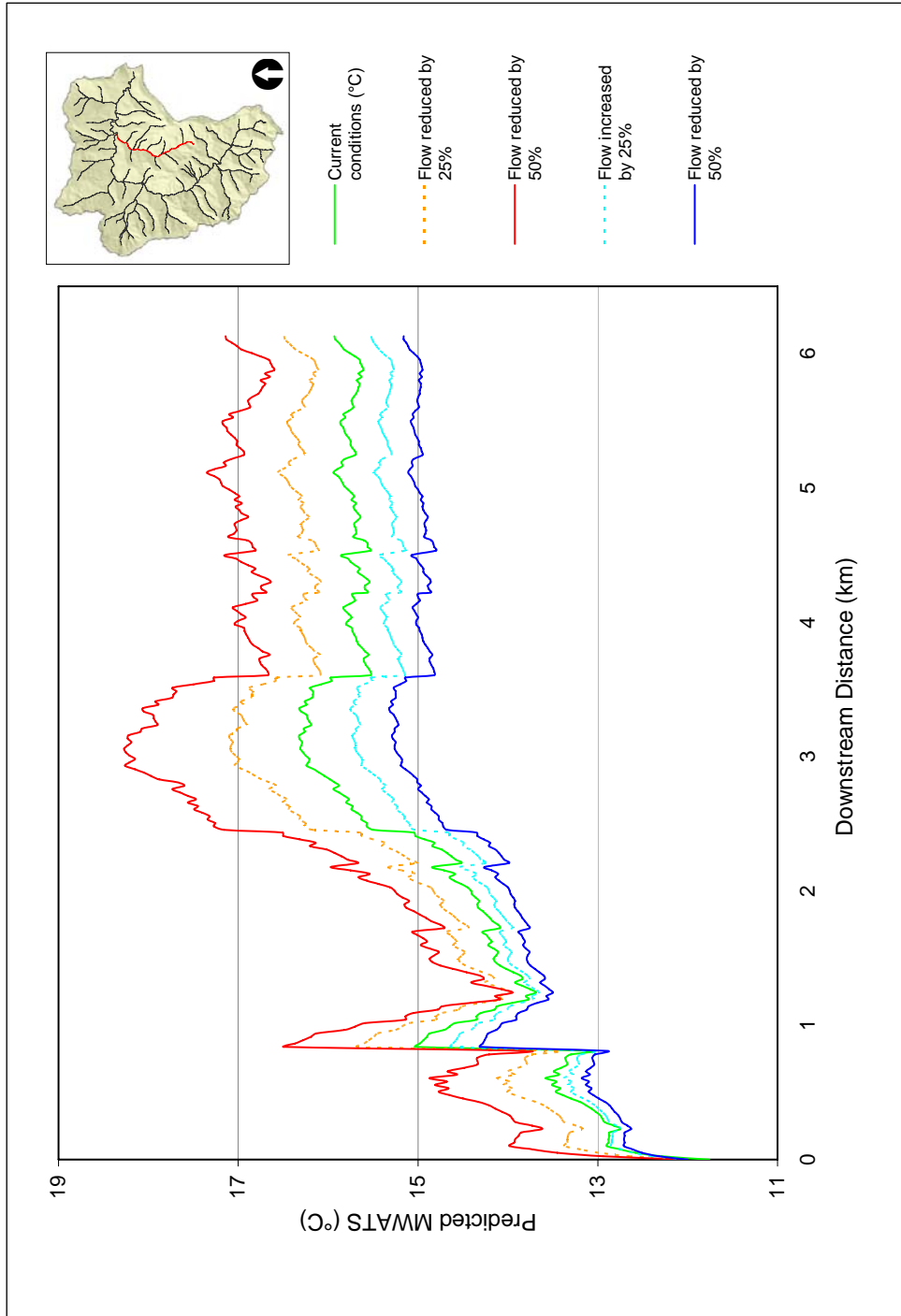
Figure 3.25   Cuneo Creek thermal long profiles: temperature effects of reducing (or
                increasing) flow by 25% and 50%
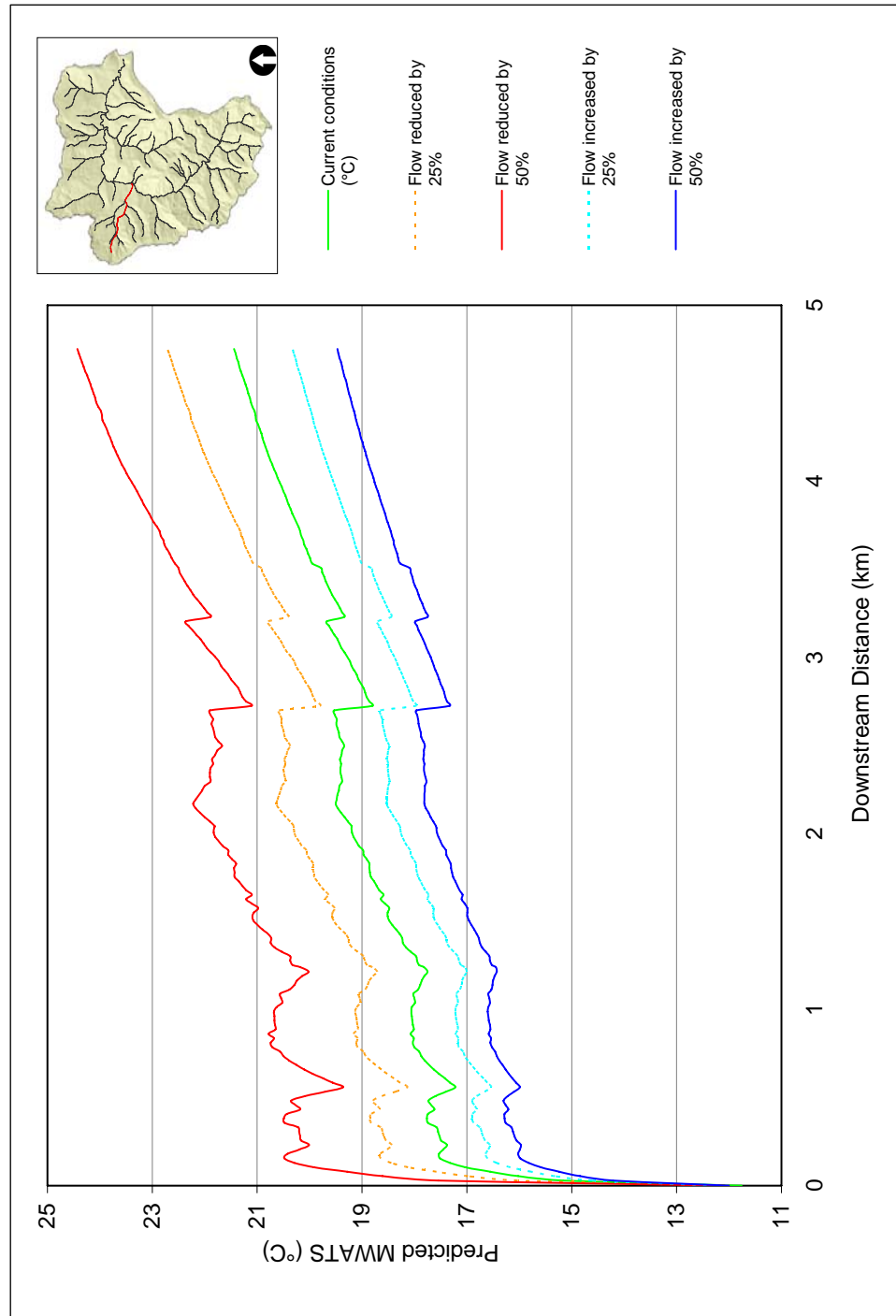
Figure 3.26   Observed versus predicted low-flow discharge. South Fork Ten Mile River, Mendocino County, Northern California
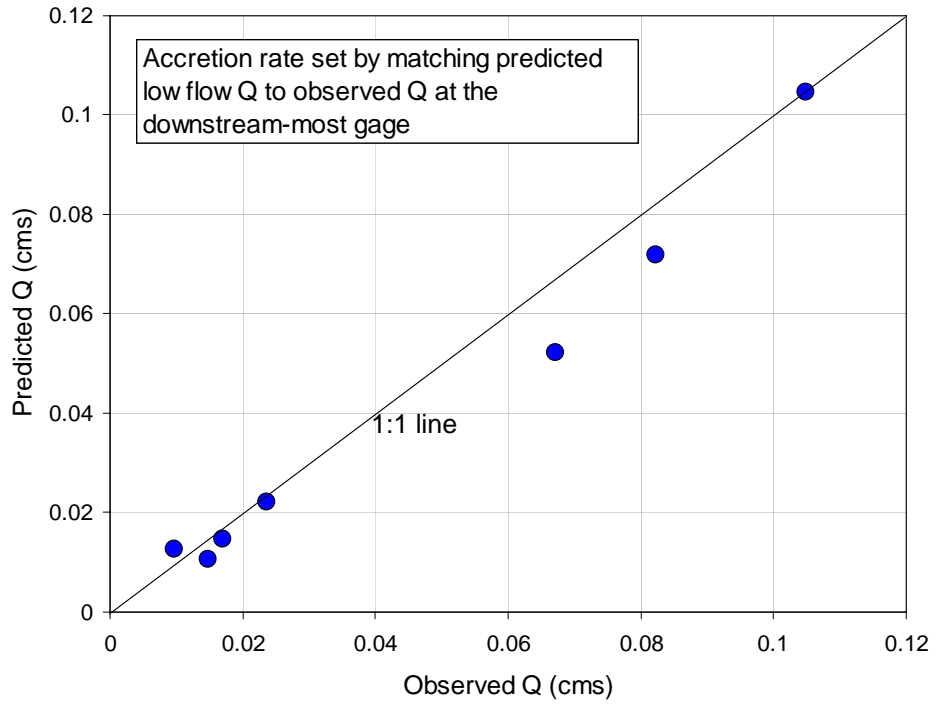
Chapter 4

Shade, discharge and temperature interactions

4.1 INTRODUCTION

In this chapter I explore through a series of model runs the influence of riparian forest management on stream temperature. I contrast the effect of vegetation removal throughout an entire watershed, with that caused by removal or addition of seral stage vegetation to just the headwaters of watersheds. The latter explores the possible downstream cumulative temperature effects (see Glossary, Appendix A) of different headwater shade scenarios. While there is general agreement about which mechanisms are responsible for summertime stream heating, vigorous debate persists over which factors predominate and whether elevated stream temperatures are cumulative and persist downstream. Finally I show how the effects of shading are magnified under low-flow conditions. I conclude that seral stage management of headwater riparian vegetation may be most important during dry years (the frequency of which is likely to increase with global warming).

Timber harvesting and riparian shade impacts

Most studies, both empirical and theoretical, strongly support the conclusion that direct solar radiation receipt in small stream channels is the most important mechanism responsible for stream heating, hence protection of riparian vegetation is argued to be essential (Beschta et al., 1987, Beschta and Wetherred 1984, Sansone and Lettenmaier 2001, Beschta, 1997). Several studies have measured diurnal temperature differences

between closed and open stands ranging from 3°C to 6°C (Brosofske et al. 1997, Spittlehouse et al. 2004, Chen et al. 1995). Brown and Krygier (1970) recorded diurnal temperature increases following harvesting of up to 15°C for small headwater streams in coastal Oregon. Johnson and Jones (2000) showed that following timber harvesting in three basins in the H.J. Andrews Experimental Forest, maximum temperatures increased by 7°C and occurred earlier in the summer. They reported increases in diurnal temperatures ranging from 2°C to 8°C (Johnson and Jones 2000). Johnson (2004) recorded temperatures downstream of small, artificially shaded stream in the H.J. Andrews Experimental Forest in the Oregon Cascades. While mean and minimum temperatures recorded in the study remained the same, maximum temperatures downstream of the artificially shaded reach were 1 to 3°C lower (Johnson 2004). A few studies have challenged the assumption that riparian shade is an essential control over summertime stream heating and instead suggest that a warm environment and ambient air temperature are more important (Larson and Larson 1996, 1997, Sullivan et al. 1990, Zwieniecki and Newton 1999).

Timber harvesting and downstream cumulative heating effects

Several studies have provided empirical and theoretical support demonstrating the importance of downstream cumulative heating effects. Beschta and Taylor (1988) reported increase of 6°C in the average daily maximum temperatures over a 30-year period in a forested Oregon watershed which over the same period experienced cumulative increases in timber harvesting. In a study of trout-bearing streams in Canada, Barton et al. (1985) showed that maximum average stream temperatures recorded over a

three week period were determined by the upstream extent of forested buffer strips. They

showed that removal of upstream vegetation resulted in elevated maximum stream

temperatures for 11 sampling sites. Shrimpton et al (2000) evaluated the role downstream

cumulative stream heating effects for small streams in central British Columbia and

observed that increased stream heat loading following upstream forest removal was

carried several hundred meters downstream.

Berman (1990), in a study of the Yakima River in Washington state, applied the

Tempest stream temperature model (Adams and Sullivan 1989) to characterize thermal

regimes historically tolerated by spring Chinook salmon and tested the effects of forest

practices on salmon viability. The results indicated that cumulative effects as a result of

upstream habitat degradation had the most significant affect on predicted stream

temperatures. Alteration in the model of upstream characteristics to reflect assumed post-

harvest conditions resulted in increases in predicted maximum temperatures of 6.5°C.

Bartholow (2000) applied the reach-based Stream Segment temperature model

(SSTEMP) to assess the role downstream cumulative effects. Model results showed a

2.4°C increase in mean daily temperatures downstream of a clearcut reach while

maximum predicted daily temperatures increased by 3.6°C downstream of a clearcut.

A handful of studies have challenged the concept of cumulative downstream

heating and suggest that local effects of clear-cutting or other disturbance are rapidly

ameliorated. Burton and Likens (1973) showed rapid recovery of stream temperatures

that flowed through clearcut reaches and then passed through fully forested reaches in the

Hubbard Brook Experimental Forest, although the authors could provide no explanation

for this recovery. Zwieniecki and Newton (1999) measured stream temperatures in

upstream 'clearcut' and downstream 'recovery' zones, and concluded that elevated

temperatures as a result of removing riparian shade upstream rapidly return to normal

trends in downstream 'recovery zones'. However, Johnson (2004) argued that the average

longitudinal temperature trend concept proposed by Zwieniecki and Newton were applied

to reaches which were far too short (150 to 300 meters) to compute 'average' temperature

trends. Caldwell et al. (1991) found no evidence of downstream cumulative effects in a

study of small stream in Washington State under a variety of vegetation conditions.

However, the sample size (n=9) used to generate their conclusions was very small

(NCASI 2001), while shade measurements were made using canopy densiometers which

have been shown to provide highly unreliable estimates of riparian shade (Ice 2001).

Understanding and quantifying the role and importance riparian shade effects on

stream temperature is important because of all the factors controlling stream

temperatures, riparian shade is most commonly altered by landuse and is the factor that

state and federal water quality regulators use when assessing temperature mitigation

strategies (EPA 1999, Poole and Berman 2001, Poole et al. 2001a). Furthermore most of

the watershed area and length of channel network (MacDonald and Coe 2007) is drained

by small, headwater channels which receive little or no protection under state Forest

Practice Rules. For example, Table 4.1 defines, and summarizes the level of protection

afforded to, Class I, II, and III streams in California. Class III channels, which typically

comprise most of the channel network, are provided minimal protection under current

California Forest Practice Rules (Ligon et al. 1999).

In this chapter, the stream temperature model, developed in chapter 3, is used to

quantify the affects of different riparian shade treatments on stream temperature

throughout the basin. The results from numerical experiments are presented for 'whole basin' and headwaters-only riparian shade scenarios. Results for the latter scenario offer important insights into the interaction of headwater riparian shade protection, land management impacts, and downstream temperature effects.

4.2 METHODS

Three kinds of numerical experiments resulting in 12 distinct runs were conducted to explore riparian management and stream flow effects on stream temperature (Table 4.3): 1) whole basin changes in vegetation (Runs 1 to 6); 2) only tributary (headwater) vegetation management (Runs 7 and 8); and 3) vegetation management (whole and headwater changes) in combination with increases or decreases in stream flow (Runs 9 to 12). All three basins in the South Fork Eel are used in the first set of Runs. I use the Bull Creek watershed to perform the second and third set of experiments because it is underlain by a single rock type and has been influenced by logging and park management practices. Furthermore, the model performance (as measured by the RMSE) for Bull Creek was the best among all three basins. These experiments explore the case where all the tributaries of the mainstem are either free of vegetation or bordered by tall, late seral stage trees. This is to be distinguished from the case in which just a portion of the headwater tributaries experience vegetation management. These latter simulations tend to typify the practice of providing mainstem channels riparian buffer strips while affording less protection to tributaries (e.g., Class III streams which are considered fishless and therefore less essential to protect, Table 4.1).

4.2.1 'Whole basin' shade provision (Runs 1 to 6)

Predicted temperatures were generated for two shade scenarios for all three South Fork Eel River watersheds: (1) a topography-only shade scenario, and (2) late seral (reference state) shade scenario. The topography-only scenario assumes no riparian vegetation anywhere and hence topography alone controls the amount of solar radiation

predicted to reach the stream surface. The late seral (reference state) scenario, assumes undisturbed conditions in the riparian zone and assigns late seral tree height values to streamside vegetation. The same diameter-at-breast height relationships (DBH) outlined in the first chapter were used to calibrate late the seral tree height model for the South Fork Eel River basins. Table 4.2 details late seral tree heights assigned to riparian vegetation. For the three South Fork Eel River sub-basins, where the dominant vegetation was grassland and shrubs in existing conditions, these areas were assigned mixed-hardwood tree heights. Figure 4.1 shows the assumed reference vegetation conditions for all three South Fork Eel watersheds

4.2.2 Headwaters shade provision (Runs 7 and 8)

Downstream cumulative effects were examined for Bull Creek alone. Two scenarios were tested: (1) a topography-only headwater shade scenario (Run 7), and (2) a full reference vegetation headwater shade scenario (Run 8). In the first scenario, no riparian shade (except for that provided by topography) was supplied to headwaters. The rest of the channel network was attributed with existing vegetation shade conditions. In the second scenario, headwater channels were attributed with full, reference vegetation shade (Table 4.2) while the rest of the channel network was attributed with existing vegetation shade conditions. The downstream cumulative effects tested by the two scenarios are limited to thermal effects alone. Headwater channels were defined using the Strahler stream order system (Strahler 1957). Bull Creek is a fourth order basin using 1:24,000 USGS blueline hydrography. All Strahler order one and two channels were assumed to comprise the headwater channel network (Figure 4.2). According to this

Strahler stream order criteria headwater channels drain 81% of the Bull Creek basin area and comprise 85% of the total length of channel. Both are consistent with values proposed by MacDonald and Coe (2007).

4.2.3 Flow adjustments (Runs 9 to 12)

A 50% flow adjustment (both increase and decrease) was applied to 'whole basin' and headwater shade scenarios to Bull Creek. Bull Creek was calibrated using lowflow discharge data from the USGS Weott gage for the end of July, 1996. Flows for that period were very comparable (approximately 12% greater) to the long term average flows (1961-2007) recorded at the Weott gage. Reducing (or increasing) flow by 50% offers the opportunity to explore temperature effects of drought and high flow. Furthermore both a 50% increase and decrease in flow are well within the maximum and minimum flows recorded at the Weott gage (Table 2.1).

4.3 RESULTS

Table 4.2 summarizes the results of the 12 runs conducted and Figures 4.3 to 4.15 display the findings on maps. Below I describe the detailed findings for each Run.

4.3.1 Bull Creek: whole basin shading effects (Run 1 and 2)

The spatial distribution of predicted temperature change for topography-only shade conditions are shown in Figure 4.3 and summarized in Table 4.2 (Run 1). Temperature changes (relative to current conditions) of up to 5°C are apparent for North-South oriented tributaries in the Northwest portion Bull Creek. West-to-East oriented channels in the Western portion of the basin also show increased temperatures but no more than 2 to 3°C. Most of the mainstem Bull Creek show temperatures increasing by 2 to 3 °C. Downstream of the Squaw Creek confluence, predicted temperatures show substantial warming, with a change of up to 5°C down at the mouth. In contrast (Run 2), predicted temperatures for the reference shade scenario shown in Figure 4.4 show cooling throughout the basin but the magnitude of change is significantly less than with the relative warming under the topography-only scenario. The spatial pattern of temperature change for reference shade provision shows only modest reductions in temperature for tributaries in the Northwest portion of the basin (Squaw, Harper, and Cow Creeks). Predicted temperatures for tributaries in the Western portion of the basin (Cuneo, Mill, and Burns Creek) show more significant temperature reductions (up to 2.5°C). Predicted temperatures for the mainstem Bull Creek are lower everywhere by at least 1.5°C, and downstream of the Slide Creek, down to Albee Creek, temperature reductions of at least 2.5°C are achieved.

Thermal longitudinal profiles plotted for all three shade scenarios (existing conditions, reference conditions, and topography-only) are shown for the mainstem Bull Creek (Figure 4.5), Cuneo Creek (Figure 4.6), and Squaw Creek (Figure 4.7). All thermal profiles show characteristic asymptotic forms, warming up quickly and continuing to warm but at reduced rates downstream. Contributions from cooler (or warmer) water from tributary inflows are apparent, especially for the existing vegetation and reference vegetation shade profiles. For the mainstem Bull Creek, temperatures warm downstream for all three scenarios, but at different rates (Figure 4.5). Predicted temperatures for topography-only (Run 1) continue to increase down through the entire profile. By contrast, temperatures level off for both the existing conditions and reference shade scenarios. The thermal dilution effects provided by Squaw Creek (approximately 17 km downstream) are very apparent for the existing vegetation conditions, less so for reference conditions, and almost non-existing for topography-only shade conditions (Figure 4.5).

Thermal profiles for Cuneo and Squaw Creeks demonstrate the temperature effects of existing shade conditions and the impacts of different shade scenarios. For Cuneo Creek (Figure 4.6), the strong similarities between the topography-only and existing vegetation shade scenarios suggests shade provision under current conditions is generally absent. Thermal profiles for existing conditions and reference conditions for Squaw Creek (Figure 4.7) are almost identical, demonstrating that current condition shade provision is at or near reference. An even more striking result is revealed for topography-only shade provision for Squaw Creek (Figure 4.7), which shows an initial

rapid rise in temperature within the first 1 kilometer, and then continues to increase, exceeding 21°C at the downstream-most end.

4.3.2 Elder Creek: 'whole basin' shading effects (Run 3 and 4)

Predicted temperatures for topography-only shade provision are shown in Figure 4.8a (Run 3). The magnitude of temperature increase is comparable to Bull Creek. Mainstem temperatures increase everywhere by at least 3°C, and by more than 4°C down at the mouth. Even for small North-South oriented tributaries where terrain shade effects should be greatest, temperatures increase by up to 3°C. Predicted temperature change for reference shade provision (Run 4) shows only modest cooling (Figure 4.8b). Mainstem Elder Creek temperatures decrease by no more than 1.5°C, while most of the mainstem decreases by 1°C. Tributary temperatures show even more limited temperature reductions. Thermal profiles for the three shade scenarios for Elder Creek are shown in Figure 4.9. The shape of each profile is very similar to Squaw Creek thermal profiles shown in Figure 4.7. Elder Creek thermal profiles for existing conditions and reference vegetation conditions are almost identical, demonstrating that existing vegetation shade conditions are close to full reference shade conditions. As with Squaw Creek, the topography-only thermal profile for Elder Creek (Figure 4.9) shows rapid initial temperature increase and continues to increase down through the profile, exceeding 21°C at the mouth.

4.3.3 Rattlesnake Creek: 'whole basin' shading effects (Run 5 and 6)

Predicted temperature changes for the topography-only shade scenario (Run 5) are shown in Figure 4.10. Temperatures increases of up to 5°C occur for some tributaries. Foster Creek for example, shows an increase of more than 5°C down towards the mouth. However, Foster Creek headwaters which are oriented East-to-West indicate temperature increases of only 2 to 3°C, compared to the North-South oriented downstream end. Strong orientation-led warming of up to 4°C is also apparent along Elk Creek. Cummings Creek is also largely North-South oriented but the tributary flows through Coastal Belt Franciscan lithology. As a result, the higher modeled groundwater seepages for this terrain results in temperature increases of no more than 3°C at the downstream end of Cummings Creek. Predicted temperatures for the mainstem Rattlesnake Creek increase everywhere by at least 2 to 3°C, but by up to 4°C downstream of tributaries draining through mélange terrain.

Predicted temperature changes for reference shade conditions (Run 6) are shown in Figure 4.11. The magnitude of change for this scenario is similar to the topography-only scenarios. Reductions of up to 5°C are predicted for several headwater reaches associated with mélange terrain. However, reductions of only to 2 to 3°C are achieved for the mainstems for these tributaries (which include Foster Creek, Elk Creek, and the headwaters of Rattlesnake Creek). For tributaries draining Coastal Belt lithology, notably Cummings Creek, temperatures decrease by up to 2°C, but for most of the Cummings Creek tributaries, temperatures decrease by no more than 1°C.

Thermal long profiles for the three shade scenarios for Rattlesnake Creek are shown in Figure 4.12. All three profiles show the characteristic asymptotic form and each

119

profile shows rapid heating within the first 1 kilometer. The topographic-only shade profile (Run 5) continues to warm downstream, while both the existing condition and reference shade profiles show significant cooling between 1 to 2 kilometers before continuing to warm downstream. Reference shade conditions (Run 6) results in significant downstream cooling compared to the topography-only shade profile. At the downstream-end of Rattlesnake Creek, predicted reference shade temperatures are more than 5°C lower than topography-only temperatures.

4.3.4 Bull Creek: downstream cumulative effects (Run 7 and 8)

Thermal profiles for two Bull Creek headwater (Figure 4.2) shade scenarios (Figure 4.13) show results for: (1) all tributary (headwater) channels assigned topography-only shade (Run 7), and (2) all tributary assigned reference shade tree heights (Run 8). Predicted temperatures follow the same general pattern of downstream temperature variation predicted for the existing shade conditions (Figure 4.13). The magnitude of increased warming (topography-only headwater shade scenario (Run 7)) is more significant than cooling (reference shade headwater scenario (Run 8)) within the first 10 kilometers and in the final 5 km. Downstream of the 10 kilometer mark there is slight convergence of the profiles, although below a major tributary and where current vegetation enters nearly reference conditions, the topography-only profile stays relatively warm as compared to current or reference conditions (Figure 4.13). For the reference headwater scenario, downstream cooling effects are relatively small. The difference between existing and reference shade profiles down toward the mouth is less than 1°C. Cumulative downstream warming is more apparent for the topography-only headwater

shade scenario. The difference in temperature between existing and headwater topography-shade is initially about 2°C but down at the mouth is slightly more than 1°C.

4.3.5 Bull Creek: whole basin and downstream cumulative shade and discharge effects

Thermal profiles along the mainstem Bull Creek for combined discharge and shade effects are shown for 'whole basin' (Figure 4.14, Run 9 and 10) scenarios and headwater scenarios (Figure 4.15, Run 11 and 12). These are compared to the thermal profile for current shade conditions and characteristic low flow used throughout the dissertation. As summarized in Chapter 3, the predicted current condition stream temperature profile rises quickly up to about 5 km and then drops downstream of Slide Creek (8 km) where the mainstem passes through a narrow, confined, north-south oriented valley. Downstream of Burns Creek (10 km), the mainstem emerges out on to a flood plain and predicted temperatures rise accordingly (Figure 4.15), before mainstem cooling downstream of the well-forested Squaw Creek confluence (approximately 17 km) causes an abrupt drop in temperature of about 1°C. The whole basin and tributary (headwater) vegetation changes combined with increases and decreases of discharge of 50% greatly influences the stream temperature locally, but the general pattern seen in the current conditions is mostly preserved (Figures 4.14 and 4.15). Note that here and in what follows, we will discuss warming or cooling relative to current conditions.

Whole basin vegetation removal (topography-only shade) combined with a 50% *reduction* in discharge causes the largest increases in stream temperature (Run 9a). The mainstem would quickly be 5°C warmer than current conditions. This difference persists,

even as the mainstem passes through the shaded narrow canyon at 8 km, and increases to about 7°C by the mouth.

The combination of whole watershed vegetation removal and a flow *increase* by 50% shifts the profile by about –5°C relative to the low discharge case (Run 9b versus 9a). This drop causes the warming to be a maximum of about 2°C upstream of the 5 km mark, and to differ little with current conditions from there until Squaw Creek. The cooled water coming in from Squaw Creek under current conditions drops the current temperature, but this cooling is not reproduced even with the increased discharge for Run 9b, hence the relative warming grows to almost 3°C. Surprisingly, the increased flow dampens out the relative cooling caused by flow through the narrow canyon at 8 km.

Full reference shade conditions combined with a 50% flow *decrease* causes in the first 5 km a compensating effect and there is little net difference in temperature relative to current conditions (Run 10a). Further downstream, despite the reduced flow, the mainstem is cooler by 1 to 2°C relative to current conditions due to full mainstem reference shading. This difference disappears once Squaw Creek flow enters the mainstem.

Full reference conditions combined with a 50% *increase* in flow causes the largest relative cooling, dropping by 3°C by 5 km and reaching about –3°C (relative to current conditions) just before Squaw Creek (Run 10b). As in the topographic-shade only case, with increased flow the cooling caused by flow entering the narrow canyon at 8 km in the reference shade case is also relatively minor.

These whole basin experiments show that temperature changes due to increases or decreases in shading can be compensated by decreases or increases in flow such that the

122

net temperature change is minor. If shading and flow both increase or decrease, however, large net temperature changes occur.

Vegetation removal (shade only) conditions in the tributaries (headwater case) and a 50% *decrease* in discharge (Run 11a) causes up to 7°C of warming upstream of 5 km, but then the difference declines to approximately 3°C for the rest of the profile. Interestingly, absolute temperatures decline for approximately the last 10 km of the profile. Hence, compared to the whole basin shade removal, the warming is the same initially, and then is significantly less (more than 4°C) down towards the mouth (Run 11a versus Run 9a).

Vegetation removal (shade only) conditions in the tributaries and a 50% *increase* in discharge (Run 11b) results in less warming within the first 5 km (maximum of about 2°C) which drops to zero difference at 5 km and then progressively shifts to relative cooling of about 1°C before the entrance of Squaw Creek.

Reference vegetation in the tributaries and *reduced* flow by 50% (Run 12a) is generally compensating (although fluctuations of at least 2°C are apparent) upstream of 5 km, but further downstream the relative warming climbs to about +2°C before the Squaw Creek confluence. In contrast, reference shading in the tributaries and *increased* flow by 50% (Run 12b) causes a 3°C cooling by the first 5 km, which narrows slightly before Squaw Creek.

Comparison of these runs shows that when 'signs' are the same on the change (i.e. reduced vegetation and reduced flow, or increased vegetation and increased flow) the response of the stream temperature is similar for the whole basin and headwater vegetation manipulations. When vegetation is eliminated and flow is reduced by 50%

(Runs 9a and 11a), average stream temperature dropped by about 5 to 6°C for the whole basin and 4 to 5°C for the tributaries only. When full reference vegetation and with a 50% increase in flow (Runs 10b and 12b), then the whole basin stream temperature was 3 to 4°C cooler and the reference tributary shading (with the 50% increase in flow) gave 2 to 3°C cooler.

The opposing effects in vegetation and discharge lead to opposite signs in predicted stream temperature for whole versus headwater manipulations. When whole basin vegetation was removed, but the discharged was increased by 50% the stream became slightly *warmer* (Run 9b), whereas when the vegetation was removed just on the tributaries (but with increased discharge) (Run 11b) the stream was slightly *cooler* (after the first 5 km). Similarly, when the whole basin was fully vegetated but the flow was reduced by 50% (Run 10a) downstream of the first 5 km the stream was 1 to 2°C *cooler*, but when the just the tributaries were fully vegetated with this flow, the stream beyond 5 km (Run 12a) was about 2°C *warmer*. It appears this difference in sign is due to the shading effects on the mainstem. Removal of all vegetation includes that along the mainstem, hence even with increased discharge there is still warming due to this reduced shading. Similarly, addition of reference vegetation to the entire watershed including the mainstem caused cooling even at reduced flows whereas if just the tributaries had reference vegetation this was not enough to compensate for the reduced flows, and mainstem warming is predicted.

4.4 DISCUSSION

Model predictions for all three basins for the different shade scenarios strongly demonstrate the temperature benefits of tall trees, even for areas which are already in near reference state conditions (for example, Elder Creek, and Squaw, Cow, and Harper Creeks with the Bull Creek basin). For 'whole basin' reference vegetation shade, the magnitude of temperature reduction ranges from 0.5 to 3°C, with the higher reductions associated with areas where little or no existing shade exists (e.g. Cuneo Creek in the Bull Creek basin).

Removal of all vegetation results in significant increases in temperatures for all three South Fork Eel basins, although the distribution of temperature increase is not uniform. The magnitude of predicted temperature increase is more than 5°C for areas which are characterized by late seral vegetation (Elder Creek, three Bull Creek tributaries (Squaw, Cow, and Harper Creeks)). Similar increased temperatures are also predicted for two tributaries in Rattlesnake Creek (Foster and Elk Creek), both of which were already predicted to be very warm for current conditions. Both tributaries drain through mélange lithologic terrain. The combination of increased heat loading and low water volume appears to explain the elevated predicted water temperatures.

A comparison of the discharge and shade scenarios for whole basin and headwaters suggests that mainstem shading moderates the effects of uplands vegetation and discharge reduction. Mainstem shading in particular provides significant temperature benefits at reduced flows. This shading also dampens downstream cumulative effects. Note that in Figure 4.5 and Figure 4.14 whole watershed shade removal (topography-only shade) leads to the highest temperatures and these temperatures continue to rise even at

125

the mouth. The downstream cumulative effects of removing shade on the tributaries, however, does not lead to progressively increasing stream temperature due to mainstem shading.

These results offer important insight into potential climate change impacts. A warmer climate in California is likely to lead to increased drought frequency and persistent low flows (Kiparsky and Gleick 2003, Barnett et al. 2002). Throughout this dissertation, the effects of flow have been shown to be strongly non-linear, particularly for flow reductions. The thermal profiles shown in Figures 4.13 and 4.15 suggest important headwater shade and discharge interactions, and that the temperature response to these controls is largely a function of position in the watershed. The headwater reference shade scenario with a 50% reduction in flow suggests higher up in the watershed (i.e., upstream of 5 kilometers in Bull Creek), tall trees can moderate stream temperature and offset reductions in flow. The whole basin reference shade profiles for a 50% reduction in flow shows that mainstem reference shading offers additional and important temperature benefits.

Because clear cutting commonly increases baseflow (Swank et al. 1988), it might be argued that the benefits of cooling that result from logging would offset the loss off headwater shade provision. The relative cooling or heating will depend on the relative increase in discharge, the duration of increased discharge, the amount of riparian shade reduction, and other factors not directly addressed in the model (e.g. soil temperature heating (e.g., St-Hilaire et al. 2000)). However, if there are any benefits to increased flows, they are likely to be transient. Empirical studies at the Beaver Creek watershed in Arizona have shown that for some treatments, water yields return to pre-harvest levels

126

within 3 years. Similar studies at the Caspar Creek watershed in Northern California have shown water yields return to pre-harvest levels in 5 years (Ziemer 1998). If riparian shade trees were also harvested, we would expect the net effect of clearcutting to be warming, because riparian vegetation regrowth and the shade benefits it provides, would take longer than 3 to 5 years. Thus considering stream temperature effects alone (and not other environmental impacts of clearcutting such as bank instability, sediment supply, and nutrient supply, for example), it is highly unlikely that clearcutting would offer general and long term temperature benefits through increased water yields.

The results from the headwater shade and discharge scenarios are consistent with the general sensitivity analyses presented in chapter two and reproduced by the stream temperature model applications presented in chapter three. These show that at small watershed areas (and hence shallow depths) water temperature is extremely sensitive to even moderate levels of heat loading. This has important implications regarding protection of riparian forest for headwater locations, which as indicated earlier, often receive little protection under land management protocols (e.g., California Forest Practice Rules, Table 4.1). Based on the headwater shade and discharge scenarios, persistent drought conditions are likely to result in elevated temperatures even for fully forested reaches, and as demonstrated by the reference headwater scenario with 50% reduced flow, downstream temperatures are predicted to be significantly warmer with important implications for aquatic habitat quality and quantity.

4.5 CONCLUSION

The numerical experiments conducted with the stream temperature model presented in chapter 3 strongly demonstrate the interplay of shading and stream flow on stream temperature along the mainstem of Bull Creek. The model predictions show the important role of shading – both on tributaries and the mainstem – in moderating the effects of flow reduction. It is anticipated that a warmer climate in California will lead to increased drought frequency (Kiparsky and Gleick 2003), hence the results of these numerical experiments offer important insights into likely future stream temperature response. For example, even with a reduction of flow of 50%, converting the entire watershed to late seral vegetation from its current mix of mature trees, secondary re-growth, and shrubs and grassland, would completely offset the warming effects of this low flow. While the model highlights the important controls exerted by shade (topographic and riparian vegetation), more significantly, it suggests that establishment of mature riparian forest should be implemented now so that as warmer ambient air temperatures and increased drought cycles are realized, the small, headwater streams that comprise most of the watershed area and provide vital aquatic habitat, are given maximum protection.

Table 4.1   Riparian buffer protection for Class I, II, and III streams as defined by California Forest Practice Rules[1].

Class I (Fish always or seasonally present. Includes habitat to sustain fish migration and spawning)	Class II [(1) Fish always or seasonally present offsite within 1000 feet downstream, and/or, 2) Aquatic habitat for non-fish species]	Class III (No aquatic life present. Capable of sediment transport to Class I and II streams under normal high water flow conditions.)
75 ft selective harvest on < 30% slope	50 ft selective harvest on < 30% slope	Determined on a case by case basis
100 ft selective harvest on 30-50% slope	75 ft select harvest on 30-50% slope	25ft equipment exclusion zone on slopes > 30%
150 ft selective harvest on > 50% slope[3]	100 ft selective harvest on > 50% slope[4]	50 ft equipment exclusion zone on slopes > 30%

[1]CDF (2002)

Table 4.2   Diameter-at-breast height (DBH) to reference tree height conversions[1].

DBH (inches)	Tree Height (Meters)							
	Shrubs[3]	Mixed Hardwood	Mixed Pine	Mixed Fir	Mixed Conifer and Hardwood	Mixed Oak	Mixed Hardwood and Conifer	Mixed Conifer
<= 24[2]	25	30	30	30	30	25	35	35
> 24	25	30	30	30	30	25	35	35

[1] Areas identified as wet marsh or meadow for existing vegetations conditions are left unchanged for reference condition scenarios. We assume that wet marsh and meadow vegetation types were also the reference conditions vegetation type.
[2]Reference heights for all vegetation classes are only changed for those habitat types with DBH <= 24". For DBH > 24", the tree heights are kept the same as for current vegetation conditions.
[3] Includes all grassland, shrub, and forbs vegetation assemblages.

Table 4.3   Summary of shade and discharge scenarios tested for the three South Fork Eel River basins

Basin	Run Number	Area changed	Shade scenario	Discharge scenario	Temperature Response
Bull Creek	1	Whole basin	No Trees	Current	> 5ºC warming for some N/S tributaries. 2-3ºC warming for some E/W tributaries. Mainstem warming ranging from 2ºC (upper mainstem) to ~ 5ºC down towards the mouth.
	2	Whole basin	Reference vegetation	Current	General cooling everywhere; biggest reductions (2-3ºC) observed for western tributaries. Biggest mainstem reductions (2-3ºC) along midsection at the confluences of western tributaries.
Elder Creek	3	Whole basin	No trees	Current	Mainstem Elder Creek warming ranging from 3-4ºC. Larger tributaries warm up to 3ºC
	4	Whole basin	Reference vegetation	Current	Modest cooling everywhere. Mainstem generally only cools by 0.5 to 1.0 ºC. Tributaries show similar range of cooling
Rattlesnake Creek	5	Whole basin	No Trees	Current	Warming everywhere, but especially (>5ºC) for tributaries (Foster Creek; Elk Creek draining mélange terrain
	6	Whole basin	Reference vegetation	Current	Similar magnitude of cooling (~5 ºC) observed for headwater streams draining mélange terrane tributaries (Foster Creek, Elk Creek)
Bull Creek	7	Headwaters	No Trees	Current	Rapid warming within first 5 km. Little or no apparent tributary inflow effects. Thermal profile shows slightly cooling downstream of 15 km.
	8	Headwaters	Reference Vegetation	Current	Less rapid warming within first 5 km. Thermal profile more closely tracks current conditions. Shows strong cool tributary inflow effects.
	9a,b	Whole basin	No Trees	±50% Discharge	+50% Q shows rapid warming in first 10km then leveling off. -50% Q warms more slowly, continues throughout profile.
	10a,b	Whole basin	Reference Vegetation	±50% Discharge	-50% Q profile closely tracks current vegetation condition while +50% Q warms slowly throughout profile.
	11a,b	Headwaters	No Trees	±50% Discharge	-50% Q warms rapidly; fluctuates significantly; slight downstream cooling. +50% Q warms rapidly; but much more slowly downstream of 5 km.
	12a,b	Headwaters	Reference Vegetation	±50% Discharge	+50% Q shows general, but steady warming. Tributary inflow effects apparent. -50% Q fluctuates significantly within first 5 km, then warms rapidly downstream. Cool tributary inflow effects at approximately 17 km.

Figure 4.1   Assumed reference vegetation conditions. Bull, Rattlesnake, and Elder
              Creeks. South Fork Eel River Basin.
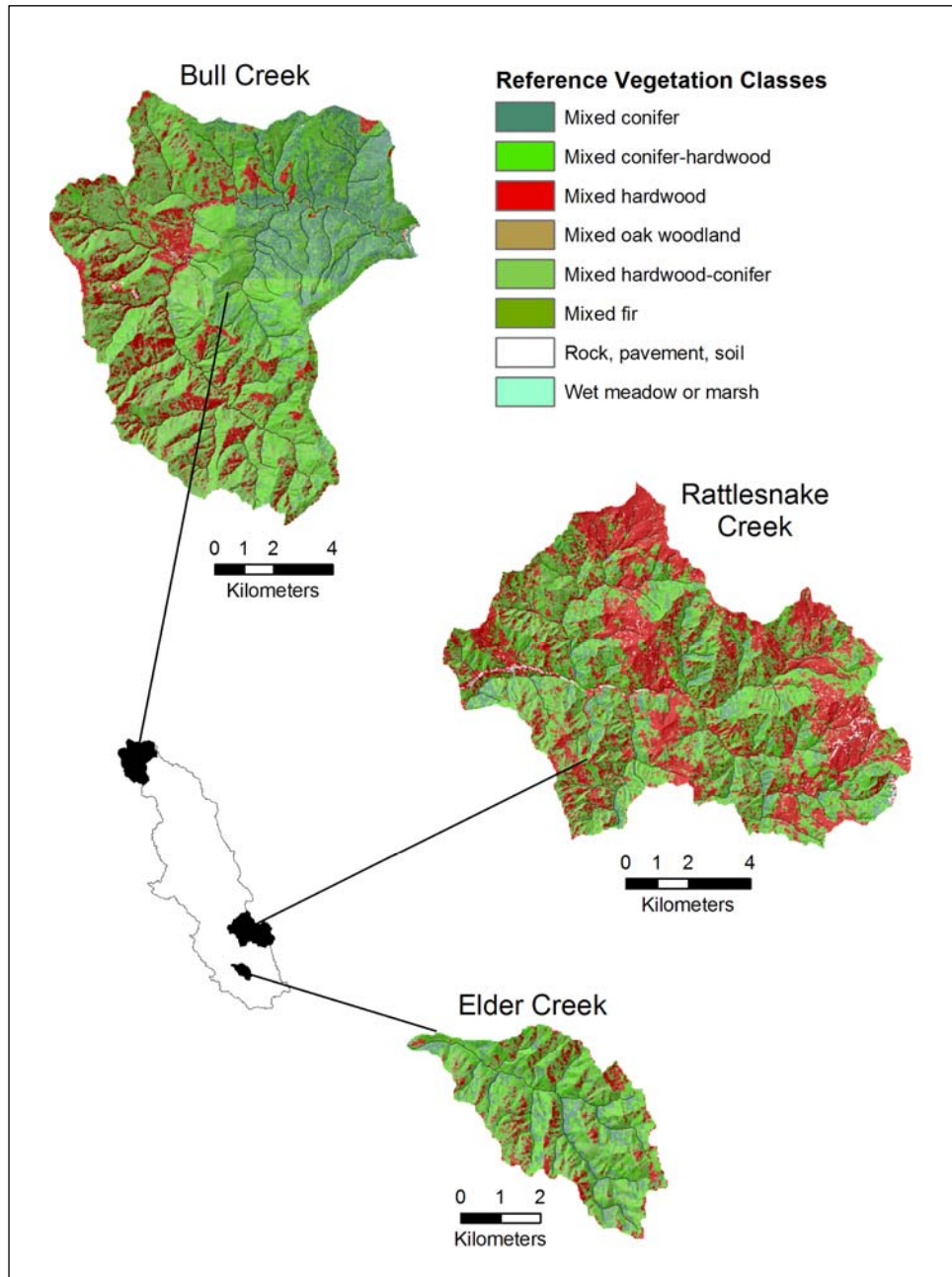
Figure 4.2   Headwater channels as defined by Strahler Order 1 and 2 channels. Bull
             Creek.
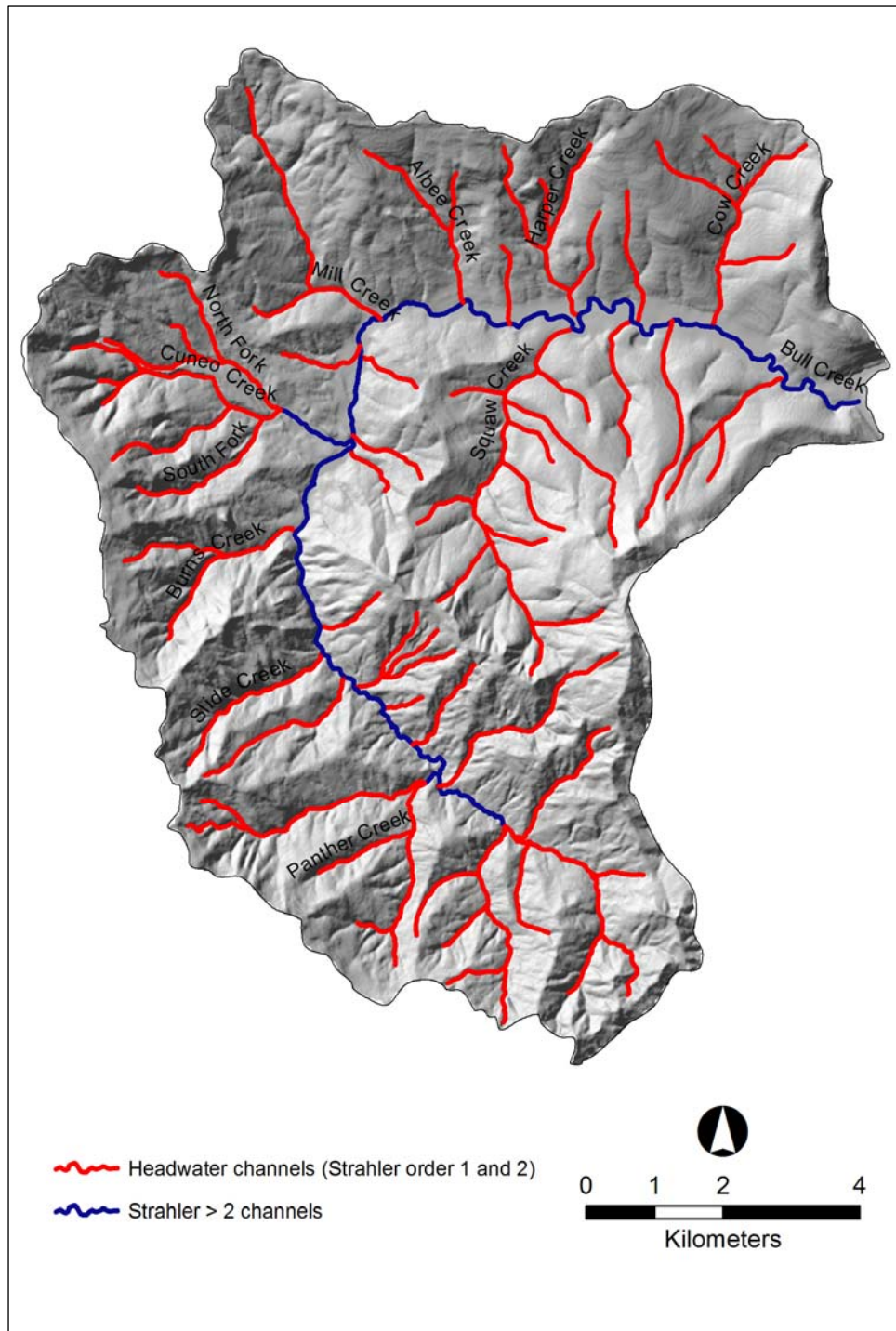
Figure 4.3   Change in predicted temperature Bull Creek between existing vegetation
              conditions and topography-only shade conditions
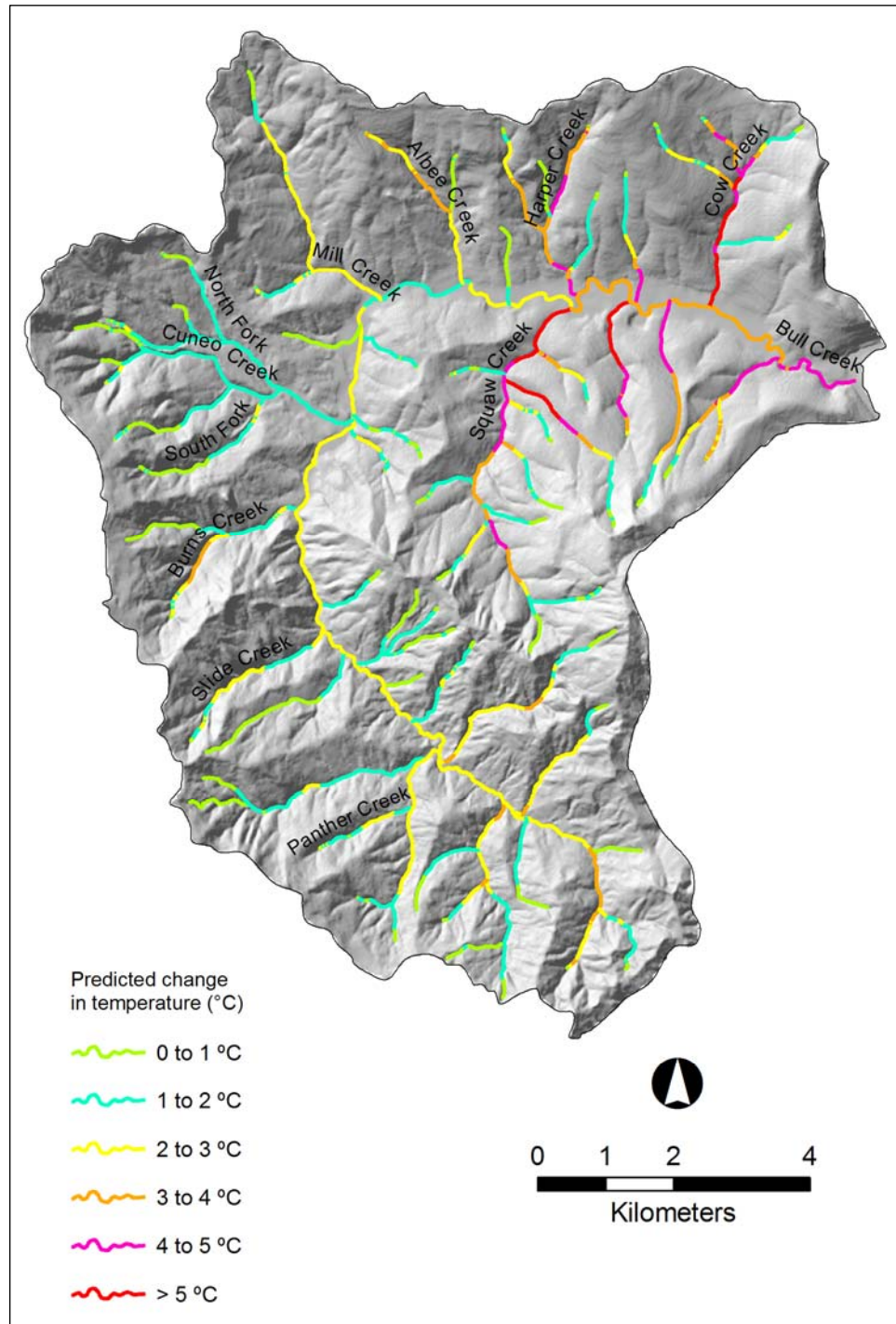
Figure 4.4   Change in predicted temperature between existing vegetation conditions
and reference shade conditions. Bull Creek
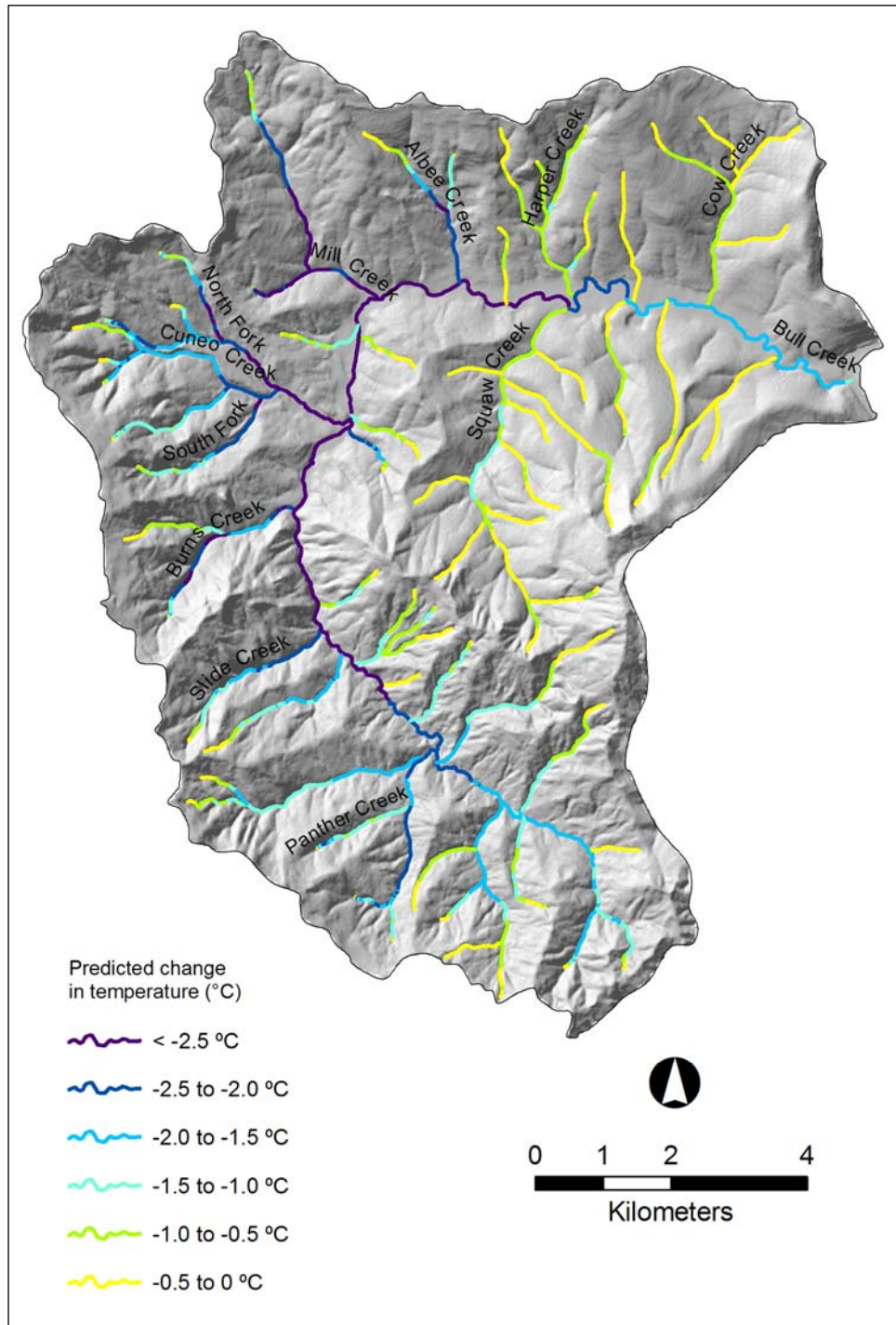
Figure 4.5   Thermal long profiles for three different shade scenarios. Mainstem Bull
              Creek
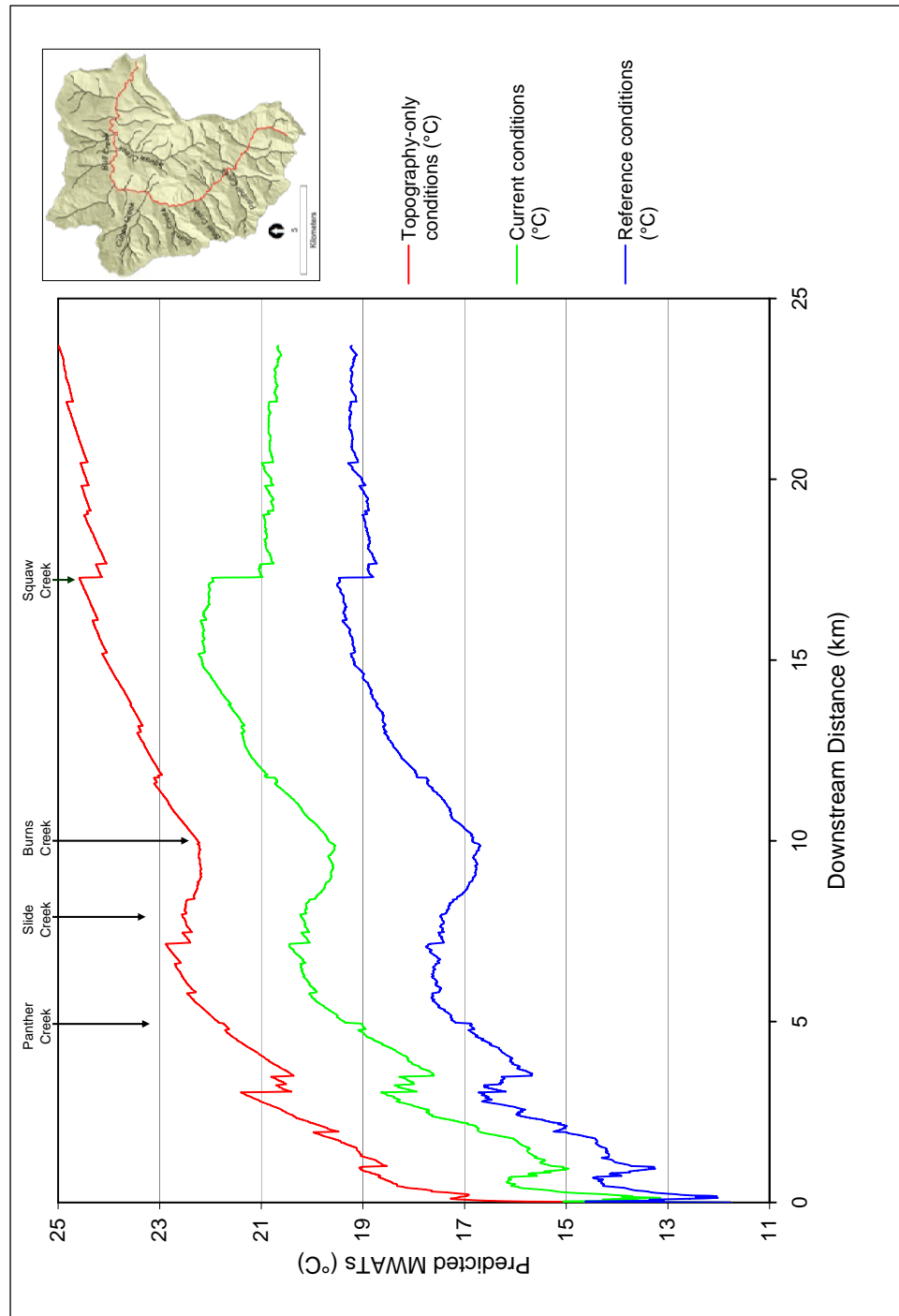
Figure 4.6   Thermal long profiles for three riparian shade scenarios. Cuneo Creek, Bull Creek.
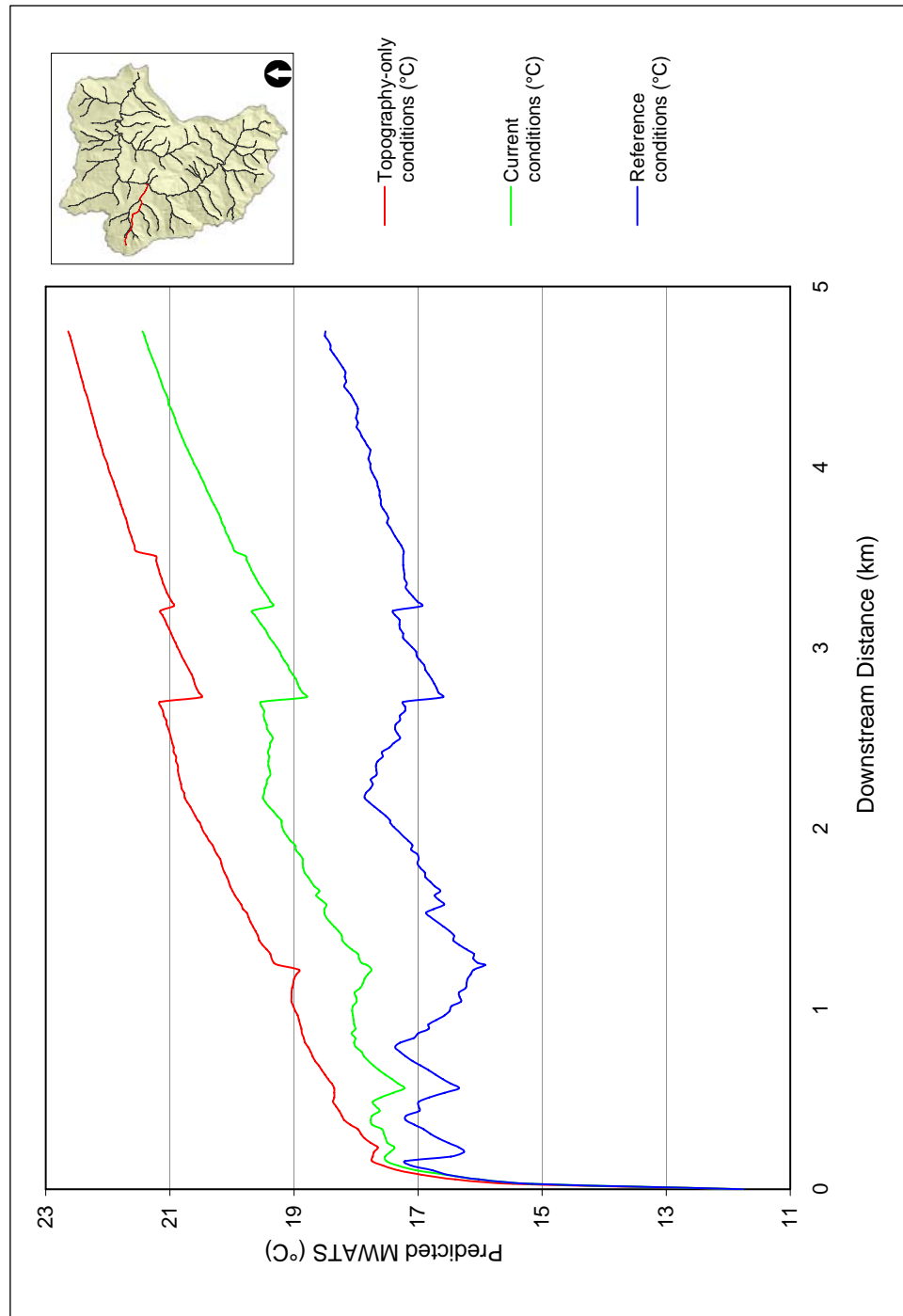
Figure 4.7   Thermal long profiles for three riparian shade scenarios. Squaw Creek, Bull Creek
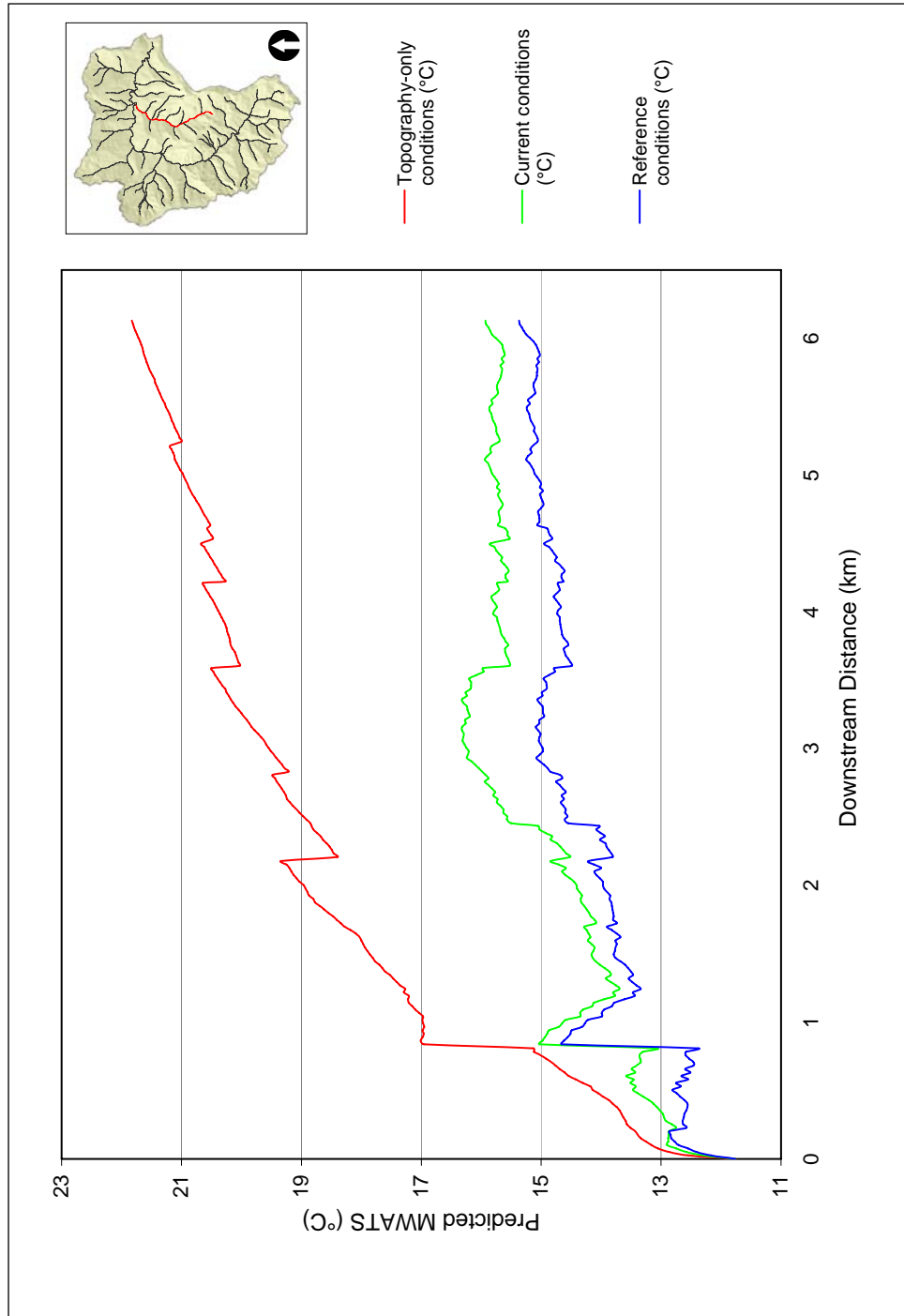
Figure 4.8   Change in predicted temperature between existing vegetation shade
conditions and (a) reference vegetation shade, and (b) topography-only
shade conditions. Elder Creek.
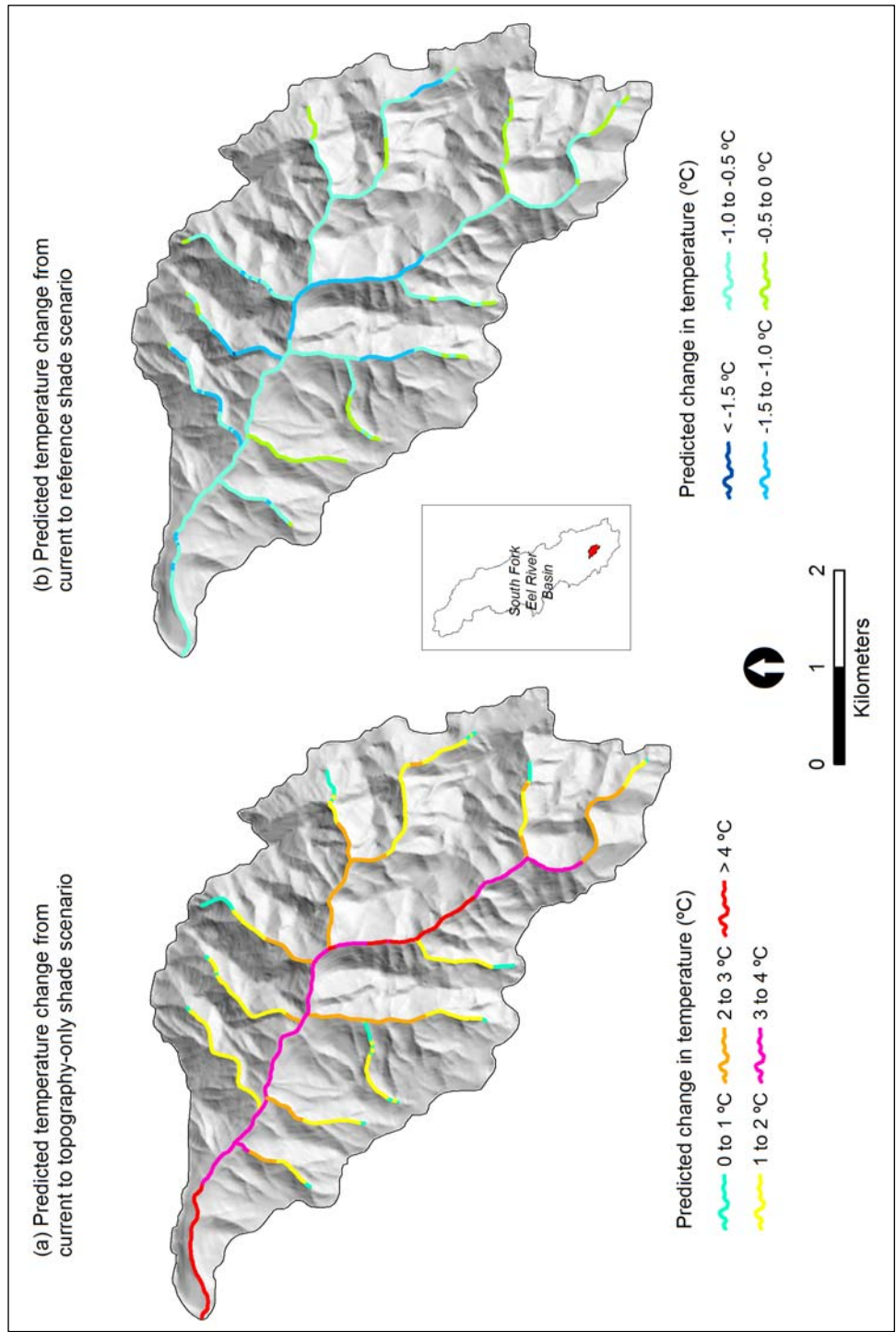
Figure 4.9   Thermal long profiles for three riparian shade scenarios. Elder Creek
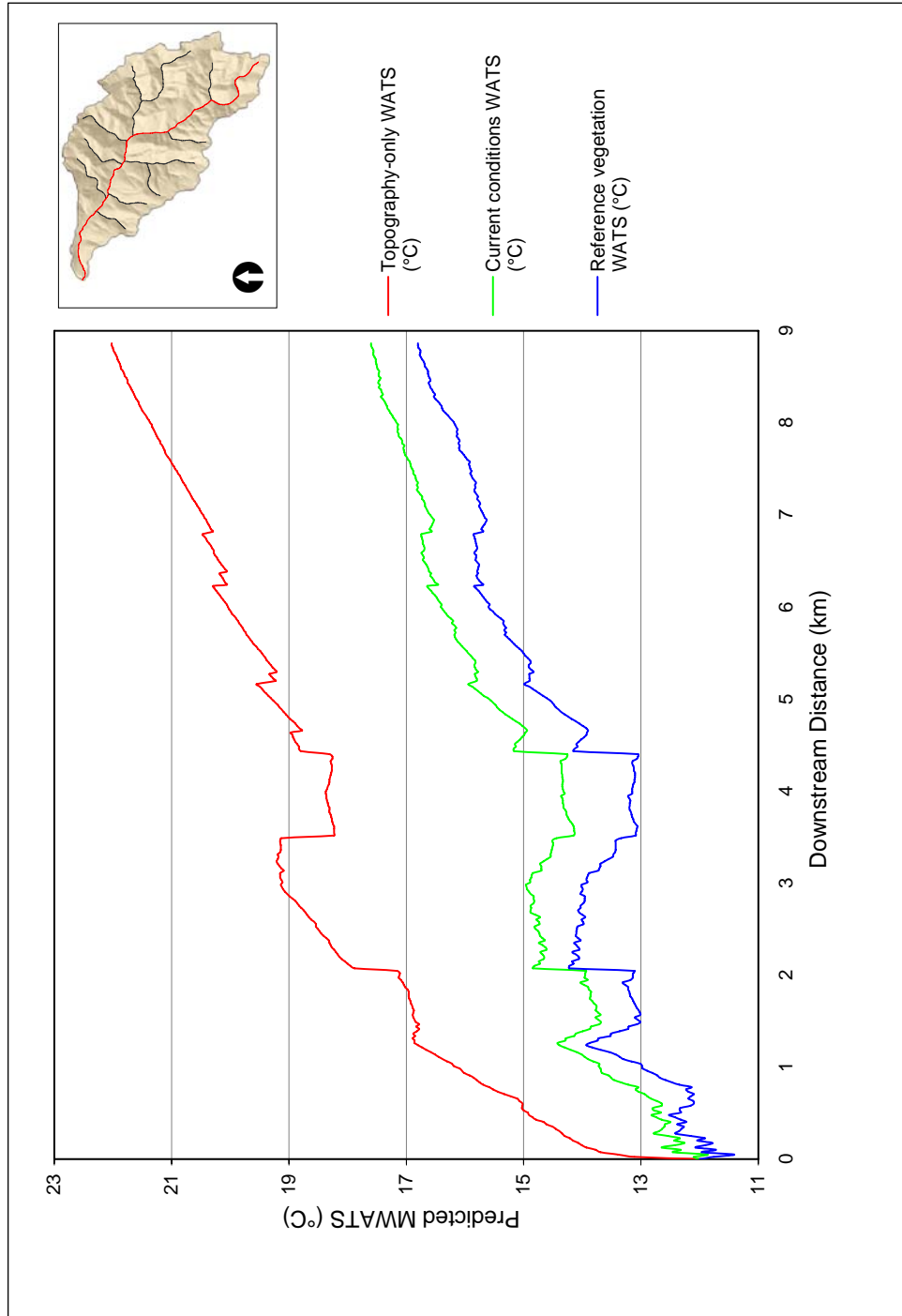
Figure 4.10   Change in predicted weekly average temperature (WATS) between existing vegetation and topography-only shade conditions. Rattlesnake Creek.
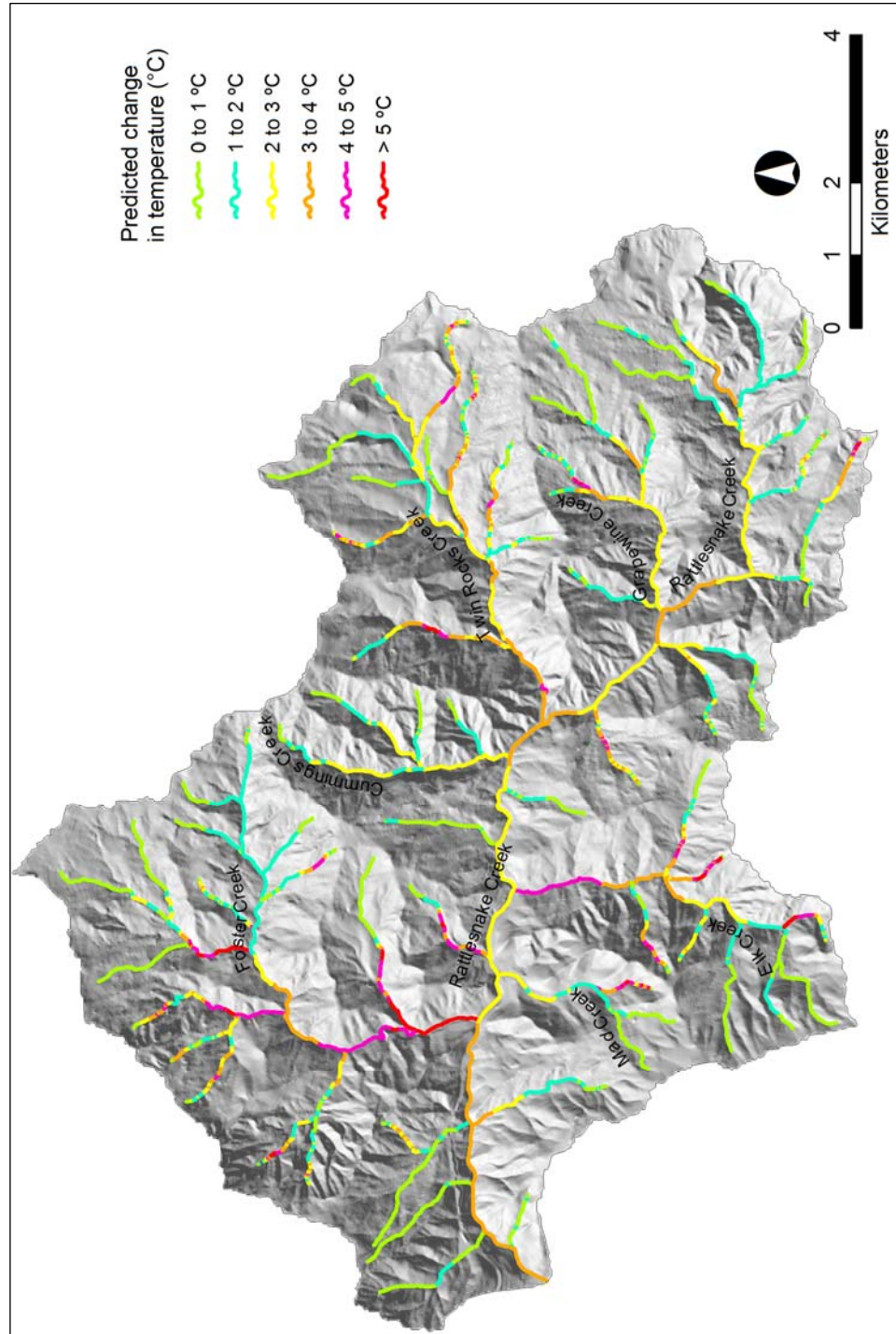
Figure 4.11   Change in predicted weekly average temperature (WATS) between existing vegetation and reference vegetation shade conditions. Rattlesnake Creek.
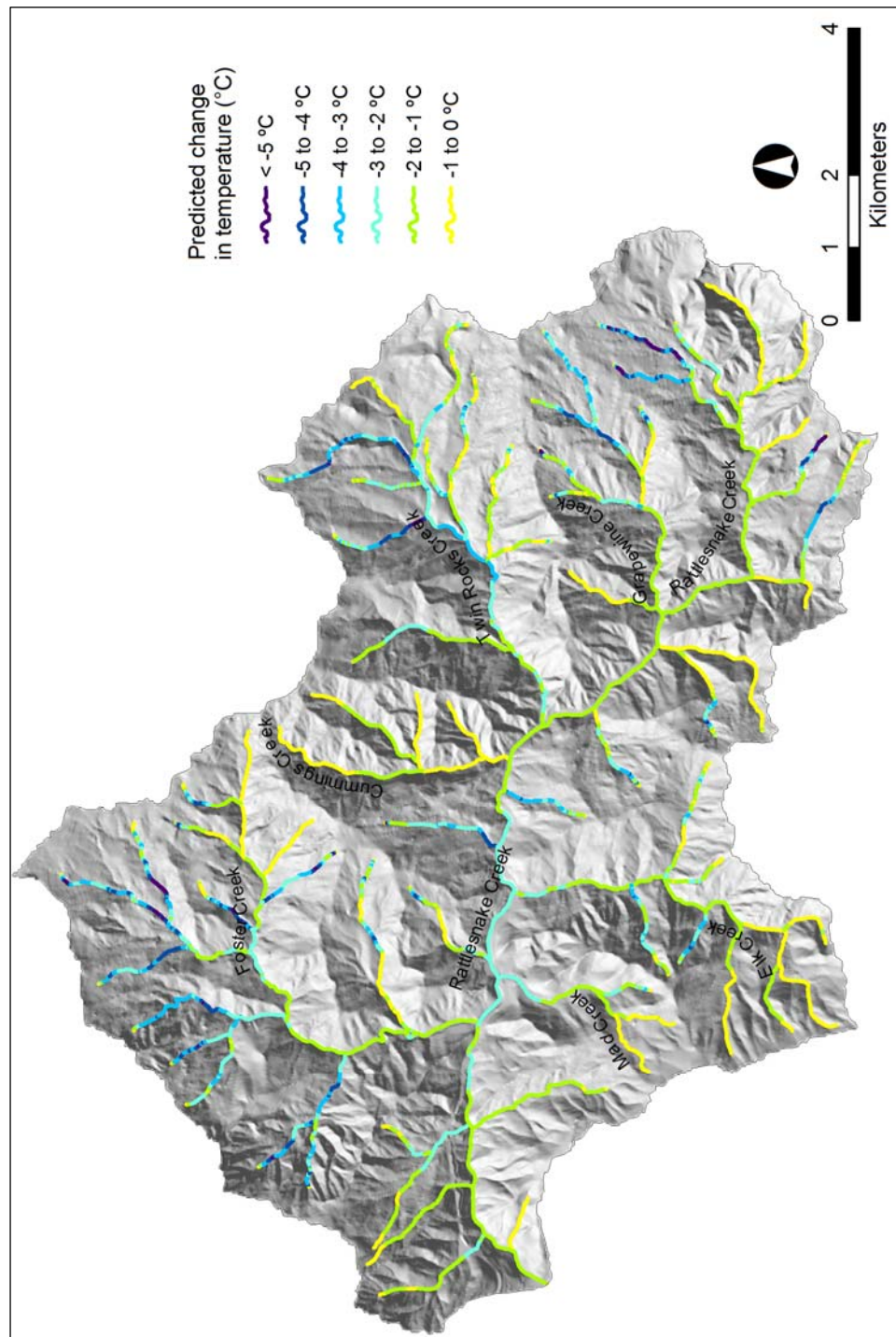
Figure 4.12   Predicted thermal longitudinal profiles for three riparian shade scenarios.
Mainstem Rattlesnake Creek
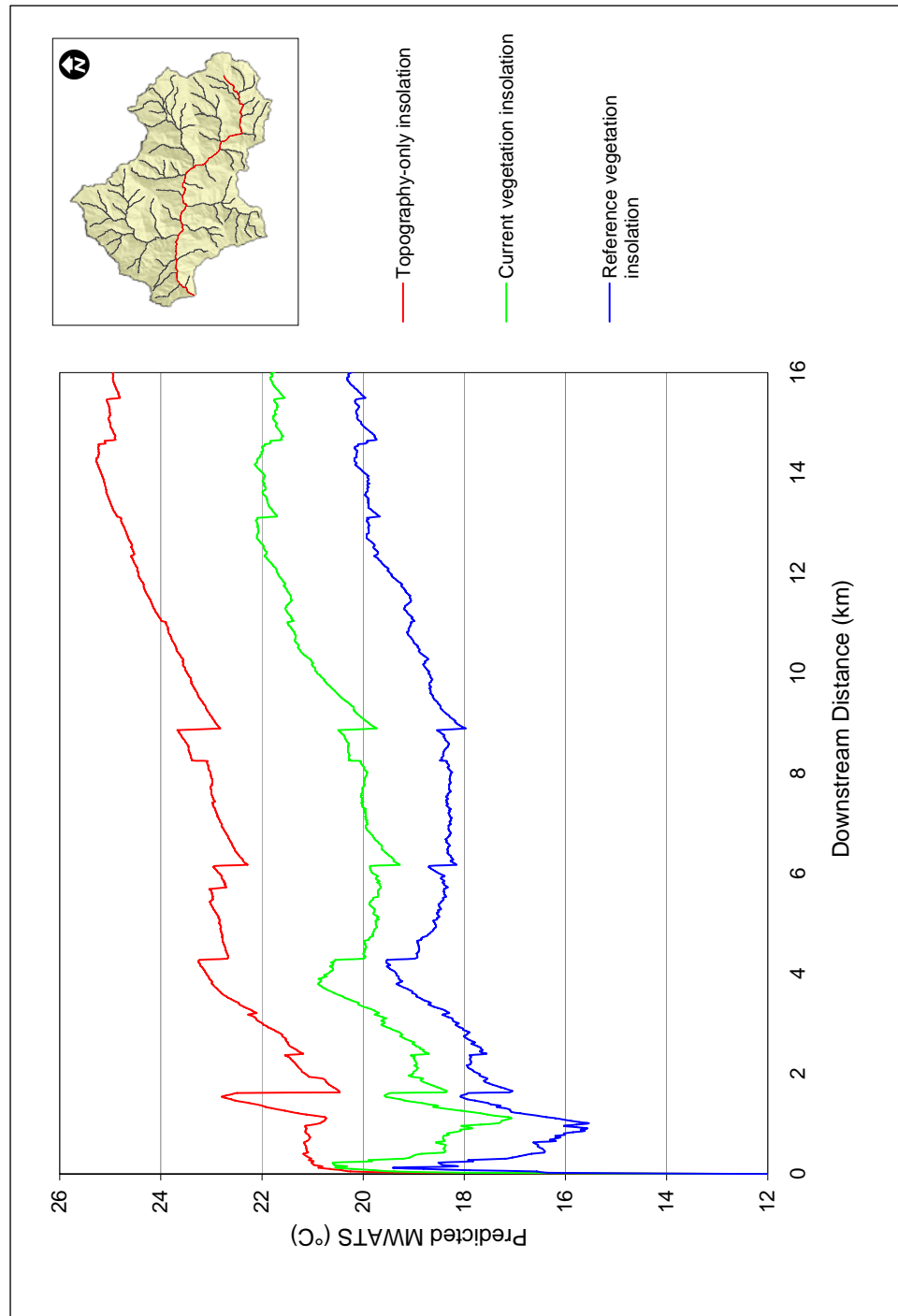
Figure 4.13   Thermal long profiles for different headwater shade scenarios. Mainstem
Bull Creek

143
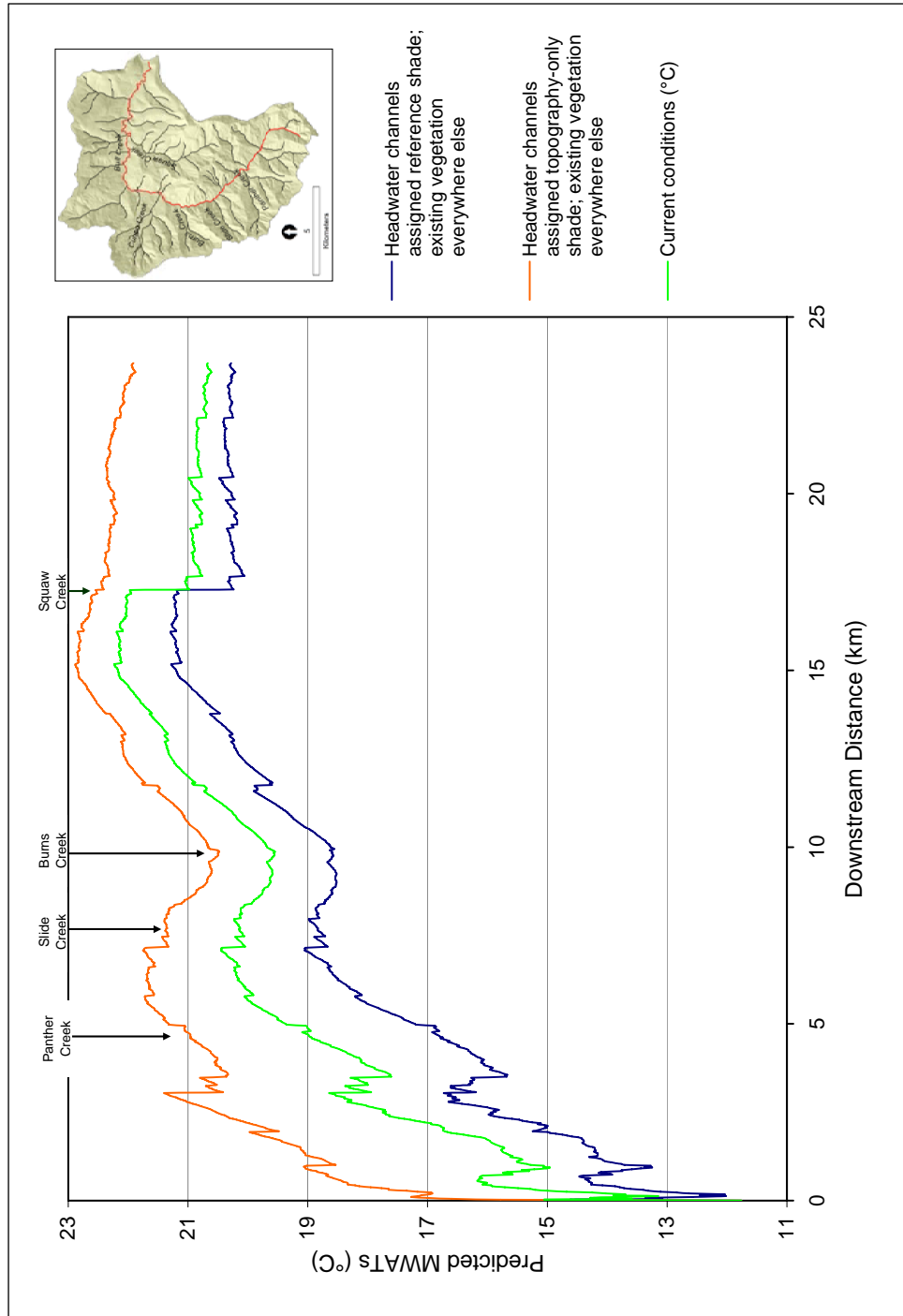
Figure 4.14   Whole basin thermal long profiles applying different shade and flow Mainstem Bull Creek.
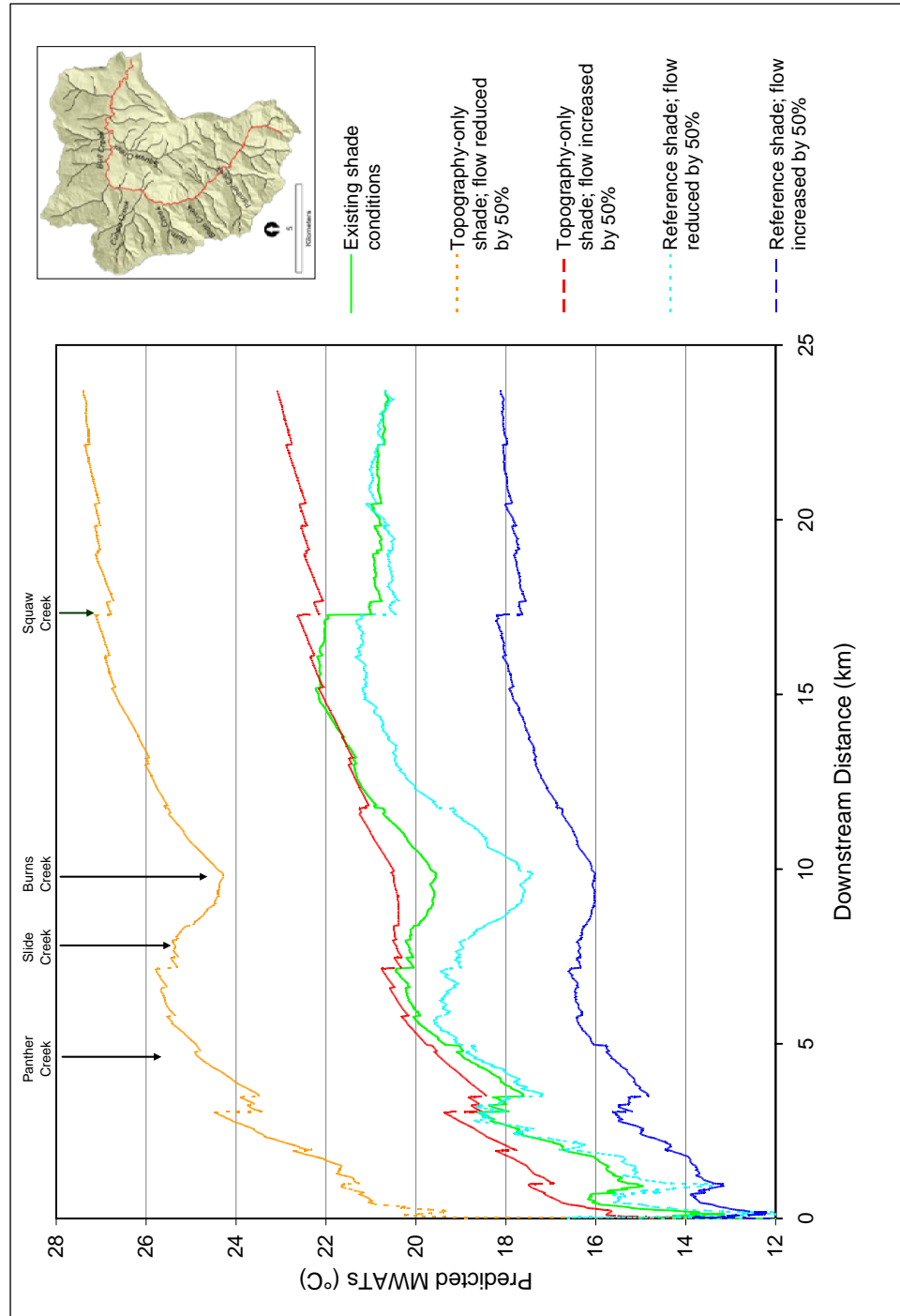
Figure 4.15   Thermal long profiles for different headwater shade and flow scenarios.
                Mainstem Bull Creek
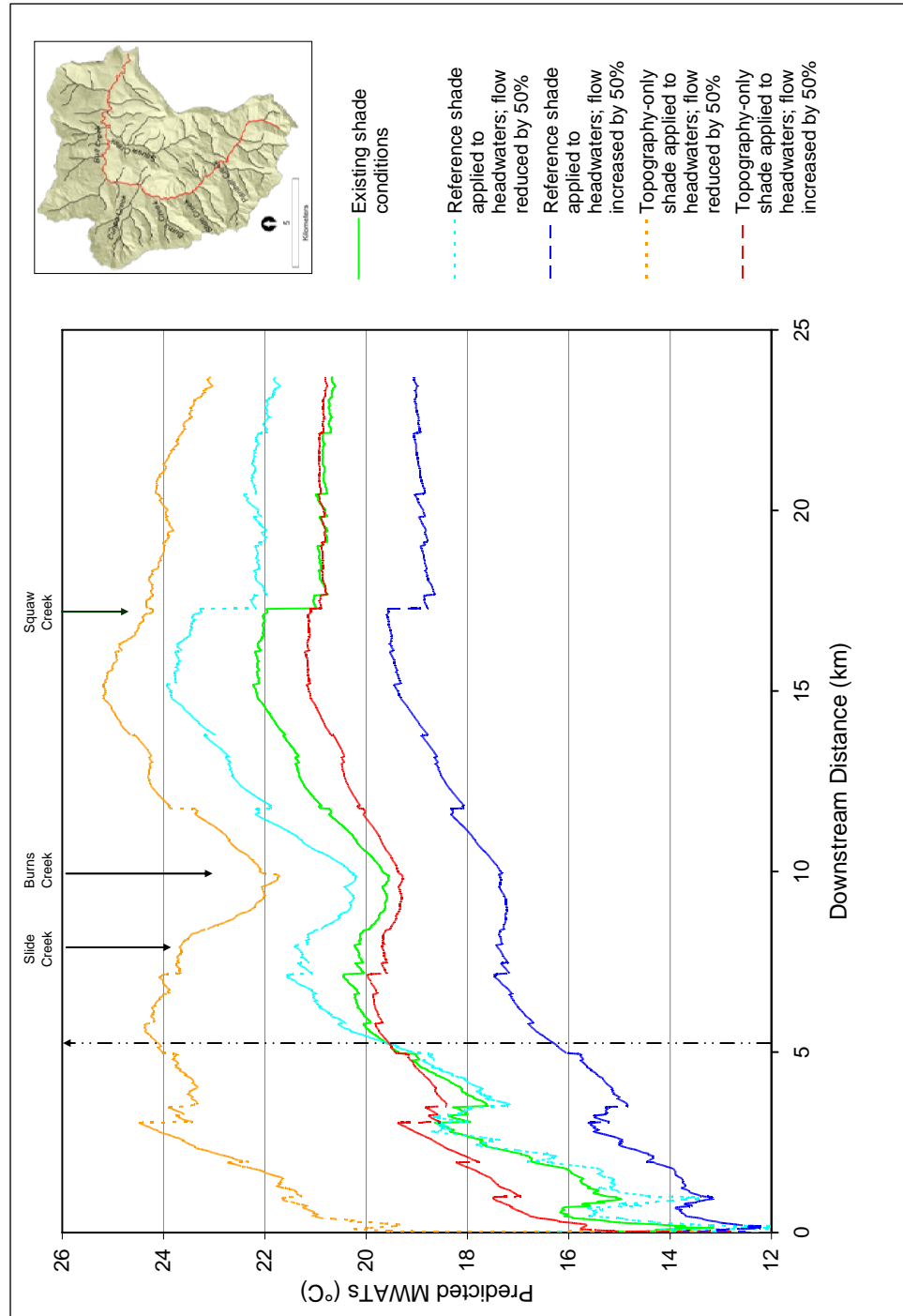
BIBLIOGRAPHY

Adams, T.N., and K. Sullivan. 1989. The physics of forest stream heating: a simple

    model. Washington DNR Timber/Fish/Wildlife Report TFW-WQ3-90-007.

Allen, D.McK., Dietrich, W.E., Baker, P.F, Ligon, F.K., and B.K. Orr. 2007.

    Development of a mechanistically based, basin-scale stream temperature model:

    applications to cumulative effects modeling. *In*: Standiford, R.B., Giusti, G.A.,

    Valachovic, Y., Zielinski, W.J., Furniss, M.J., (editors). Proceedings of the

    redwood region forest science symposium: What does the future hold? Gen. Tech.

    Rep. PSW-GTR-194. Albany, CA: Pacific Southwest Research Station, Forest

    Service, U.S. Department of Agriculture; p. 11-24.

Averett, R.C. 1968. Influence of temperature on energy and material utilization by

    juvenile coho salmon. Ph.D. thesis, Oregon State University, Corvallis. 74pp.

Baker, M.B., Jr. 1999. History of research in the Central Highland of Arizona. USDA

    Forest Service, General Technical Report RMRS-GTR29.

Bartholow, J.M. 2000. Estimating cumulative effects of clearcutting on stream

    temperatures. Rivers, Vol. 7(4): 284-297.

Barnett, T., R. Malone, W. Pennell, D. Stammer, A. Semtner, and W. Washington. 2004.

    The effects of climate change on water resources in the west: Introduction and

    Overview. Climatic Change, 62, 1-11

Bartholow, J.M. 1989. Stream temperature investigations: Field and analytic methods.

    Instream Flow Information Paper No. 13. Washington, D.C. US Fish and

    Wildlife Service (Biological Report 89(17). 139pp.

Barton, D.R., W.D. Taylor, and R.M. Biette. 1985. Dimensions of riparian buffer strips

    required to maintain trout habitat in southern Ontario streams. North American

    Journal of Fisheries Management, Volume 5:364-378.

Berk, A., L.S. Bernstein, and D.C. Robertson. 1989. MODTRAN: A Moderate

    Resolution Model for LOWTRAN 7. GL-TR-89-0122, Geophysics Directorate,

    Phillips Laboratory, Hanscom AFB, MA 01731 (April 1989) ADA214337.

Berman, C. H. 1998. Oregon Temperature Standard Review. U.S. EPA, Region 10.

    Seattle, WA.

Berman, C.H. 1990. The effect of elevated holding temperatures on adult spring Chinook

    salmon reproductive stress. Unpublished M.S. thesis. School of Fisheries,

    University of Washington. Seattle, Washington.

Beschta, R.L. 1997. Riparian shade and stream temperature: an alternative perspective. Rangelands, Vol. 19(2): 25-28.

Beschta, R.L. 1989. The effects of riparian vegetation on channel morphology, sediment, and temperature in streams. In: Silvicultural Management of Riparian Areas for Multiple Resources, A COPE Workshop, December 12-13; Gleneden Beach, OR, pp. 1-8.

Beschta, R.L., McIntosh, B.A., and C.E. Torgersen. 2003. Comment- "Perspectives on water flow and the interpretations of FLIR images" ,Journal of Range Management 55: 106-111 2002. Journal of Range Management, 56(1): 97-99.

Beschta, R. L., and J. Weatherred. 1984. TEMP-84: A computer model for predicting stream temperatures resulting from the management of streamside vegetation. WSDG Report WSDG-AD-00009. U. S. Forest Service, Watershed Systems Development Group, Fort Collins, Colorado.

Beschta, R. L., R. E. Bilby, G. W. Brown, L. B. Holtby, and T. D. Hofstra. 1987. Stream temperature and aquatic habitat: fisheries and forestry interactions. Pages 191-232 in E. O. Salo and T. W. Cundy, editors. Streamside management: forestry and fishery interactions. Contribution No. 57. College of Forest Resources, University of Washington, Seattle.

Beschta, R. L., and R. L. Taylor. 1988. Stream temperature increases and land use in a
forested Oregon watershed. Water Resources Bulletin 24: 19-21.

Bicknell, B.R., Imhoff, J.C, Kittle, J.L., Donigian, A.S., Jr. and R.C. Johanson. 1997.
Hydrological Simulation Program in FORTRAN, user's manual for version 11.
EPA/600/R-97/080. US Environmental Protection Agency, National Exposure
Research Laboratory, Athens, GA.

Bisson, P.A., Quinn, T.P, Reeves, G.H., and S.V. Gregory. 1992. Best management
practices, cumulative effects, and long-term trends in fish abundance in Pacific
Northwest river systems. *In:* Naiman, R.J. (ed). Watershed management:
balancing sustainability and environmental change. Springer Verlag, New York.

Boyd, M., and B. Kasper. 2003. Analytical Methods for Dynamic Open Channel Heat
and Mass Transfer: Methodology for the Heat Source Model Version 7.0.
Available from http://www.heatsource.info.

Brown, L.R., P.B. Moyle, and R.M. Yoshiyama. 1994. Historical decline and current
status of coho salmon in California. North America Journal of Fisheries
Management. Volume 4(2): 237-261.

Brown, G.W. 1983. Forest and Water Quality. Oregon State University Bookstore.
Corvallis, Oregon.

Brown, G.W. 1972. An improved temperature prediction model for small streams. Oregon Water Resources Research Institute, Corvallis, Oregon, 20pp.

Brown, G.W. 1970. Predicting the effect of clearcutting on stream temperature. J. Soil and Water Conservation, Vol. 25: 11-13.

Brown, G. W. 1969. Predicting temperatures of small streams. Water Resources Research 5: 68-71.

Brown, G.W., and J.T. Krygier. 1967. Changing Water Temperatures in small mountain streams. J. Soil Water Cons., Vol.22: 242-244.

Brown, G.W., and J.T. Krygier. 1970. Effects of clear-cutting on stream temperatures. Water Resources Research, Vol. 6(4): 1133-1139.

Brown, L.C., and T.O. Barnwell Jr. 1987. The enhanced stream water quality models QUAL2E and QUAL2E-UNCAS, documentation and user manual. U.S. EPA, EPA/600/3-87/007, Athens, Georgia.

Burkholder, B., Grant, G.E., Haggerty, R., Khangaonkar, T., and P.J. Wampler. 2008. Influence of hyporheic flow and geomorphology on temperature of a large,

gravel-bed river, Clackamas River, Oregon, USA. Hydrological Processes, Volume 22: 941-953.

Brungs, W. A., and B. R. Jones. 1977. Temperature criteria for freshwater fish: protocol and procedures. EPA-600/3-77-061. U. S. Environmental Protection Agency, Environmental Research Laboratory, Duluth, Minnesota.

Burns, R. M., and B. H. Honkala, 1990. Silvics of North America. Agriculture Handbook 654. USDA.

Cafferata, P. 1990. Watercourse Temperature Evaluation Guide. JDSF Newsletter No. 39. Jackson Demonstration State Forest, California Department of Forestry and Fire Protection, Fort Bragg.

Caldwell, J., K. Doughty, and K. Sullivan. 1991. Evaluation of downstream temperature effects of Type 4/5 waters. Timber/Fish/Wildlife Report TFW-WQ5-91-004. Washington Department of Natural Resources, Olympia.

California Department of Forestry and Fire Protection. 2002. California Forest Practice Rules: Title 14, California Code of Regulations, Chapters 4 and 4.5, and 10. California Department of Forestry and Fire Protection, Resource Management, Forest Practice Program. Sacramento, California.

California Department of Fish and Game. 2002. Status review of California coho salmon north of San Francisco: report to the California Fish and Game Commission. California Department of Fish and Game Candidate Species Status Review Report 2002-3.

California Department of Forestry and Fire Protection. 1999. Draft habitat conservation plan and sustained yield plan for Jackson Demonstration State Forest. Prepared by Stillwater Sciences, Berkeley, California.

California Department of Fish and Game. 1997. Eel River Salmon and Steelhead Restoration Action Plan. Inland Fisheries Division.

Campbell, G.S., and J.M. Norman. 1998. An introduction to environmental biophysics. Springer Verlag.

Chen, D.Y., Carsel, R.F., McCutcheon, S.C., and W.L. Nutter. 1998a. Stream temperature simulation of forested riparian areas: I. Watershed-scale model development. J. Env. Eng., Vol. 124(4): 304-311.

Chen, D.Y., McCutcheon, S.C., Norton, D.J., and W.L. Nutter. 1998b. Stream temperature simulation of forested riparian areas: II. Model application. J. Env. Eng., Vol. 124(4): 316-328.

Chen, J., J.F. Franklin, and T.A. Spies. 1995. Growing-season microclimatic gradients from clearcut edges into old-growth Douglas-fir forests. Ecological Applications 5:74-86

Deas, M.L., and C.L. Lowney. 2000. Water temperature modeling review. California Water Modeling Forum, Central Valley, California. Available online: (http://cwemf.org/Pubs/BDMFTempReview.pdf)

Dennis Jr., J.E., and R.B. Schnabel. 1996. Numerical methods for unconstrained optimization and nonlinear equations. SIAM, Philadelphia.

Dingman, S.L. 2002. Physical Hydrology, 2nd Edition. Prentice Hall, Inc. Upper Saddle River, New Jersey.

Dozier, J., and J. Frew. 1990. Rapid calculation of terrain parameters for radiation modeling from digital elevation data. IEEE Transactions on Geoscience and Remote Sensing, Volume 28: 963-969.

Dubayah, R. 1994. Modeling a solar radiation topoclimatology for the Rio Grande basin. Journal of Vegetation Science, Volume 5: 627-640.

Dubayah, R. 1991. The topographic variability of solar radiation. Unpublished Ph.D dissertation, Department of Geography, University of California, Santa Barbara.

153

Dubayah, R. J. Dozier, and F.W. Davis. 1990. Topographic distribution of clear-sky radiation over the Konza prairie, Kansas. Water Resources Research, Volume 26: 679-690.

Dubayah, R., and P.M. Rich. 1991. Topographic solar radiation models for GIS. International Journal of Geographic Information Systems. Volume 9(4): 405-419.

Dunham, J., Lockwood, J., and C. Mebane. 2001. Salmonid distributions and temperature. EPA Region X Temperature Water Quality Criteria Guidance Development Project Issue paper 2, Seattle, WA.

Dunne, T., J. Agee, S. Beissinger, W. Dietrich, D. Gray, M. Power, V. Resh, and K. Rodrigues. 2001. A scientific basis for the prediction of cumulative watershed effects. Report 46. Berkeley: University of California, Wildland Resources Center.

Environmental Protection Agency. 2002. National Water Quality Inventory: 2000 Report. EPA-841-R-02-001. U.S. Environmental Protection Agency.

Environmental Protection Agency. 2001. Technical synthesis: Scientific issues relating to temperature criteria for salmon, trout, and char native to the Pacific Northwest.

Report submitted to the Policy Workgroup, EPA Region 10 Temperature Criteria Guidance Project. EPA 910-R-01-007, August 2001. 21p.

Environmental Protection Agency. 1999. South Fork Eel River Total Maximum Daily Loads for Sediment and Temperature. U.S. Environmental Protection Agency Region XI. San Francisco, California. December 1999.

Feller, M.C. 1981. Effects of clearcutting and slashburning on stream temperature in Southwest British Columbia. Water Resources Bulletin, 17: 863-867.

FEMAT. 1993. Forest Ecosystem Management Assessment Team Report. Sponsored by USDA Forest Service, US Environmental Protection Agency, USDOI Bureau of Land Management, National Park Service. Portland, Oregon.

Fowells, H.A., ed. 1965. Silvics of forest trees of the United States. U.S. Department of Agriculture, Agricultural Handbook 271. Washington, DC. 203 p.

Fox, L., Bonser, G.L., Trehey, G.H., Buntz, R.M., Jacoby, C.E., Bartson, A.P., and D.M. La Brie. 1997. A wildlife map and database for the ORCA (Oregon-California) Klamath Bioregion derived from Landsat imagery. Klamath Bioregional Assessment Project, College of Natural Resources, Humboldt State University, Arcata, CA.

Fox, L., and S.A. Carslon. 1996. Using a GIS and vegetation cover derived from Landsat-TM image classification to assess the health of the Klamath river hydro-basin in North America. Commission VII, Working Group 3, Departments of Forestry and Natural Resources Planning and Interpretation Humboldt State University, Arcata, California.

Friedrichsen, G. 1998. Eel River water quality monitoring report. Final report, 205(j) submitted to California State Water Quality Control Board. Humboldt County Resource Conservation District, Fields Landing, California.

Frew, J. 1990. The Image Processing Workbench. Unpublished Ph.D dissertation, Department of Geography, University of California, Santa Barbara.

Gaffield, S.J., Potter, K.W., and L. Wang. 2005. Predicting the summer temperature of small streams in Southwestern Wisconsin. Journal of the American Water Resources Association, Vol. 41(1): 25-36.

Garman, S. L., S. A. Acker, J. L. Ohmann, and T. A. Spies. 1995. Asymptotic height diameter equations for 24 tree species in western Oregon. Research Contribution 10. Forest Research Laboratory, College of Forestry, Oregon State University, Corvallis, Oregon.

Gleick, P.H. 2000. Water: the potential consequences of climate variability and change for the water resources of the United States. Report of the Water Sector Assessment Team of the National Assessment of the Potential Consequences for Climate Variability and Change, Pacific Institute for Studies in Development, Environment, and Security, Oakland, California.

Groot, C., L. Margolis, and W. C. Clarke, editors. 1995. Physiological ecology of Pacific salmon. University of British Columbia Press, Vancouver.

Gu, R.R., and Y. Li. 2002. River temperature sensitivity to hydraulic and meteorological parameters. Journal of Environmental Management, Vol. 66: 43-56.

Gu, R.R., McCutcheon, S., and C-J. Chen. 1999. Development of weather-dependent flow requirements for river temperature control. Environmental Management, Vol. 24(4): 529-540.

Gu, R.R., Montgomery, S., and T. Al Austin. 1998. Quantifying the effects of stream discharge on summer river temperature. Hydrological Sciences, Vol. 43(6): 885-904.

Handcock, R. N., Gillespie A.R., Cherkauer, K.A., Kay J.E., Burges S.J., and S. K. Kampf. 2006. Accuracy and uncertainty of thermal-infrared remote sensing of

stream temperatures at multiple spatial scales, Remote Sensing of Environment, 100: 427-440.

Hanus, M. L., D. D. Marshall, and D. W. Hann. 1999. Height diameter equations for six species in the coastal regions of the Pacific Northwest. Research Contribution 25. Forest Research Laboratory, College of Forestry, Oregon State University, Corvallis, Oregon.

Harr, R.D. and R.L. Fredriksen. 1988. Water quality after logging small watersheds within the Bull Run Watershed, Oregon. Water Resources Bulletin, 24(5): 1103-1111.

Harris, D.D. 1977. Hydrologic changes after logging in two small Oregon Coastal watersheds. Geological Survey Water-Supply Paper 2037, U.S. Geological Survey, Washington, D.C. 31pp.

Hewlett, J.D., and J.C. Fortson. 1982. Stream temperature under an inadequate buffer strip in the Southeast Piedmont. Water Resources Bulletin, Vol. 18(6): 983-988.

Hockey, J.B, Owen, I.F., and N.J. Tapper. 1982. Empirical and theoretical models to isolate the effect of discharge on summer water temperatures in the Hurunui River. Journal of Hydrology (NZ), Vol.21: 1-12.

Holtby, L.B. 1982. Effects of logging on stream temperatures in Carnation Creek, British Columbia, and associated impacts on the Coho Salmon (Oncorhynchus kisutch). Can. J. Fish. Aquat. Sci., Vol. 45: 502-511.

Ice, G.G., J. Light, and M. Reiter. 2004. Use of Natural Temperature Patterns to Identify Achievable Stream Temperature Criteria for Forest Streams. Western Journal of Applied Forestry, 19(4): 252-259.

Ice, G.G. 2001. How direct solar radiation and shade influences temperature in forest streams and relaxation of changes in stream temperature. Cooperative Monitoring Evaluation Research (CMER) Workshop. Heat Transfer Processes in Forested Watersheds and their Effects on Surface Water Temperature, Lacy, Washington. February, 2001.

Iqbal, M. 1983. An introduction to solar radiation. Academic Press.

James, S.M. 1983. South Fork Eel watershed erosion investigation. Calif. Dept. of Water Resources. 95pp.

Johnson, S.L. 2004. Factors influencing stream temperatures in small streams: substrate effects and a shading experiment. Can. J. Fish. Aquat. Sci. 61: 913-923.

Johnson, S.L. 2003. Stream temperature: scaling of observations and issues for modeling. Hydrological Processes, 17, 497-499.

Johnson, S.L., and J.A. Jones. 2000. Stream temperature response to forest harvest and debris flows in western Cascades, Oregon. Canadian J. Fish. Aquat. Sci., Volume 57(Suppl. 2): 30-39.

Kiparsky, M., and P. Gleick. 2003. Climate change and California water resources: a survey and summary of the literature. California Energy Commission Report 500-04-073.

Koslowski, D.R, and L.M. Edwards. 2007. An Analysis and Summary of the July 2006 Record-Breaking Heat Wave Across the State of California.   Western Region Technical Attachment No. 07-05, February 27, 2007. National Weather Service, California-Nevada River Forecast Center.

Krumland, B.E., and L.C.Wensel. 1988. A generalized height-diameter equation for coastal California species. Western Journal of Applied Forestry 3:113-115.

Larson, L. and P. Larson. 1997. The natural heating and cooling of water. Rangelands: 19:6-8.

Larson, L.L., and S.L. Larson. 1996. Riparian shade and stream temperature: a perspective. Rangelands, Vol. 18(4): 149-152.

LeBlanc, R.T., and R.D. Brown. 2000. The use of riparian vegetation in stream-temperature modification. Journal of the Chartered Institution of Water and Environmental Management, Vol. 14(4): 297-303.

LeBlanc, R.T., Brown, R.D, and J.E. FitzGibbon. 1997. Modeling the effects of land use change on the water temperature of unregulated urban streams. Journal of Environmental Management, Vol. 49: 445-469.

Levno, A., and J. Rothacher. 1967. Increases in maximum stream temperatures after logging in old-growth Douglas-fir watersheds. Research Note PNW-61. Pacific Northwest Forest and Range Experimental Station, Portland, OR. 12pp.

Lewis, T.E., D.W. Lamphear, D.R. McCanne, A.S. Webb, J.P. Krieter, and W. D. Conroy. 2000. Regional Assessment of Stream Temperatures Across Northern California and Their Relationship to Various Landscape-Level and Site-Specific Attributes. Forest Science Project. Humboldt State University Foundation, Arcata, CA. 420pp.

Lichatowich, J. 1999. Salmon without rivers: A history of the Pacific salmon crisis. Island Press, Washington D.C.

Ligon, F.K, Rich, A., Rynearson, G., Thornburgh, D., Trush, W. 1999. Report of the Scientific Review Panel on California Forest Practice Rules and Salmonid Habitat. Prepared for The Resources Agency of California and the National Marine Fisheries Service. Sacramento, California

Lufkin, Alan. 1996. The Story of the Eel River Commercial Salmon Fishery. The Humboldt Historian. Vol 44(2): pp 4 - 8.

Lynch, J.A., Sopper, W.E, Corbett, E.S., and D.W. Aurand. 1975. Effects of management practices on water quality and quantity: The Penn State Experimental Watersheds. *In* Proceedings of the Symposium on Municipal Watershed Management, p.32-46. USDA Forest Service General Technical Report, NE-13. Northeastern Forest Experimental Station, Broomall, PA.

Macdonald, J.S., H. Herunter, and R.D. Moore. 2003. Temperatures in aquatic habitats: the impacts of forest harvesting in the interior of B.C. *In*: Forestry impacts on fish habitat in the Northern Interior of British Columbia: a compendium of research from the Stuart-Takla Fish-Forestry Study, E. MacIsaac (Editor). Canadian Technical Report on Fisheries and Aquatic Science 2509, Fisheries and Oceans Canada, Vancouver, B.C., Canada, pp101-116.

MacDonald, L.H., and D. Coe. 2007. Influence of headwater streams on downstream reaches in forested areas. Forest Science, Volume 53(2):148-168.

Marks D., J. Domingo, and J. Frew. 1999. Software tools for hydro-climatic modeling and analysis: Image Processing Workbench ARS – USGS Version 2. ARS Tech. Bull. 99-1, Northwest Watershed Research Center, USDA Agricultural Research Service, Boise, ID. [Available online at http://www.nwrc.ars.usda.gov/ipw.].

Mast, M.A., and D.W. Clow. 2000. Environmental characteristics and water-quality of Hydrologic Benchmark Network stations in the Western United States. U.S. Geological Survey Circular 1173-D, 115 pp.

Mattax, B. L., and T. M. Quigley. 1989. Validation and sensitivity analysis of the stream network temperature model on small watersheds in northeast Oregon. Pages 391-400 in W. W. Woessner and D. F. Potts, editors. Proceedings of the symposium on headwaters hydrology. American Water Resources Association, Bethesda, Maryland.

Matthews, Graham and Associates. 2000. Sediment source analysis and preliminary sediment budget for the Ten Mile River, Mendocino County, CA. Prepared for Tetra Tech, Inc. VOLUME 1: Text, Tables, and Figures. Fairfax, VA. 143 pp. October 2000.

Mayer, K.E. and W.F. Laudenslayer, Jr., eds. 1988. A guide to wildlife habitats of California. State of California, Resources Agency, Department of Fish and Game, Sacramento, CA.

McGurk, B.J. 1989. Predicting stream temperature after riparian vegetation removal. USDA Forest Service General Technical Report, PSW-110.

McMahon, T.E. 1983. Habitat suitability index models: coho salmon. USDI. Fish and Wildlife Service, Division of Biology. Washington, DC. 29p.

Meador, W.E., and W. R. Weaver. 1980. Two-stream approximations to radiative transfer in planetary atmospheres: a unified description of existing methods and a new improvement. J. Atmos. Sci., 37, 630-643.

Meehan, W.R, and T.C. Bjornn. 1991. Salmonid distributions and life histories. In: Meehan, W.R., ed. Influences of forest and rangeland management on salmonid fishes and their habitats. American Fisheries Society Special Publication 19: 47-82. Bethesda, MD.

Meehan, W.R. 1970. Some effects of shade cover on stream temperatures in southeast Alaska. USDA Forest Service Note PNW-113. PNW Forest and Range Experimental Station, Portland, OR. 9p.

Mitchell, S. 1999. A simple model for estimating mean monthly stream temperatures after riparian canopy removal. Environmental Management, Vol. 24(1): 77-83.

Monteith, J.L., and M. Unsworth. 1990. Principles of environmental physics. 2nd edition. Routledge, Chapman, and Hall. London, UK.

Moore, J.A., Miner, J.R., Bower, R., and Buckhouse, J.C. 1999. The effect of shade on water: a tub study. pp70-86: *In* Innovative approaches to the Oregon Salmon Restoration Program. Special Report 997: Corvallis, OR: Oregon State University Extension Service.

Moore, R.D., D.L. Spittlehouse, and A. Story. 2005. Riparian microclimate and stream temperature response to forest harvesting: a review. J. Am. Wat. Res. Assoc. 41(4): 813-834.

Moring, J. R. 1975. The Alsea watershed study: effects of logging on the aquatic resources of three headwater streams of the Alsea River, Oregon. Part 2— Changes in environmental conditions. Fishery Research Report 9. Oregon Department of Fish and Wildlife, Corvallis.

Morse, W.L. 1970. Stream temperature prediction model. Water Resources Research, Vol. 6(1): 290-302.

Nakamura, F., and T. Dokai. 1989. Estimation of the effect of riparian forest on stream temperature based on heat budget. Journal of the Japanese Forestry Society, Volume 71: 387-394.

National Council for Air and Stream Improvement, Inc. 2001. Annotated/abstracted bibliography: Riparian canopy cover, microclimate, and stream temperatures. Available online: (www.ncasi.org/Publications/Detail.aspx?id=2623).

National Marine Fisheries Service and U.S. Fish and Wildlife Service. 1997. Aquatic properly functioning condition matrix. NMFS, Southwest Region, Northern California Area Office, Santa Rosa and USFWS, Arcata, California.

National Marine Fisheries Service, 1996. Coastal salmon conservation: Working guidance for comprehensive salmon restoration initiatives on the Pacific Coast. NMFS, Northwest Region, Seattle, WA. 6p.

Norman, J.M. 1975. Radiative transfer in vegetation. *In* Heat and mass transfer in the biosphere, edited by D.A. deVries and N.H. Afgan. Scripta Book Company, Washington, D.C.

Oke, T.R. 1987. Boundary Layer Climates. Routledge, 435 pp.

Peterson, B., Stringham, T., and W. Krueger. 1999. The impact of shade on the
temperature of running water, pp: 176-184. In: Krueger, W.C., Stringham, T.K.,
and C.E. Kelley (eds), Environmental and management impacts on stream
temperature. Final Report, Dept. of Rangeland Resources, Oregon State U.,
Corvallis, OR.

Pluhowski, E.J. 1972. Clear-cutting and its effects on the water temperature of a small
stream in Northern Virginia. USGS Professional Paper 800-C, pages C257-C262.

Poole, G.C., J.B. Dunham, D.M. Keenan, S.T. Sauter, D.A. McCullough, C. Mebane, J.C.
Lockwood, D.A. Essig, M.P. Hicks, D.J. Sturdevant, E.J. Materna, S.A. Spalding,
J. Risley, and M. Deppman. 2004. The case for regime-based water quality
standards. BioScience, 54(2): 155-161.

Poole, G.C. and C.H. Berman. 2001. An ecological perspective on in-stream temperature:
natural heat dynamics and mechanisms of human-caused thermal degradation.
Environmental Management, Vol. 27(6): 787-802.

Poole, G.C.; Risley, J.; Hicks, M. 2001a. Spatial and temporal patterns of stream
temperature. EPA Region X Temperature Water Quality Criteria Guidance
Development Project Issue paper 3, EPA-910-D-01-003, Seattle, WA.

Poole, G.; Dunham, J.; Hicks, M.; Keenan, D.; Lockwood, J.; Materna, E.; McCullough, D.; Mebane, C.; Risley, J.; Sauter S.; Sturdevant, D. 2001b. Scientific issues relating to temperature criteria for salmon, trout, and char native to the Pacific Northwest. EPA 910-R-01-007, Technical Report, U.S. Environmental Protection Agency, Seattle, WA.

Railsback, S., and S. Jackson. 2004. Water temperature model. Included as part of the EcoSwarm software suite available online at: http://www.humboldt.edu/~ecomodel.

Raphael, J.M. 1962. Prediction of temperature in rivers and reservoirs. J. Power Division, Am. Soc. Civil Eng., 88: 158-181.

Reeves, G.H., Everest, F.H., and T.E. Nickelson. 1989. Identification of physical habitats limiting the production of coho salmon in Western Oregon and Washington. General Technical Report, PNW GTR-245. U.S. Forest Service, PNW Research Station, Portland, OR.

Reifsnyder, W.E., Furnival, G.M., and J.L. Horowitz. 1971. Spatial and temporal distribution of solar radiation beneath forest canopies. Agricultural Meteorology, 9: 21-37.

Reifsnyder, W.E., and H.W. Lull. 1965. Radiant energy in relation to forests. Washington, D.C. USDA Forest Service. Technical Bulletin No. 1344. 108pp

Ricchiazzi, P., Yang, S.R., Gautier, C., and D. Sowle. 1998. SBDART – a research and teaching software tool for plane-parallel radiative transfer in the earth's atmosphere. Bulletin of the American Meteorological Society, 79(10): 2101-2114.

Rishel, G.B, Lynch, J.A., and E.S. Corbett. 1982. Seasonal stream temperature changes following forest harvesting. J. Environ. Qual., Vol. 11(1): 112-116.

Rodriguez-Iturbe, I., and L.A. Escobar. 1982. The dependence of drainage density on climate and geomorphology. Hydrological Sciences Journal, Volume 27(2): 129-137.

Rutherford, J.C, N.A. Marsh, P.M. Davies, and S.E. Bunn. 2004. Effects of patchy shade on stream water temperature: how quickly do small streams heat and cool. Marine and Freshwater Research, 55: 737-748.

Rutherford, J.C., J.B. Macaskill, and B.L. Williams. 1993. Natural water temperature variations in the lower Waikato River. New Zealand Journal of Marine and Freshwater Research, Vol. 27: 71-81.

Rutherford, J.C., Blackett S., Blackett C., Saito L., and R.J. Davies-Colley. 1997. Predicting the effects of shade on water temperature in small streams. New Zealand J. Marine and Freshwater Research, Vol. 31: 707-721.

Sansone, A.L. and D. P. Lettenmaier. 2001. A GIS-based temperature model for the prediction of maximum stream temperatures in the Cascade mountain region. Water Resources Series: Technical Report No. 168, University of Washington, Seattle, WA.

St-Hilaire, A., G. Morin, N. El-Jabi, and D. Caissie. 2000. Water temperature modelling in a small forested stream: implication of forest canopy and soil temperature. Canadian Journal of Civil Engineering, 27: 1095-1108.

Sawyer, J. O., and T. Keeler-Wolf. 1995. A manual of California vegetation. California Native Plant Society, Sacramento, CA.

Sedell, J.R., F.N. Leone, and W.S. Duval. 1991. Water transportation: In Influences of forest and rangeland management on salmonid fishes and their habitats. AFFS Special Publication 19.

Shrimpton, J.M., Bourgeois, J.F., Quigley, J.T., and D.M. Blouw. 2000. Removal of riparian zone during forest harvesting increase stream temperature: are the effects cumulative downstream? *In*: L. M. Darling, editor. 2000. Proceedings of a

Conference on the Biology and Management of Species and Habitats at Risk, Kamloops, B.C., 15 - 19 Feb.,1999. Volume Two. B.C. Ministry of Environment, Lands and Parks, Victoria, B.C. and University College of the Cariboo, Kamloops, B.C. 520pp.

Sinokrot, B.A., and J.S. Gulliver. 2000. In-stream flow impact on river water temperatures. J. Hydraulic Research, Vol. 38(5): 339-349.

Sinokrot, B. A., and H. G. Stefan. 1993. Stream temperature dynamics: measurements and modeling. Water Resources Research 29: 2299-2312.

Smith, K. 1981. The prediction of water temperatures. Hydrological Sciences Bulletin, Volume 26(1): 19-33.

Spence, B.C. et al. 1996. An ecosystem approach to salmonid conservation. TR-4501-96-6057. ManTech Environmental Research Services Corp. Corvalis, OR.

Sridhar, V., Sanson, A.L., LaMarch, J., Dubin, T., and D.P. Lettenmaier. 2004. Prediction of stream temperatures in forested watersheds. Journal of the American Water Resources Association, Vol. 40(1): 197-213.

Stefan, H.G., and E. B. Preud'homme. 1993. Stream temperature estimation from air temperature. Water Resources Bulletin, Volume 29(1): 27-41.

Stillwater Sciences. 2006-2009 stream temperature assessment of the South Fork Ten Mile River, Mendocino County, Northern California. In preparation for Campbell Timberland Management, Fort Bragg, California. Berkeley, California.

Stillwater Sciences. 2002. Stream temperature indices, thresholds, and standards used to protect coho salmon habitat: A review. Unpublished white paper prepared for Campbell Timberland Management, Fort Bragg, California. March 2002

Strahler, A. N. 1957. Quantitative analysis of watershed geomorphology. Transactions of the American Geophysical Union (38):913-920.

Sugimoto, S., Nakamura, F., and A. Ito. 1997. Heat budget and statistical analysis of the relationship between stream temperature and riparian forest in the Toikanbetsu River basin, northern Japan. Journal of Forest Research, Vol.2(2): 103-107.

Sullivan, K., J. Tooley, K. Doughty, J. Caldwell, and P. Knudsen. 1990. Evaluation of prediction models and characterization of stream temperature regimes in Washington. Timber/Fish/Wildlife Report No. TFW-WQ3-90-006. Washington Department of Natural Resources, Olympia.

Swank, W.T., Swift Jr., L.W., and I.E. Douglas. 1988. Streamflow changes associated with forest cutting, species conversions, and natural disturbances. In: Swank,

W.T, and D.A. Crossley Jr. (Eds), Ecological Studies, Vol.66: Forest Hydrology and Ecology at Coweeta. Springer-Verlag. New York, NY.

Swift, L. W., Jr., and J. B. Messer. 1971. Forest cuttings raise temperatures of small streams in the southern Appalachians. Journal of Soil and Water Conservation 26: 111-116.

Tague, C., Farrell, M., Grant, G., Lewis, S., and S. Rey. 2007. Hydrogeologic controls on summer stream temperatures in the McKenzie River basin, Oregon. Hydrological Processes, 21: 3288-3300.

Tennessee Valley Authority (TVA). 1972. Heat and mass transfer between a water surface and the atmosphere. Water Resources Research, Laboratory Report No. 14, Norris, Tennesse.

Theurer, F.D., I. Lines, and T. Nelson. 1985. Interaction between riparian vegetation, water temperature, and salmonid habitat in the Tucannon River. Water Resources Bulletin, 21: 53-64.

Theurer, F.D. K.A. Voos, and W.J. Miller. 1984. Instream Water Temperature Model. Instream Flow Information Paper No. 16. Washington, DC: US Fish and Wildlife Service (FWS/OBS-84/15).

U.S. Environmental Protection Agencey. 2003. EPA Region 10 guidance for Pacific
Northwest state and tribal temperature water quality standards. EPA 910-B-03-
002. Region 10 Office of Water. Seattle, WA.

U.S. Environmental Protection Agency. 1999. South Fork Eel River Total Maximum
Daily Loads for Sediment and Temperature. U.S. EPA Region IX Water
Division, San Francisco, CA. Available online at:
http://www.epa.gov/region09/water/tmdl/final.html

Webb, B.W. 1996. Trends in stream and river temperature. Hydrological Processes, 10:
205-226.

Webb, B.W. and Y.Zhang. 2004. Inter-annual variability in the non-advective heat
energy budget in Devon streams and rivers.Spatial and seasonal variability in the
components of the river heat budget. Hydrological Processes, 18: 2117-2146.

Webb, B.W. and Y.Zhang. 1997. Spatial and seasonal variability in the components of
the river heat budget. Hydrological Processes, 11: 79-101.

Webster, I.T., and C.R.B. Day. 1993. The impacts of shade on evaporation rates and
temperatures in stock watering troughs. Australian Journal of Agricultural
Research, 44: 287-98.

Welsh, Jr. H.H, Hodgson G.R, Harvey B.C., and M.E. Roche. 2001. Distribution of
juvenile coho salmon in relation to water temperatures in tributaries of the
Mattole River, California. North American Journal of Fisheries Management 21:
464-470.

Whitney, S. 1985. Western Forests. National Audubon Society Nature Guides,
Chanticleer Press, Inc., New York.

Ziemer, R.R. 1998. Proceedings of the conference on coastal watersheds: the Caspar
Creek story. Albany, CA: USDA Forest Service Pacific Southwest Research
Station, General Technical Report PSW-GTR-168.

Zwieniecki, M.A., and M. Newton. 1999. Influence of streamside cover and stream
features on temperature trends in forested streams in Western Oregon. W. J.
Appl. For., Vol.14(2): 106-113

APPENDIX

A   GLOSSARY

Broadband radiation – integrated values of solar irradiance over the complete electromagnetic spectrum. *BasinTemp* applications generated predicted insolation over a coarse spectral range of 0.3μm to 3.0μm.

Downstream cumulative effects –repeated, synergistic downstream impacts as a result of changes in land management practices upstream and which result in these changes being propagated and amplified downstream (Dunne et al. 2001, FEMAT 1993)

Model trust region method – any of a family of globally-convergent modifications to Newton's method for minimizing smooth multivariate functions, which are based on the idea of minimizing a quadratic function (the model) over an ellipsoid within which the model is known to be a good approximation to the objective function (the trusted region).

Monochromatic radiation – irradiance calculated for infinitesimally small wavelengths. Practically, it can apply to wavelength ranges of 0.1μm.

Optical depth – the mass of an absorbing or emitting material within a vertical column of unit cross-sectional area and extending to a specified depth in the atmosphere. The optical depth is a dimensionless measure of how much the radiation is reduced between

176

two points, i.e., from the top of atmosphere to an altitude z. The optical depth is equal to the integral of extinction over altitude

Scattering asymmetry factor – the fraction of the incident radiation scattered forward after striking an aerosol particle.

Single scattering albedo – the ratio of the scattering extinction to the total extinction, and therefore the fraction of incident radiation that is scattered when sunlight interacts with aerosol particles.

Sky view factor – the ratio of diffuse sky irradiance at a point to that on an unobstructed horizon. The sky view factor accounts for the slope and orientation of a terrain facet and the portion of the overlying hemisphere visible to it, determined by the local horizon in all directions.

Terrain configuration factor – for an individual point, reflected radiation from surrounding terrain is adjusted by the terrain configuration factor, which incorporates anisotropy of the radiation and geometric effects between the point and surrounding terrain points that are mutually visible.

Transmittance – the fraction of direct short wave radiation that penetrates through the atmosphere. For T=0, no solar radiation penetrates through the atmosphere, and at the opposite end of the scale, for T=1, all radiation penetrates through the atmosphere. The

amount of solar radiation reaching the ground surface is functionally related to the amount of dust particles, water vapor, and gas compounds in the atmosphere. Transmittance is also a function of elevation. At higher elevations in the atmosphere, density is reduced and thus the number of particles that attenuate and scatter solar radiation is reduced. Consequently the amount of solar radiation penetrating the atmosphere at higher elevations is greater.

B   General stream temperature sensitivity analysis

The sensitivity analysis adopts the stream temperature model implementation

presented by Railsback and Jackson (2004) as part of the EcoSwarm software suite. The

flux equations used in their implementation are the same as those applied in the Stream

Network Temperature Model (SNTEMP) (Theurer at al. 1984, Bartholow et al. 1989).

Incoming shortwave radiation, q_{sw}, is provided as input. Values range from 0 to

400 (J m^{-2} s^{-1}), encompassing the full range of daily averaged shortwave radiation for

mid-latitude regions (Boyd and Kaspar 2003, Deas and Lowney 2000).

Atmospheric (downwelling) longwave radiation, $q_{lw\downarrow}$ (J m^{-2} s^{-1}), is given by,

$$q_{lw\downarrow} = (1-r)\varepsilon_a \cdot \sigma (T_a + 273.16)^4 \qquad \text{[B.1]}$$

where $r = 0.03$, ε_a is the atmospheric emissivity = 9.062 x 10^{-6} (T$_a$ + 273.16)^2, σ is the

Stefan-Boltzman constant (5.67 x 10^{-8} J m^{-2} sec^{-1} K^{-4}), and T_a is air temperature (ºC).

The upwelling longwave radiation flux from the water surface, $q_{lw\uparrow}$ (J m^{-2} sec^{-1}), is

given by,

$$q_{lw\uparrow} = -\varepsilon_w \sigma (T_w + 273.16)^4 \qquad \text{[B.2]}$$

where ε_a is the emissivity of the water body and set to a constant value (0.9526), and T_w is

the water temperature (ºC).

Latent heat (evaporation) and convective fluxes are computed using 'lake-type'

equations applied in the Stream Network (SNTEMP) temperature model (Theurer et al.

1984, Bartholow 1989). The latent heat flux, q_l (J m^{-2} sec^{-1}), is given by,

$$q_l = (26.0 \cdot u) \left[R_h (1.0640)^{T_a} - (1.0640)^{T_w} \right] \qquad \text{[B.3]}$$

where u is the wind speed (m/sec), and R_h is relative humidity (%).

The convective flux, q_h (J m^{-2} sec^{-1}), is calculated using,

$$q_h = \left(2.55 \times 10^{-3} \cdot u\right) P_{atm} \left(T_w - T_a\right)$$ [B.4]

where P_{atm} is the atmospheric pressure (mb).